



universität  
wien

## Dissertation

Titel der Dissertation

Quantification of tectonic movement in the Vienna Basin

Verfasserin

Mag. Monika Hölzel

Angestrebter akademischer Grad

Doktorin der Naturwissenschaften (Dr. rer. nat.)

Wien, Juni 2009

Studienkennzahl lt. Studienblatt

A 091 431

Dissertationsgebiet lt. Studienblatt

Geologie

Betreuer

Ao. Prof. Michael Wagreich



## Content

<i>Abstract</i>	<i>iii</i>
<i>Zusammenfassung</i>	<i>v</i>
<i>Acknowledgement</i>	<i>vii</i>
<b>1 Introduction</b>	<b>1</b>
1.1 Aims and Approaches	2
1.2 Outline of scientific and economic oriented investigations through history	2
1.3 Short geological overview of the Vienna Basin	4
1.4 Definition of (normal) faults and their evolution	4
1.5 Methods and Data	6
1.6 Outlook and unsolved questions	7
<b>2 Subsidence Analysis</b>	<b>9</b>
2.1 Abstract	10
2.2 Kurzfassung	10
2.3 Introduction	11
2.4 Geological Outline of the Vienna Basin	12
2.5 Principles of Subsidence Calculations	13
2.6 Data Base	15
2.7 Generation of Subsidence Maps	16
2.8 Results and Interpretation	17
2.9 Regional Trends of Subsidence	17
2.10 Subsidence Maps	22
2.11 General Subsidence Trends	23
2.12 Conclusions	27
<b>3 Error Quantification for Subsidence Analysis</b>	<b>29</b>
3.1 Abstract	31
3.2 Introduction	32
3.3 Subsidence calculations	32
3.4 Programme description and work flow	33

3.5 Method of error calculation	34
3.6 Error sources	37
3.7 Application	37
3.8 Discussion and Conclusion	40
<b>4 Sedimentary Fault Backstripping</b>	<b>41</b>
4.1 Abstract	43
4.2 Introduction	44
4.3 Sedimentary fault backstripping	44
4.4 Application in the southern Vienna Basin	46
4.5 Results	54
4.6 Discussion	56
4.7 Errors, limitations, and requirements for sedimentary fault backstripping	57
4.8 Conclusion	58
<b>5 Synthesis I - Wedge Top Phase</b>	<b>61</b>
5.1 Abstract	63
5.2 Introduction	64
5.3 Techniques and working area	65
5.4 Stratigraphy, marker horizons and time constraints	68
5.5 Tectonic structures in the subcrop	72
5.6 Early Miocene fault kinematics derived from outcrop data	79
5.7 Evolution of the Lower Miocene wedge-top zone	81
<b>6 Synthesis II - Pull-Apart Phase</b>	<b>85</b>
<b>7 References</b>	<b>89</b>
<b>8 Appendix 1</b>	<b>101</b>
8.1 Seismic sections	103
8.2 Displacement Plots	107
8.3 Input Data for Subsidence Analysis	113
<b>9 Appendix 2</b>	<b>131</b>
Curriculum Vitae	132
List of Publications	135

## Abstract

This cumulative Ph.D. consists of four publications published in or submitted to international peer-reviewed scientific journals. The publications are all related to the structural development of the Vienna Basin. The main focus was on the quantification of fault movement, based on subsidence analysis.

Chapter 2 (based on Hölzel, M., Wagreich, M., Faber R., Strauss, P. (2008). *Regional subsidence analysis in the Vienna Basin (Austria)*. *Austrian Journal of Earth Sciences*, 101, 88 – 98) summarises the results of subsidence analysis with data from 50 wells in the southern and the central area of the Austrian part of the Vienna Basin. The subsidence analysis is based on the decompaction of the sedimentary record at the time of interest, with the results displayed as total basement and tectonic subsidence curves and tectonic subsidence rates for the pull-apart phase of the Vienna Basin. Three types of subsidence curves have been distinguished, representing combinations of three main subsidence phases; in the early Badenian (~16.1 – 14.2 Ma), the Sarmatian (~12.7 – 11.5 Ma), and the middle Pannonian (~10.2 – 9.8 Ma).

To be sure errors are minimised during generation of the base data, software for the calculation of subsidence data with error quantification has been established. Chapter 3 (based on Hölzel, M., Faber, R., Wagreich, M. (2008). *DeCompactionTool: Software for subsidence analysis including statistical error quantification*. *Computers and Geosciences*, 34, 1454-1460) presents the applied programme in detail. Input data consists of factors like strata thickness, lithology, age constraints, lithological properties, porosity, palaeobathymetry, sea-level changes and heat flux, amongst others. Uncertainties of these input parameters are not independent, so within the subsidence calculation a Monte Carlo Simulation routine was implemented. In this, the range of possible input values (minimum, maximum, most likely number) is assigned to each of the parameters used. A random number generator chooses values within the defined intervals and calculates results for every combination. The probability that a number is selected by the generator may follow a uniform distribution, a power distribution, a symmetric normal distribution or an asymmetric normal distribution. The results are mean values with two extreme values quantifying the error range.

Sedimentary fault backstripping is a rather new method for the quantification of vertical fault displacement to assess the fault movement behaviour of fault surfaces. Chapter 4 (based on Hölzel, M., Wagreich, M. (submitted 2009). *Sedimentary fault backstripping of a complex fault system – Results and limitations of a case study in the southern Vienna Basin*. *Marine and Petroleum Geology*) describes the workflow in detail. The method has been applied to the southern Vienna Basin. Major normal faults as the Leopoldsdorf Fault with an overall offset of 4000 m are compared to more complex fault arrays forming a negative flower structure and relay ramps. All faults have in common that they were synsedimentary active. The thickness of the sediments overtops the thickness of the footwall strata. So displacement has been conserved during ongoing sedimentation. After discriminating the structural build-up by seismic data and 3D modelling, basement subsidence data from the different fault blocks are compared. Results are very inhomogeneous. The more isolated huge fault surface of the Leopoldsdorf Fault

shows normal slip through time. The more complex faults of the negative flower structure are kinematically linked and display normal as well as reverse slip periods. Data indicate alternating activity on converging fault surfaces.

The first part of the Synthesis (Chapter 5) is based on the publication *Hölzel, M., Decker, K., Zamolyi, A., Strauss, P., Wagneich, M. (submitted 2008): Lower Miocene structural evolution of the central Vienna Basin (Austria). Marine and Petroleum Geology*, which deals with the structural evolution of the basin during the Lower Miocene wedge top phase. These investigations are based on stratigraphic and structural seismic mapping and 3D visualisation. It gives an overview about the evolution of the basin prior to the pull-apart phase.

The second part of the Synthesis (Chapter 6) summarises the results of subsidence analysis in the southern and central and the results of *Sedimentary Fault Backstripping* in the southern part during the pull-apart phase.

## Zusammenfassung

Diese kumulative Dissertation besteht aus 4 Publikationen, die in peer-reviewten wissenschaftlichen Journalen publiziert oder eingereicht wurden. Die Themen aller stehen in Beziehung mit der strukturellen Entstehungsgeschichte des Wiener Beckens. Der Fokus liegt auf der Quantifizierung von Störungsversatz, basierend auf Subsidenzanalyse.

Kapitel 2 (basierend auf: Hölzel, M., Wagreich, M., Faber R., Strauss, P. (2008). *Regional subsidence analysis in the Vienna Basin (Austria)*. *Austrian Journal of Earth Sciences*, 101, 88 – 98) fasst die Ergebnisse der Subsidenzanalyse mit Daten aus 50 Bohrungen des südlichen und zentralen österreichischen Anteils des Wiener Beckens zusammen. Die Subsidenzanalyse basiert auf der Dekompaktion der Sedimente zu bestimmten Zeitpunkten. Die Ergebnisse werden als Gesamt-Basement- und tektonische Subsidenz und Kurven tektonischer Subsidenzraten für die Pull-Apart Phase des Wiener Beckens dargestellt. Beim Vergleich der Form dieser Kurven ergaben sich 3 Hauptsubsidenzphasen für das frühe Badanium (~16,1 – 14,2 Ma), für das Sarmatium (~12,7 – 11,5 Ma) und im Mittelpannonium (~10,2 – 9,8 Ma).

Um sicher zu stellen, dass Fehler während der Berechnungen der Grunddaten so klein wie möglich sind, wurde eine Software für die Berechnung von Subsidenz mit einer implementierten Funktion zur Quantifizierung von Fehlerbereichen entwickelt. Kapitel 3 (basierend auf: Hölzel, M., Faber, R., Wagreich, M. (2008). *DeCompactionTool: Software for subsidence analysis including statistical error quantification*. *Computers and Geosciences*, 34, 1454-1460) präsentiert das Programm im Detail. Die eingegebenen Daten bestehen unter anderen aus Faktoren wie der Mächtigkeit der sedimentären Schichten, der Lithologie, Alter der Schichten, Gesteinseigenschaften, Porosität, Paläobathymetrie, Meeresspiegelvariationen und Wärmefluss. Die Unsicherheiten dieser Faktoren sind im Resultat abhängig von einander zu betrachten und so wurde eine gleichzeitig mit der Subsidenzberechnung einhergehende Monte Carlo Simulation Routine eingebaut. In dieser wird ein Wert aus einem Intervall möglicher Eingabefaktoren einem Parameter per Zufallsabfrage zugeordnet. Ein Zufallsgenerator wählt Werte innerhalb der definierten Intervallgrenzen und rechnet Resultate für jede Kombination. Die Wahrscheinlichkeit, dass ein Wert vom Zufallsgenerator ausgewählt wird, richtet sich nach zu wählenden uniformen Verteilungen, einer Power Verteilung, einer symmetrischen Normalverteilung oder einer asymmetrischen Normalverteilung. Die Resultate sind Mittelwertkurven mit jeweils 2 Extremwertkurven, die den Fehlerbereich quantifizieren.

*Sedimentary fault backstripping* ist eine neue Methode zur Quantifizierung von vertikalem Störungsversatz, um das Verhalten entlang von Störungsflächen abschätzen zu können. Kapitel 4 (basierend auf: Hölzel, M., Wagreich, M. (submitted 2009). *Middle to Upper Miocene fault history analysis of the southern Vienna Basin (Austria)*. *Marine and Petroleum Geology*) beschreibt den Arbeitsablauf dieser Methode im Detail. Sie wird im südlichen Teil des Wiener Beckens angewandt und getestet. Dort existieren mächtige Abschiebungen wie der Leopoldsdorf Bruch mit einem Gesamtversatz von 4000 m, daneben aber auch komplexere Strukturen, die eine negative *Flower Structure* und *Relay Ramps* formen. Die Gemeinsamkeit aller Störungen ist ihre ehemals synsedimentäre Aktivität. Die Dicke des Sedimentstapels

der Hangendschollen überragen die Mächtigkeiten auf den Liegendblöcken. Der Versatz wurde durch die gleichzeitige Sedimentation konserviert.

Nachdem der strukturelle Aufbau in der Seismik kartiert und ein 3D Modell erstellt wurde, konnte die Basementsubsidenz der verschiedenen Störungsblöcke miteinander verglichen werden. Diese Resultate sind sehr inhomogen. Die einigermaßen isolierte große Störungsfläche des Leopoldsdorf Bruch zeigt Abschiebungen während der untersuchten Zeitspanne. Die komplexeren Störungen der negativen *Flower Structure* sind kinematisch miteinander verbunden und weisen abschiebende und aufschiebende Phasen auf. Die Daten zeigen auch wie Störungen, die in der Tiefe konvergieren, abwechselnd aktiv sind.

Der erste Teil der Synthese (Kapitel 5) basiert auf einer Publikation (Hölzel, M., Decker, K., Zamolyi, A., Strauss, P., Wagreich, M. (submitted 2008): *Lower Miocene structural evolution of the central Vienna Basin (Austria). Marine and Petroleum Geology*), die die strukturelle Evolution des Beckens während des Unteren Miozäns in der Wedge Top Phase zum Inhalt hat. Die Arbeit ist Ergebnis von stratigraphischer und struktureller Kartierung von Seismik-Daten und 3D Visualisierung. Das Kapitel gibt einen Überblick über die Zeit vor der Pull-Apart Phase des Wiener Beckens.

Der zweite Teil der Synthese fasst die Ergebnisse von Subsidenzanalyse in südlichen und zentralen und des *Sedimentary Fault Backstripping* im südlichen Teil des Wiener Beckens während der Pull-Apart Phase zusammen.

## Acknowledgement

The Austrian Academy of Sciences supported this Ph.D. with a DOC scholarship for 18 month. The development of DeCompactionTool has been funded by a scholarship promoting scientific research by the University of Vienna. The publication about wedge top zone is a product of my collaboration in the project *Karpatian Tectonics* at the Department of Geodynamics and Sedimentology (University Vienna), funded by OMV E&P Austria.

All additional well data, interpreted horizons and 2D seismic were provided by OMV. Therefore, I would like to thank the responsible managers Kurt Wagner and Christian Astl for the uncomplicated data exchange. My special thanks go to Philipp Strauss, who was always interested in my research activity and with whom I had lively discussions about the geology of the Vienna Basin.

From my promoter Michael Wagneich I got permanent support over all the years. He proposed the basic concepts of this Ph.D. and I am very thankful for his patience and ideas.

I was very happy to join the *Karpatian Tectonics* group and work together with Kurt Decker and Andras Zamolyi. I learned a lot within this active team and would never miss the time during field work in Slovakia.

Ralph Hinsch provided lots of his data and guidance throughout the first steps of seismic interpretation within his former working area, the southern Vienna Basin. Bernhard Grasemann motivated me with providing brand new literature and discussions.

I thank all my other colleagues for their support as solving computer problems, providing literature or having just good working climate and a good time, especially Ulli Exner, Stefi Neuhuber, Andreas Beidinger, Bernhard Salcher, Marcus Ebner, Olga Wronska, Anna Berger and Nelli Tschegg.

Norbert Irrnberger helped me improving my figures for the paper in the Austrian Journal of Earth Sciences to enable publication nearly immediately.

Without the genial programming skills of Robert Faber from *TerraMath* ([www.terramath.com](http://www.terramath.com)) the programme DeCompactionTool would have never been possible. I thank him for his time and support by solving all the upcoming problems with Monte Carlo Simulation and statistics.

Matthias Harzhauser supported the work with his advises about the stratigraphic zonation of the Vienna Basin. Godfried Wessely always found some interesting topics to discuss about the structural inventory of the Vienna Basin.

I would like to thank Hugh Rice and Ruth Kremer, who were my first readers and had to improve my English and sometimes the confusing contents of the manuscripts.

My friend Lukas always had to have calming words when I was frustrated about all my data mess and encouraged me to go on. I thank him for motivating me for things which I would never have tried without him and for enjoying these moments together!

Finally I would like to thank my parents Luzia and Herbert, who supported me over a long time and who never lost their faith that my studies of Earth Sciences could come to a happy end.



## **1 Introduction**

### **1.1 Aims and Approaches**

There are numerous interesting basins in the world with diverse geological evolutions. In many cases someone would search for spots where geological results seem to be new, where the key problems are still unsolved. The Vienna Basin is the contrary example as hydrocarbon exploration started in the 1920ties. The basin is very well known and provides a huge data base.

The main task of this Ph.D. is to quantify the kinematics of Miocene fault movements resulting to better understand the mechanics, timing and sedimentary evolution of the Vienna Basin and of pull-apart basins in general. In literature, there are numerous analogue and numerical models investigating the geometric development of pull-apart basins and the arrangement of their fault systems. Comparisons between models and existing pull-apart basins focus mainly on the parameters that control their geometries and not on the changing behaviour of actual fault surfaces through time.

The southern part of the Vienna Basin, south of the river Danube, has been chosen as area of investigations. There are prominent faults with normal displacement as well as strike-slip offset.

The method applied, *sedimentary fault backstripping*, was developed by ten Veen and Kleinspehn (2000) and up to recent it was only adopted on neotectonic structures in Crete (Greece). After a pilot study of Wagreich and Schmid (2002) in the central Vienna Basin, it is the aim to test and check this method on its applicability in a bigger area with a comprehensive dataset.

Accordingly, to apply *sedimentary fault backstripping* it is necessary to know the exact structural build-up. Horizon and fault mapping within 3D and 2D seismic datasets allows getting information about the subsurface geologic features. To obtain the relationship between the mapped structures in 3D, the digital reconstruction should be undertaken resulting in a subsurface 3D model. This is a useful tool to cross-check the results for their quality.

As subsidence analysis is the data base for *sedimentary fault backstripping*, one focus is on the quantification of errors during subsidence calculations to have good quality data for fault displacement determination. Subsidence maps should be generated for the Middle- to Late Miocene pull-apart history as well as for distinct time intervals.

### **1.2 Outline of scientific and economic oriented investigations through history**

The evolution of the Vienna Basin has interested generations of investigators so far. There is a voluminous amount of literature about the basin including all branches of Earth Sciences. The following paragraphs give an outline of (mostly overview) works investigating the structural and tectonic evolution of the Vienna Basin.

One of the first geological descriptions about the Vienna Basin comes from the 19th century (Keferstein, 1828). Then, geological research became intensified during the 1920ies due to the occurrence of natural oil seeps in the Slovakian part of the basin. Petraschek (1922) and Friedl (1927; 1929) recognised the occurrences of large fault systems, like the Leopoldsdorf Fault and Steinberg Fault at the western margin of the basin, with estimated minimum displacements of

500 to 1000 m (“mit ungeheuerlichen Sprunghöhen”). A major change in view was the insight that activity of these faults were not longer seen as post-Pannonian, but as a steady process starting during the Badenian (former Tortonian) ongoing through the Sarmatian, Pannonian and post-Pannonian to neotectonic activity.

During World War II the Vienna Basin was exploited intensively and the data network became dense very quickly. Janoschek (1942) gives a review about large fault systems known at that time, like the Steinberg Fault in the northern Vienna Basin, where large anticlines in the hanging wall form hydrocarbon reservoirs. In the following, the debate about genesis and tectonics of major fault systems was ongoing (Stowasser, 1958). Modern interpretations, concentrating on the Steinberg Fault were later given in the 1960ies. Stowasser (1966) defines the fault and related fault blocks as rollover structure. He tries to explain the compensation of the enormous normal displacement with an “under thrusting” (Unterschubung) at the eastern margin of the basin. Today in this eastern area (Lasse Fault System) we know from seismic data that a negative flower structure is bordering the basin.

The Austroalpine Units underlying the Neogene sediments, especially the nappes of the Northern Calcareous Alps, became more and more the focus of interest for the oil industry (first gas bearing reservoirs were discovered in 1959) as alternative reservoirs to the Neogene basin fill (Kapounek et al., 1963; Kröll and Wessely, 1973; Hamilton et al., 1980; Wessely, 1988; Wessely, 1992).

The opening mechanisms of the basin were discussed since the 1980ies as Royden (1985) explained the basin as thin skinned pull-apart structure. Transtensional opening of the Vienna Basin was proposed at a stepover between two lateral strike slip faults (Royden and Baldi, 1988) to result from the north-eastward reorientation of the still escaping northern edge of the Pannonian plate. There are also alternative publications following the assumption that the basin represents a graben rift system, reactivating Variscan structures of the underlying crystalline basement of the remnants of the Bohemian Massif (Tollmann, 1985). Schopper (1991) discussed this question based on brittle structural data from the basin margin.

In the 1990ies the pull-apart theory was commonly accepted and supported by the concept of lateral orogenic float of the Eastern Alps (Ratschbacher et al., 1991). New insights about the structural evolution of the Vienna Basin were given by Fodor (1995), Decker (1996) and Decker and Peresson (1996). They could resolve the paradigm that an extensional structure could evolve in an overall compressive setting.

Later the focus of structural studies lay on active tectonics and the question about earthquakes hazards in the Austrian – Slovak border zone and in the Pannonian region (Hinsch and Decker, 2003; Hinsch et al., 2005a; Hinsch et al., 2005b; Bus et al., in press).

### **1.3 Short geological overview of the Vienna Basin**

The Vienna Basin is bordered by the Eastern Alps in the West and the Carpathians in the North-East and the Pannonian Basin System in the East. So the basin was governed and influenced by the evolution of both of these orogens, and by the formation of the Pannonian region. The modern Vienna Basin has a rhombohedral shape with a length of ca. 200 km and a width of 60 km. Tectonics, subsidence and sedimentation in the basin are characterised by two distinct stages, which are referred to as a Early Miocene piggy-back stage (Seifert, 1992; Peresson and Decker, 1997) and a subsequent Middle to Late Miocene stage of pull-apart basin formation at the sinistral Vienna Basin Transfer Fault. Basin subsidence and sedimentation terminated during a compressional phase in the Late Miocene (Decker and Peresson, 1996).

In the Early Miocene (Ottangian; ca. 18 Ma) several small basins opened on top of the thrust sheets of the Eastern Alps. These wedge top basins (piggy back basins) are aligned by fault propagation folds of the underlying Austroalpine nappes and bordered by NE-dipping normal faults. The basins are preserved under the Middle to Upper Miocene sediments of the pull-apart and could be located with seismic data. The distribution of these basins is parallel to the strike of the Alpine Units.

A major change occurred at the Early- to Middle Miocene boundary (Top Karpatian – 16.3 Ma). The kinematic regime changed to WSW-ENE extension and duplexes bordered by major sinistral strike-slip and normal faults developed. Many of these fault surfaces dissect the sedimentary basin fill and reach the basin floor as well. So the basin is divided into lower lying depocentres and higher horst blocks. Many of the faults are related to growth strata due to their synsedimentary activity over the Middle to Late Miocene. The ongoing displacement after the sediment influx stopped with the top of the Upper Pannonian (ca. 7.1 Ma) can be concluded from faults without growth strata.

### **1.4 Definition of (normal) faults and their evolution**

In general, *faults* are zones of discontinuities within rocks. They are represented by one or more surfaces having all kinds of scales (mm to hundreds of km). The general term for the relative movement of the two sides of a fault, measured in any direction is the *displacement* (Bates and Jackson, 1987). Finite displacements are produced by a number of individual slip events on a fault (Walsh and Watterson, 1987). *Dip slip* is characterised by displacement parallel to the dip of the fault surface (Reid et al., 1913). Normal and reverse faults are both dip-slip dominated.

*Throw* (Fig. 1.1) is the vertical component of dip-separation of a normal or reverse fault, measured in a vertical cross section perpendicular to the strike of the fault (e.g. Geiki, 1882; Billings, 1942; Hills, 1949), which it is not equal to the net slip (vector) of the fault. Vertical throw is equivalent to the vertical component of displacement only for a pure dip-slip fault. Stratigraphic throw is the vertical displacement between 2 tilted layers, which has to be dip corrected.

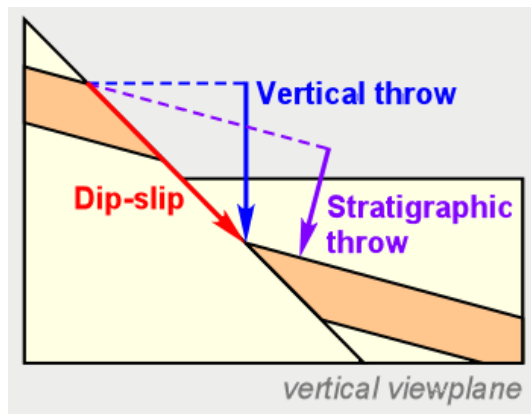


Fig. 1.1: Scheme of what is dip slip along a fault surface, vertical throw and stratigraphic throw.

The idealised normal fault (plane) has elliptical shape with slip maximum in the centre that is decreasing towards the tip lines (lines of zero displacement). However, numerical models show that slip distributions on normal faults are often asymmetric and display local maxima (Maerten et al., 1999). They can be caused by mechanical interaction between intersecting faults. Mechanical interaction between faults involves the behaviour and development of one

fault being influenced by another fault or faults (Segall and Pollard, 1980; Aydin and Schultz, 1990; Bürgmann et al., 1994). Overstepping normal faults interact across transfer zones (Morley, 1995). One type of transfer zone transferring displacement between two normal faults which overstep in map view and which have the same dip direction (Larsen, 1988) is defined as **relay ramp** (Fig. 1.2). Fault segments are unconnected, but soft-linked by ductile strain of the rock volume between them.

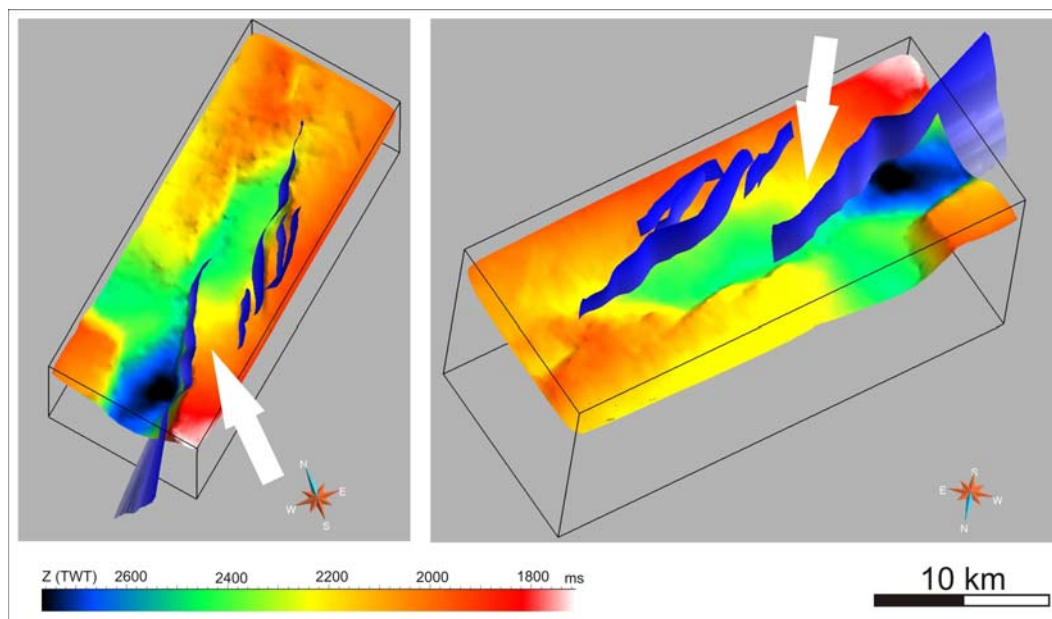


Fig. 1.2: Example of a relay ramp in the 3D seismic block Moosbrunn, southern Vienna Basin (white arrows).

Large scaled fault surfaces of some kilometres in length and 1000 m in depth with displacement from 20 to 3000 m at least are characteristic for the Vienna Basin. The structural build up

comprises a complex system of linked or overstepping normal faults, some with strike-slip components as well. They are located in a sedimentary environment showing different sediment thickness for the same stratigraphic interval at both sides of the fault surface. If the hanging wall block thickness exceeds the footwall then the fault surface is referred to have been active during sediment deposition. That indicates them as synsedimentary or growth faults. If the sediment rates are high and fault scarps are blanketed with sediment after the time of displacement it is possible to determine the amount of vertical throw.

## **1.5 Methods and Data**

### **1.5.1 Seismic**

Seismic mapping of horizon and fault surfaces have been done to get 3D relationship of the fault blocks and stratigraphic horizons. The seismic data set comprises a 3D seismic block (*Moosbrunn*) which covers an area of 192 km<sup>2</sup> and reaches a depth of 3000 ms TWT (Two-Way-Traveltime; c. 3700 m). Selected 2D seismic lines of better quality as the 3D data supported the subsurface mapping of horizons and the allocation of fault surfaces.

For the quantification of fault movement, the stratigraphic information comes from markers from 25 wells. Seismic reflectors have been tied to selected wells and are calibrated to high resolution seismic stratigraphy by Strauss et al. (2006), who defined stratigraphic boundaries at distinct reflectors of the 3D seismic cube *Moosbrunn*.

Horizons were mapped on a net of every 20<sup>th</sup> seismic line, supported by the use of random lines. For the mapping of fault surfaces lines perpendicular to the strike have been generated, supported by time sections (horizontal sections) within the 3D seismic cube *Moosbrunn*.

Mapping itself was conducted with the software Landmark Geographix (Halliburton), based on PC with Windows. This is a module-based software for interpreting geophysical data as seismic, borehole information and log data combining it with geographic data as topographic maps or DEM.

### **1.5.2 Sedimentary Fault Backstripping**

In literature the method is sometimes referred to as *fault backstripping*, but mostly with this term a different approach for quantifying fault displacement is meant (Rowan et al., 1998; Walsh et al., 2003). In this Ph.D., the method will be referred to as *sedimentary fault backstripping*.

The principle is that on both sides of a fault surface, on the hanging wall and the footwall, the sedimentary record is analysed. From both fault blocks the basement subsidence is reconstructed, because it is assumed that sediments were deposited during fault movement. Therefore the displacement could be read out the restored sedimentary column. The process of subsidence analysis is explained in detail in Chapter 2, where also the results are presented. In these calculations wells from the northern part have been incorporated.

### 1.5.3 Visualisation in 3D and modelling of geologic structures

The construction of a 3D model supports the visualisation and crosschecking of the subsurface structures. For the 3D modelling of the mapped subsurface structures the software GoCad was used. Raw data from seismic interpretation can be transferred into the programme and surfaces are constructed. They are based on TINs (*triangular irregular networks*), which means that a surface is represented by a net of triangles with variable sizes.

Fault surfaces within seismic data are sometimes not distinct reflections but are characterised by a zone of noisy and disturbed reflectors. So the termination of horizons along fault surfaces is not easy to detect. The 3D modelling of data allows the extrapolation of missing data points, especially from horizons, to be cut by fault surfaces to get the exact interference pattern between stratigraphic and fault surface.

### 1.6 Outlook and unsolved questions

The detailed reconstruction of the 2D-subsidence history using basin modelling software like *STRETCH* or *FlexDecomp*, which are available at the Department for Geodynamics and Sedimentology, would be a challenging task for future work. Also the trial of building, balancing, restoring and analysing sections, including decompaction and depth conversion with software tools like *3Dmove* (<http://www.mve.com/>). With balancing programmes it should be possible to incorporate and quantify the effects such as footwall uplift in extension, loading during basin inversion and thrusting, compaction, and fault related folding, which will result in a validated and balanced palinspastic model of a southern Vienna Basin transect and provides a necessary test for the plausibility of the reconstructed movements along the faults.

As the study area is limited to the southern part of the Vienna Basin, faults of other parts of the basin could be investigated. The seismic coverage is very dense so far.

An overlook about times of fault activity would help to understand the overall kinematics better, because some faults show growth strata and some not. To extract, which faults were active during the Middle to Late Miocene and which were active postsedimentary would be an interesting task.



## **2    Subsidence Analysis**

---

The chapter is based on:

Hölzel, M., Wagreich, M., Faber R., Strauss, P. (2008). Regional subsidence analysis in the Vienna Basin (Austria). *Austrian Journal of Earth Sciences*, 101, 88 – 98.

## **2.1 Abstract**

In the southern and central parts of the Vienna Basin in Austria, 50 wells have been investigated to quantify the subsidence during the pull-apart stage of basin evolution (Middle to Upper Miocene; 16.1 – 7.8 Ma). Subsidence analysis is based on the decompaction of the sedimentary record at the time of interest, with the results displayed as total basement and tectonic subsidence curves and tectonic subsidence rates for a given time interval. Due to the compartmentalisation of the basin floor and the overlying sediments, the results vary in detail. They show the highest tectonic subsidence rates occurred during the Upper Lagenidae Zone (14.5 – 14.2 Ma) with c. 1000 m/Ma in the southern part and around 700 m/Ma in the central part of the basin. Three types of subsidence curve have been distinguished, representing combinations of three main subsidence phases; in the early Badenian, the Sarmatian, and the Middle Pannonian. Maps of the cumulative tectonic subsidence of four selected stratigraphic tops and the interval tectonic subsidence of four stratigraphic zones are presented.

## **2.2 Kurzfassung**

Im südlichen und zentralen Teil des Wiener Beckens (Österreich) wurden zur Quantifizierung der Subsidenz 50 Bohrungen untersucht. Als Zeitraum wurde die Entwicklung der Pull-Apart Phase (Mittleres bis Oberes Miozän, 16.1 – 7.8 Ma) gewählt. Die Subsidenzanalyse basiert auf der Dekompaktion der Sedimente zu bestimmten Zeitpunkten. Die Ergebnisse sind als Gesamt-Basement- und tektonische Subsidenz und Kurven tektonischer Subsidenzraten für bestimmte Zeitintervalle dargestellt. Im Detail variieren die Kurven, weil der Beckenuntergrund und die darüberliegenden Sedimente in Blöcke zerteilt sind. Die höchsten Werte der tektonischen Subsidenzraten ergeben sich in der Oberen Lageniden Zone (14,5 – 14,2 Ma) mit ca. 1000 m/Ma im südlichen Teil und mit niedrigeren Werten um die 700 m/Ma im zentralen Teil. Beim Vergleich der Form dieser Kurven ergaben sich 3 Hauptsubsidenzphasen für das frühe Badenium, für das Sarmatium und im Mittelpannonium. Als Endergebnisse präsentieren wir Karten der kumulativen tektonischen Subsidenz von 4 ausgewählten stratigraphischen Grenzen und der Intervall-Subsidenz von 4 stratigraphischen Zeitabschnitten.

### **2.3 Introduction**

A large number of publications about the formation and geological evolution of the Vienna Basin (Vienna Basin) has been published, beginning with classic papers in the 19<sup>th</sup> century (e.g. Keferstein, 1828) up to recent articles on sequence stratigraphy and tectonics. Here, we present a detailed quantification of subsidence in the Vienna Basin through time. Subsidence analysis allows a quantitative reconstruction of basin evolution, sediment influx and deposition, and gives hints to the timing and types of tectonic driving forces. Due to the extensional basin formation, a complex fault pattern evolved in the Vienna Basin, with duplexes along sinistral strike-slip systems and normal faulting during the Middle to Upper Miocene. This resulted in the obvious tectonic segmentation of the basin fill, which, consequently, calls for detailed subsidence analysis, using a larger data base than previously used (e.g. Lankreijer et al., 1995).

The data presented here were derived from 50 wells drilled in the southern and central Vienna Basin (Austrian part, Fig. 2.1) and, due to the high density of boreholes, allows the plotting of detailed regional subsidence maps. Other publications on this topic have mainly referred to surrounding areas, such as the eastern part of the foreland-basin of the Eastern Alps (Genser et al., 2007), the Styrian Basin (Sachsenhofer et al., 1997) and the Pannonian Basin System (Sclater et al., 1980; Lankreijer et al., 1995; Lankreijer, 1998; Baldi et al., 2001). Lankreijer (1998) quantified the large-scale subsidence of the whole Pannonian system, including the Vienna Basin. Lankreijer et al. (1995) integrated 36 wells from the Slovakian northern part and 12 wells from the Austrian central part of the Vienna Basin. Our work, which mainly covers the remaining parts of the Vienna Basin, aims to give a more detailed regional study and interpretation of subsidence patterns, using a significantly revised, more accurate stratigraphy of the Vienna Basin, developed since the 1990s (Rögl, 1996; Steininger and Wessely, 1999; Rögl et al., 2002; Harzhauser et al., 2002; Harzhauser and Piller, 2004; Piller et al., 2004; Strauss et al., 2006; Hohenegger et al., 2008). Together with the high density of borehole data, this has allowed considerable refinements to be made in the timing of subsidence events and more accurate tectonic interpretations.

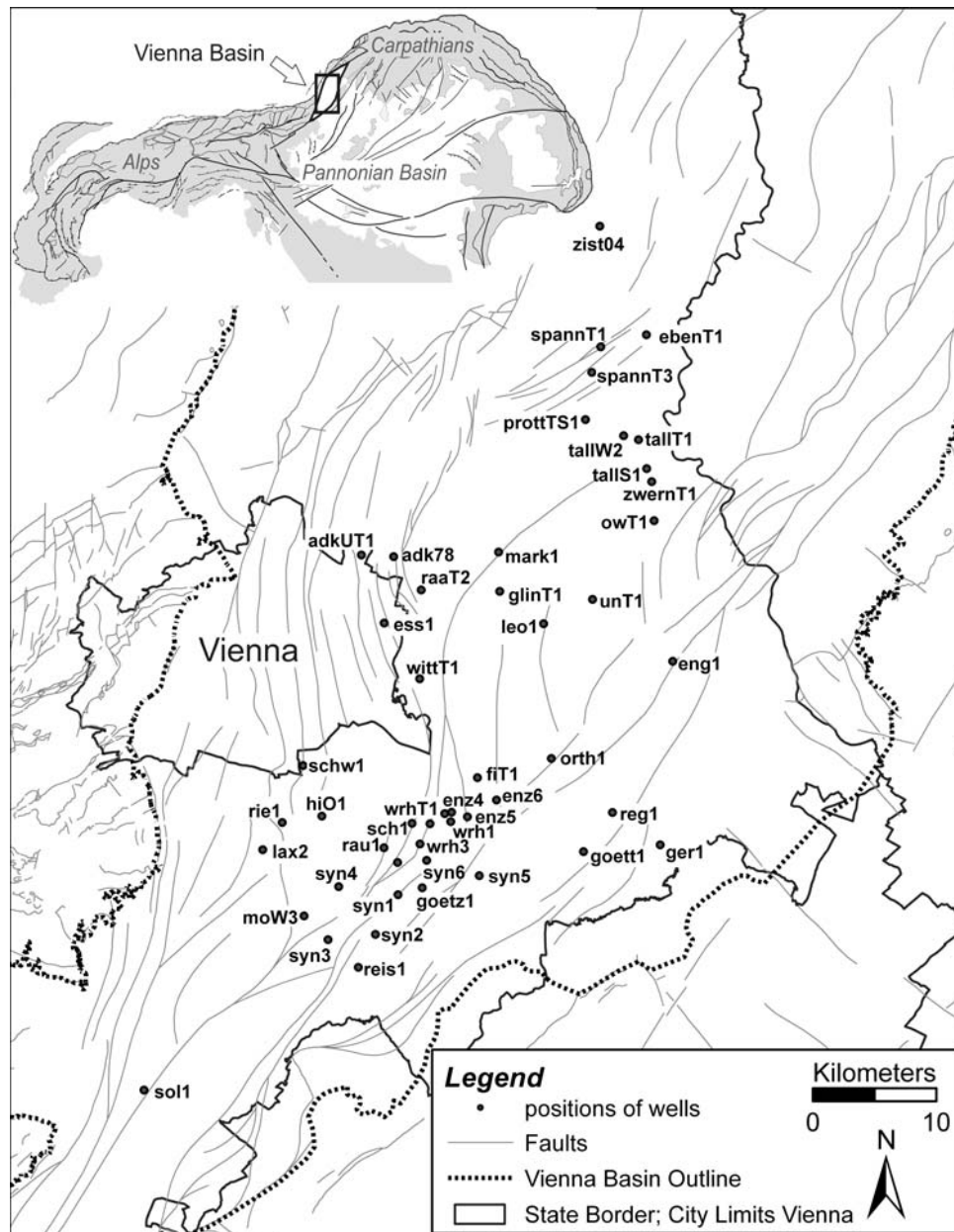


Fig. 2.1: Position of the Vienna Basin within the Alpine/Carpathian transition and overview of borehole locations used in this study.

## 2.4 Geological Outline of the Vienna Basin

The main subsidence period of the Vienna Basin was during the Miocene. The initial basin structure was a wedge-top zone (DeCelles and Giles, 1996) on the frontal parts of the north-west propagating thrust sheets of the Eastern Alps (Lower Miocene; ~18 – 16 Ma; Fig. 2.2). Within this zone, mainly fluvial sediments filled several small basins that later merged into one large basin. Due to changes in the local stress-regime, a pull-apart geometry began to develop (Fodor, 1995; Decker and Peresson, 1996), with the initiation of large-scale sinistral

strike-slip fault systems; these are often rooted in reactivated basement structures and were accompanied by significant normal faults with offsets reaching some 1000s of metres. This led to an intense segmentation of the basin into duplexes, where depocentres were filled with clastic sediments up to 5.5 km thick (Middle to Upper Miocene; ~16 – 7 Ma; Fig. 2.2). Detailed descriptions of the basin evolution can be found in Jiricek and Tomek (1981), Royden (1985), Wessely (1988), Seifert, (1992), Wessely (1992), Fodor (1995), Weissenböck (1996), Kováč et al. (2004) and Hinsch et al. (2005).

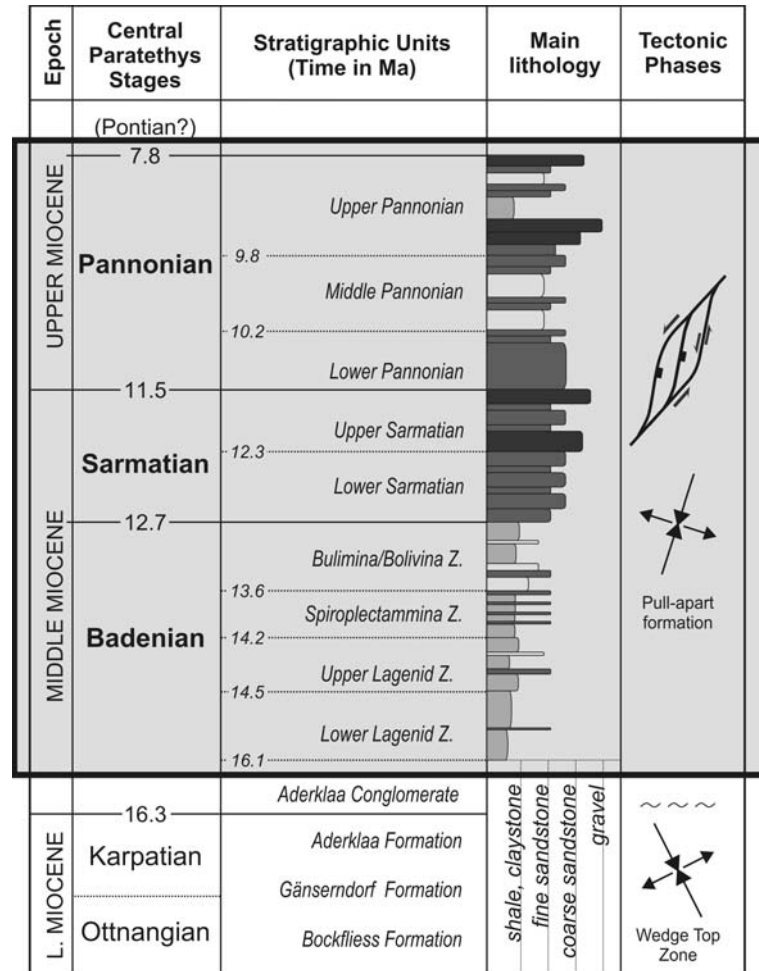


Fig. 2.2: Simplified stratigraphic table with Central Paratethys stages and local stratigraphic nomenclature used in the Vienna Basin. The grey rectangle marks the investigated time window. Tectonic phases according to Decker and Peresson (1996).

## 2.5 Principles of Subsidence Calculations

Subsidence analysis is mainly based on decompaction of the sedimentary record (Steckler and Watts, 1978; Van Hinte, 1978; Slater and Christie, 1980). This uses empirically derived curves of porosity-depth relationships, with an exponential reduction of porosity at increasing depths (Baldwin and Butler, 1985). The most important parameters are the thickness of the sedimentary

layers and the chronostratigraphy, both of which affect quantification of the subsidence rates. The total subsidence is partitioned into subsidence caused by the tectonic driving force(s) and subsidence due to the sediment load (and compaction). Backstripping removes the effect of sediment loading and compaction from the basement subsidence. Normally, an Airy isostasy model is applied, with the sediment load replaced by a column of water. The results can be used to infer types of the tectonic driving forces and for basin modelling (Lankreijer et al., 1995; Sachsenhofer et al., 1997). The difference between basement and tectonic subsidence curves are shown in Fig. 2.3. For further descriptions of the method refer to Einsele (2000) and Allen and Allen (2005).

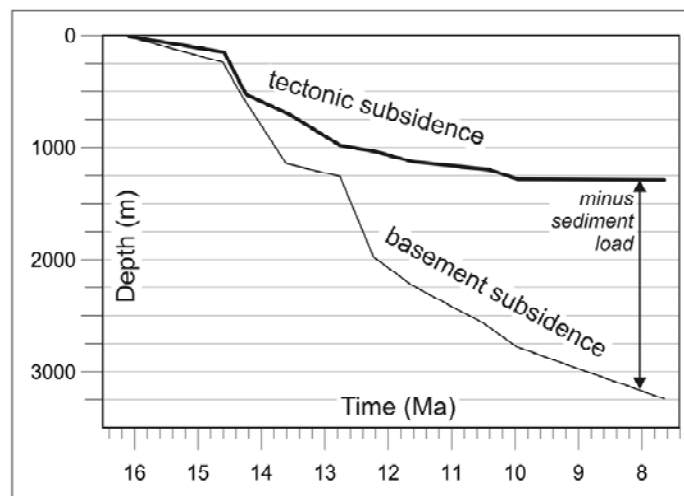


Fig. 2.3: Difference between backstripped tectonic and basement subsidence. Curve is from well *raa72*.

For calculating subsidence, the programme DeCompactionTool (DCT) has been developed (Fig. 2.4; Wagreich, 1991; Hölzel et al., 2008b). This software implements an error quantification on the subsidence analysis, based on Monte Carlo Simulation, such that a range of possible values is assigned to each parameters used. A random function chooses input parameter values within the defined ranges and these are used to calculate the subsidence. From a number of input parameter value combinations, the average subsidence is determined. The programme also incorporates for the first time, the parameter “age”, as the controlling factor for the x-axis. Inputting the correct sedimentary age of backstripped layers is particularly crucial for subsidence rate calculations and thus for identifying discrete phases of subsidence. The approach used reduced errors due to ongoing uncertainties in the Vienna Basin chronostratigraphy (Hohenegger et al., 2008).

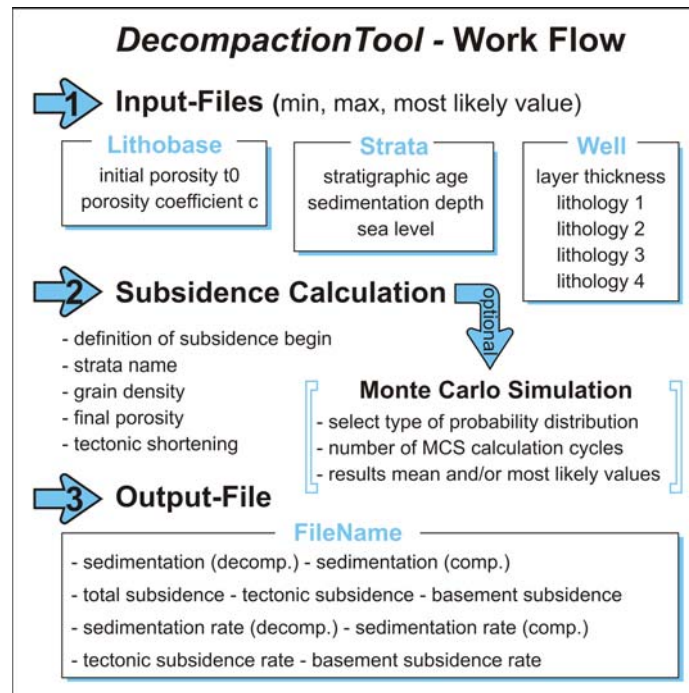


Fig. 2.4: Work flow and input parameters for the software DeCompactionTool (Hölzel et al., 2008b).

## 2.6 Data Base

Input data of wells from the southern and central parts of the Vienna Basin in Austria was provided by OMV-E&P Austria, (Fig. 2.1). The subsidence curves were calculated for the pull-apart evolution of the basin from 16 to 7 Ma, to quantify the main phase of basin evolution within a constant stress field. The basal level used in the calculations was the top of the Aderklaa Conglomerate, which has been dated to 16.1 Ma (Fig. 2.2; Weissenböck, 1996).

The Lower Miocene wedge-top phase of basin development was excluded from the subsidence calculations as it was controlled by a different stress field and different mechanisms of basin formation. Detailed data for that time-period are not available. Furthermore, the angular unconformity between the Karpatian and Badenian also indicates a major break in basin evolution (Hölzel et al., 2008a). Quaternary strata were also excluded, both because of the recent change to a regional uplifting regime (Decker and Peresson, 1996) and because the stratigraphic record is incomplete.

The following parameters were used: 1.) thickness of stratigraphic layers (metres); 2.) age of stratigraphic boundaries (Ma); 3.) lithology, with percentages attributed to different lithologies; 4.) sedimentation (palaeowater) depth (metres); 5.) decompaction parameters (porosity for  $t_0$  = initial % porosity, decompaction coefficient  $c$ , final % porosity) and 6.) physical properties (grain density, crustal density).

Values for some of these parameters were derived from borehole data and related log measurements: Depths to formation tops are necessary to measure the sediment thickness.

Most wells reached the basement below the Neogene basin-fill, so that the stratigraphic record for the Middle to Upper Miocene is complete. Chosen wells mostly lie in undisturbed fault blocks, some distance away from the basin margin. Consequently, the thickness of the sedimentary infill was not significantly influenced by faulting or erosion. Missing stratigraphic data and well-data in areas of interest have been interpolated from mapping of stratigraphic boundaries within seismic data. These sections have been termed synthetic wells (*syn*).

The chronostratigraphic time-scale for the Neogene of Austria has been used (Piller et al., 2004) together with the eco-bio-zonation terms for the Vienna Basin (Rögl, 1998; Strauss et al. 2006; M. Harzhauser, pers.comm.).

Well-log data contains information on the lithological composition of the sediments. For this, Self Potential logs (SP logs), in combination with resistivity logs, were mainly used to differentiation between sand and shale. These data were crosschecked with OMV in-house reports about the composition of well-cuttings. The lithology parameter does not show much variation, because in the investigated, largely basinal offshore area, most sediments are composed of sand (-stone), clay and/or siltstone. Carbonate rocks are of minor importance.

Palaeobathymetric data (sedimentation depth) were taken from the compilation of Wagreich and Schmid (2002), which was based on sedimentological and palaeontological investigations (Kreutzer, 1993; Seifert, 1996). Relative sea-level changes have not been incorporated in the calculations, since the basin was separated from the world ocean after 10.5 Ma (Steininger and Wessely, 1999).

Decompaction parameters were compiled from Steckler and Watts (1978), Royden and Keen (1980), Selater and Christie (1980) Sawyer (1983) and, Bond and Kominz (1984). For the present-day porosity, a value of 10 % has been generally assumed (Flügel and Walitzi, 1968).

## **2.7 Generation of Subsidence Maps**

For an area-wide visualisation of the tectonic subsidence, maps were compiled for distinct stratigraphic boundaries (Fig. 2.8) and stratigraphic zones (Fig. 2.9). For the gridding process, the software Surfer© was used. In Austrian Bundesmeldenetz Coordinates, the defined area ranges from 742,000/302,000 (lower left; UTM M33: 591,650/5 301,089) to 792,000/378,000 (upper right; UTM M33: 640,310/5 377,928). Using the Kriging algorithm, a grid with 200 rows x 100 columns, resulting in an x-spacing of c. 500 m and y-spacing of c. 380 m was generated. Due to the Kriging algorithms and the irregular distribution of data points (boreholes), some isolated spots may occur; however, we used these maps to decipher general trends in the regional distribution of subsidence. Uncertainties due to the extrapolation of isolines to the basin margin were taken into account critically during interpretation and conclusions were drawn only from the central areas of the maps.

## 2.8 Results and Interpretation

Only the Middle to Upper Miocene basin subsidence history has been studied in detail because Lower Miocene basin structures were triggered by different basin-forming mechanisms, such as fault propagation folds that were active in the underlying Alpine units (Hölzel et al., 2008a), and thus represent the fill of one or more separate basins.

Results for the Middle to Upper Miocene basin history are presented grouped (for the position of groups see Fig. 2.5) as basement subsidence in total (BS-Total), tectonic subsidence in total (TS-Total) and as tectonic subsidence rates (TS-Rate; Fig. 2.6 and Fig. 2.7).

Many curves show the highest subsidence rates in the Upper Lagenidae Zone, the duration of which has become shorter since the 1990s, due to ongoing refinements of the Central Paratethys chronostratigraphy and the local Vienna Basin-zones. Although we are aware that the time factor is one of the most influential parameters in basin analysis, the steepness of the curves in this time interval is not thought to be only an effect of its shorter length, because there are many other curves show different subsidence rates (see below). Consequently, we conclude that these results from the Upper Lagenidae Zone are not an artefact of an erroneously defined duration, but represent a robust result.

## 2.9 Regional Trends of Subsidence

To obtain an accurate impression of the regional differences in the subsidence history, the wells have been sorted into several groups (G1 – G13) based partly on their position, from south to north. Their position within the same fault block bordered by major faults or the occurrence in depocentres which reached the same depth was also used in defining the groups. All well-groups, fault names and key structural features are indicated in Fig. 2.5.

### 2.9.1 Groups G1 and G2

The southernmost well is *sol1*. Due to its isolated position, it has been put into a separate group (G1). The three G2 wells lie in the footwall of the Leopoldsdorf Fault. The BS-Total curve for *lax2*, *rie1* and *schwe1* display a continuous decrease through time. Well *moW3* indicates a stepwise subsidence, which, surprisingly, resembles the curve from well *sol1*. For the TS-Rate each curve is different as *schwe1* and *moW3* show peaks for the Upper Lagenidae Zone, Sarmatian and Middle Pannonian. Values from 250 m/Ma – 1000 m/Ma dominate during those phases, in contrast to nearly no subsidence during the remaining time intervals. Wells *lax2* and *rie1* also show the same peaks only in the Upper Lagenidae Zone and Middle Pannonian, but less total subsidence.

### 2.9.2 Group G3

This group (4 wells) comprises data from the hanging wall block of the Leopoldsdorf Fault. The common trend of the BS-Total is high subsidence within the Upper Lagenidae Zone, which also correlates with well *moW3* from G2. This may be attributed to surface growth of the Leopoldsdorf Fault, starting with the highest normal displacement in a more northern position. In the Lower Lagenidae Zone, the wells *syn4*, *him1*, *raul* and *syn3* start with moderate TS-

Rates of 250 m/Ma, which, in the Upper Lagenidae Zone, increases to 500 m/Ma – 1000 m/Ma. For the rest of the Miocene they subside in a very similar way, with values around 100 – 250 m/Ma. With this pattern of homogeneous subsidence in the hanging wall of the Leopoldsdorf Fault, slip variations along the Leopoldsdorf Fault (Hölzel and Wagreich, 2006) were probably mainly dependent on the behaviour of the footwall block.

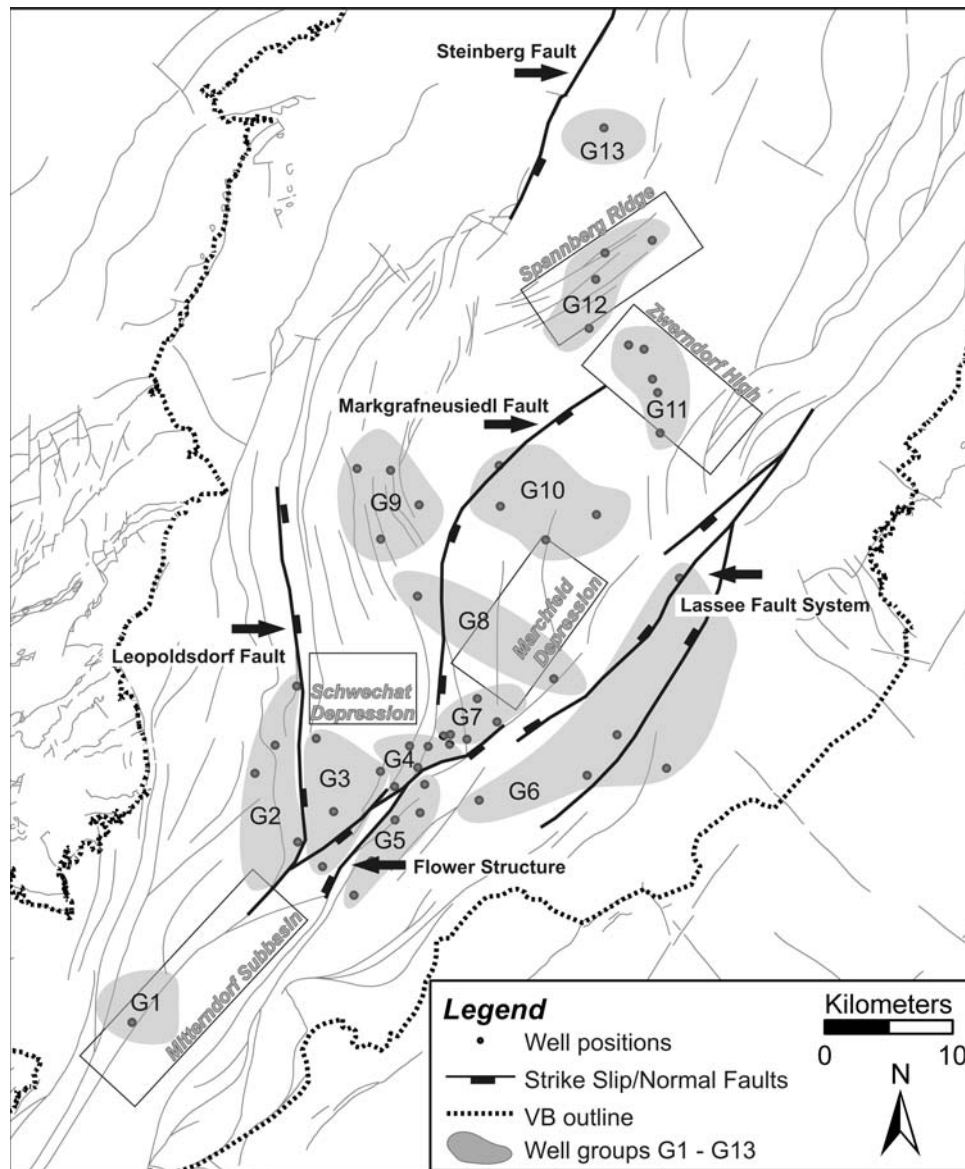


Fig. 2.5: Division of wells into groups according to fault blocks including key structural features of the Vienna Basin such as faults and highs and lows of the top of the pre-Neogene basement (for general position of Vienna Basin and names of wells see Fig. 2.1).

## Quantification of tectonic movement in the Vienna Basin – Subsidence Analysis

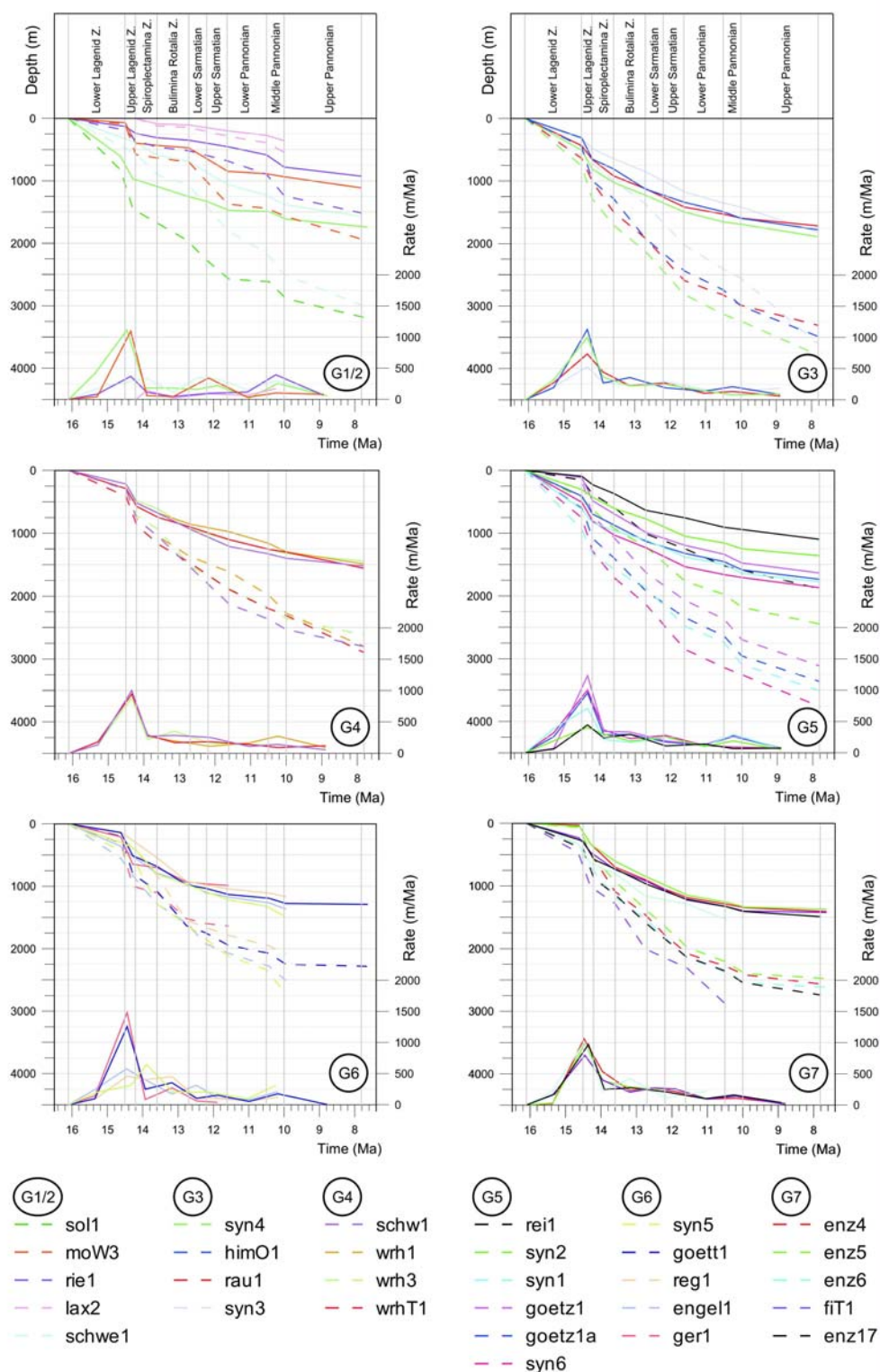


Fig. 2.6: Groups 1-7: Basement subsidence total (BS-Total, dashed lines), tectonic subsidence total (TS-Total, solid lines) and tectonic subsidence rates (TS-Rates, solid lines).

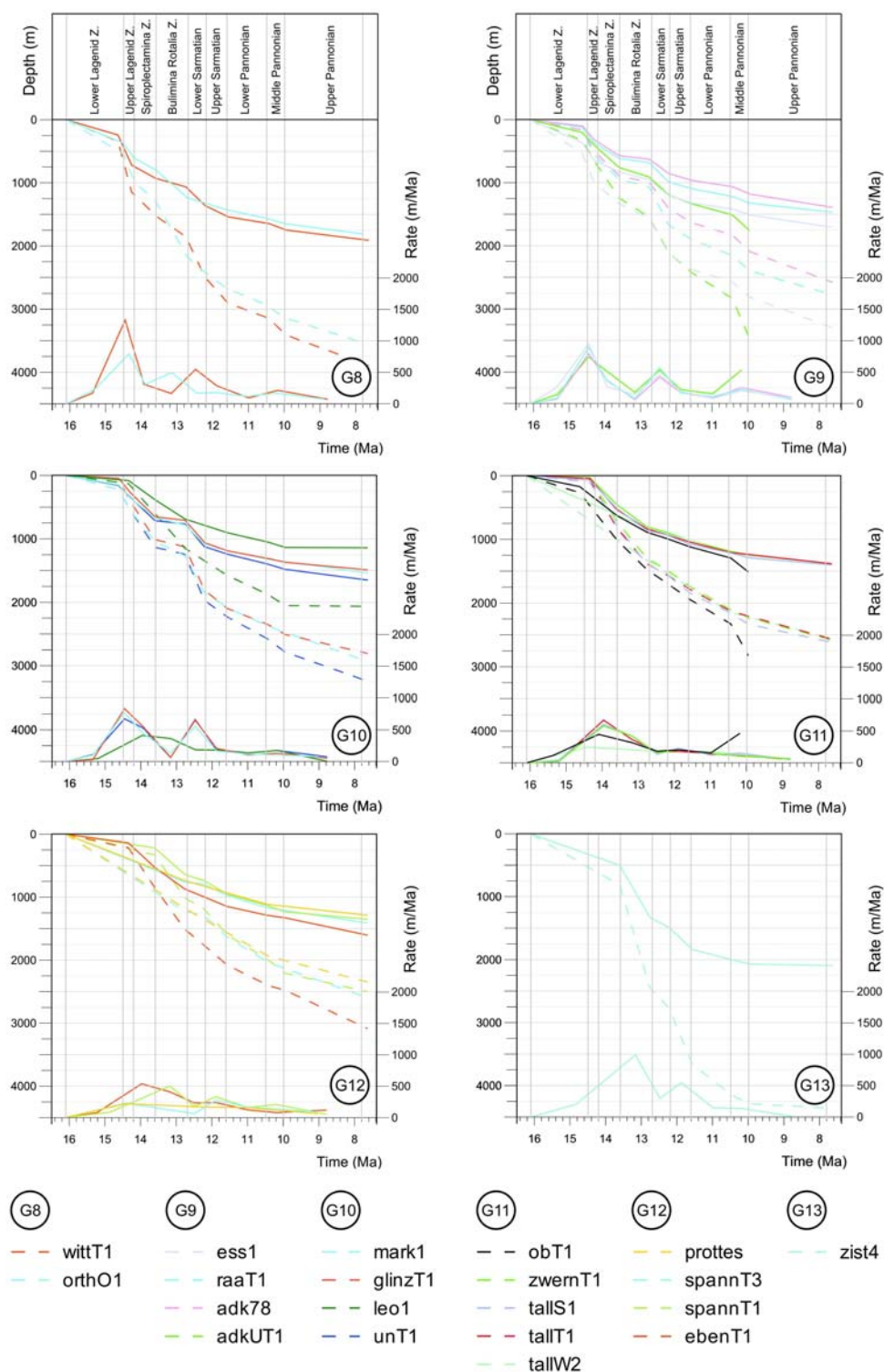


Fig. 2.7: Groups 8-13: Basement subsidence total (BS-Total, dashed lines), tectonic subsidence total (TS-Total, solid lines) and tectonic subsidence rates (TS-Rates, solid lines).

#### 2.9.3 Group G4

These wells are situated in an area where the normal faults of the negative flower structure of the Mitterndorf sub-basin (Hinsch et al., 2005) displace and rotate blocks vertically. As a result, the wells all show essentially the same subsidence history, although they are separated by faults. The subsidence rates are very similar to those of G2, although it accelerated in the Lower Lagenidae Zone, with a moderate TS-Rate of c. 250 m/Ma for the rest of the basin evolution.

#### 2.9.4 Group G5

The wells *syn2* and *rei1* are situated in the highest parts of the eastern footwall of the negative flower structure. This area forms a relay ramp to the north and all other wells of this group lie in a deeper position along the ramp. As a consequence, BS-Total of *syn2* and *rei1* do not display an increase of subsidence in the Upper Lagenidae Zone comparable to that seen in the other wells, *syn1*, *goetz1* and *syn6*. Sarmatian and Middle Pannonian phases are rather subdued or not represented in TS-Rates, indicating that this part of the basin was not affected by significant extension during later stages of basin evolution.

#### 2.9.5 Group G6

The BS-Total curves of *ger1* and *goett1* show the same development at the beginning of the Upper Lagenidae Zone, with parallel segments. The curves then differ because of the higher position of well *ger1* in the footwall of the Lassee Fault, which, therefore, could have been active, with a normal offset, from the Upper Lagenidae Zone onwards. Wells *reg1* and *syn5* are similar, because they lie in the same fault block. TS-Rates display the same pattern as G5, with no, or only very minor Sarmatian and Pannonian phases.

#### 2.9.6 Group G7

Wells of this group are situated in a strongly faulted area, in which fault blocks are bordered by various narrow branches of the negative flower structure. The BS-Total results seem to resemble steady subsidence except during the Lower Lagenidae Zone; the TS-Rates are similar to G5 and G6, with only one significant subsidence phase, in the Badenian.

#### 2.9.7 Group G8

Well *witt1* is situated at the northern flank of the Schwechat Depression and *orth01* lies within the Marchfeld Depression; both depressions display high basement subsidence values for the Vienna Basin, of up to 4000 m. Both wells have parallel BS-Total curves in the Badenian, but antithetic curves for the other time intervals. This has been interpreted as the result of switching depocentres and sediment input; if one depocentre was active, the other one was inactive and vice versa. BS-Total for well *fi1* of G7 is similar to well *orth1*, except during the Pannonian, because the sediment record ends at the top Lower Pannonian. TS-Rates indicate 3 phases of subsidence, with Badenian subsidence being the highest (up to 1500m/Ma) and Middle Pannonian subsidence being the lowest (below 250m/Ma).

#### 2.9.8 Group G9

The BS-Total trends of wells *ess1*, *raa1* and *adk78* and *adkUT1* are very similar, typical for the area between the Markgrafneusiedl Fault and the Leopoldsdorf Fault, in the central part

of the Vienna Basin, southwest of the Spannberg Ridge. TS-Rates again display a threefold pattern, similar to G8, but with lower rates in the Badenian.

#### 2.9.9 Group G10

This group largely resembles G9 for the BS-Total values. The trends of *mark1*, *glinz1* and *unT1* are the same. Well *leo1*, which shows a unique trend in having a broadly distributed Late Badenian subsidence that has been attributed to fault interference west of the Markgrafneusiedl Fault. The TS-Rates do not exceed 450 m/Ma, but the development from the Upper Sarmatian onwards coincides with the other wells of G9 and G10. Well *leo1* again shows a considerable difference to all other wells in the central part of the basin.

The areas covered by G8 – G10 subsided together in a largely similar way. This indicates that the Markgrafneusiedl Fault is a very young feature, with post sedimentary activity from the Upper Pannonian onwards.

#### 2.9.10 Groups G11 and G12

In the sedimentary columns of G11 and G12, the Lower Lagenidae Zone is missing and, consequently, subsidence curves start later. The Badenian transgression was not able to reach this area of the former coast line, at the flanks of the Spannberg Ridge and the Zwerndorf High (e.g. Weissenböck, 1996). Thus sedimentation started significantly later and a depocentre for the transgressing sediments had not been established. The basement structure of the Spannberg Ridge was uplifted during the Upper Karpatian (Hölzel et al., 2008a). Consequently, TS-Rates display a delay in subsidence in relation to data from surrounding, lower-lying areas with respect to the Spannberg Ridge, like well *ebenT1*.

#### 2.9.11 Group G13

Well *zist4* was drilled into the hanging wall of the Steinberg Fault. For the lower parts of the well, the TS-Rate shows maxima within the Spiroplectamina Zone (1000 m/Ma) and in the Sarmatian (250 – 500 m/Ma). These values contradict former assumptions that the strongest activity on this major basin forming fault was during the Lower Badenian, but it coincides with the varying thicknesses of growth strata through time observed on seismic sections. The two pronounced subsidence phases resemble curves from G10.

### 2.10 Subsidence Maps

Figures 8 and 9 show total tectonic subsidence for the central and southern part of the Vienna Basin, plotted as relative depth maps for distinct tops of stratigraphic units and interval subsidence between these stratigraphic boundaries, respectively. The time intervals range from 1.1 – 1.7 Ma, except for the Upper Lagenidae Zone, which is considerably shorter, most probably representing only 300,000 years (Fig. 2.2).

The top Lower Lagenidae Zone subsidence pattern shows the characteristic segmentation into narrow depocentres (Fig. 2.8a) due to the formation of strike-slip duplexes. In the southern part, the hanging wall of the Leopoldsdorf Fault subsided considerably in relation to the footwall, indicating the synsedimentary movement of this fault during the Lower Lagenidae Zone. In the

central part, uplifted basement blocks, such as the Spannberg Ridge, are displayed by zero values. The strong subsidence segmentation suggests major fault activity during the Lower Lagenidae Zone. The interval subsidence maps show that in the following depocentres merged (Fig. 2.9a). During the early Badenian (Fig. 9b), the Zwerndorf High developed, with only 200 m total tectonic subsidence, in contrast to the more southern regions, which subsided by up to 600 m during the same time-interval.

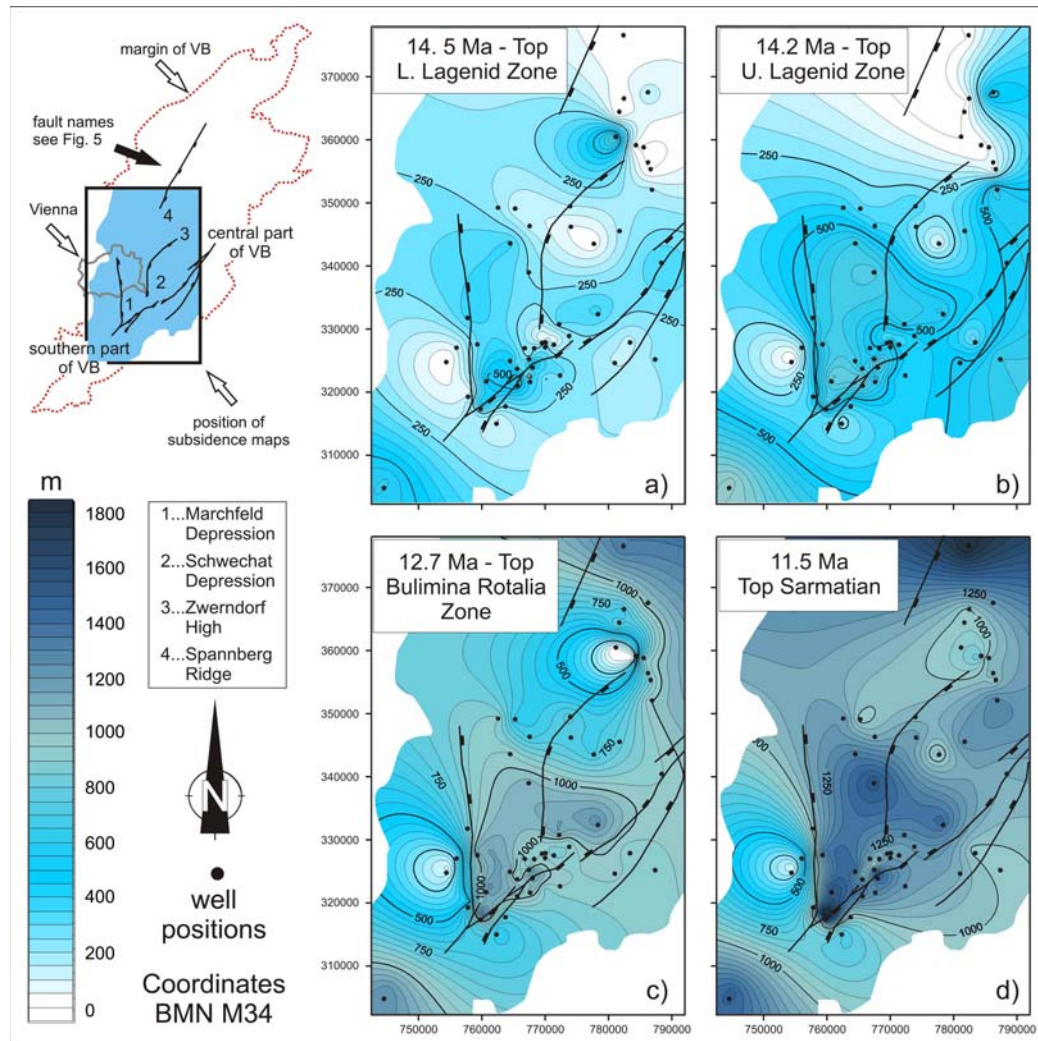


Fig. 2.8: Tectonic subsidence maps of the central and southern Vienna Basin displayed as cumulative subsidence at 4 stratigraphic boundaries. Extrapolated isolines to the basin margin must not be interpreted, because they represent artificial borders.

At the Badenian/Sarmatian boundary, the delay in subsidence from the central to the northern part is visible (Fig. 2.8c). From the late Badenian to the top Sarmatian (Fig. 2.9c), this trend reversed, with pronounced subsidence in the Zwerndorf area (600 m) and lower subsidence values within the Marchfeld Depression (only up to 400 m). In the southern part of the basin, the fault blocks of the negative flower structure subsided c. 600 m. The top Sarmatian (Fig. 2.8d) indicates that the overall tectonic subsidence was higher in the southern part (1500 m)

than in the central part (1000 m). The Sarmatian to Middle Pannonian pattern (Fig. 2.9d) shows ongoing uniform subsidence with moderate values affecting the deeper parts of the Vienna Basin, whereas the marginal areas remain nearly stable.

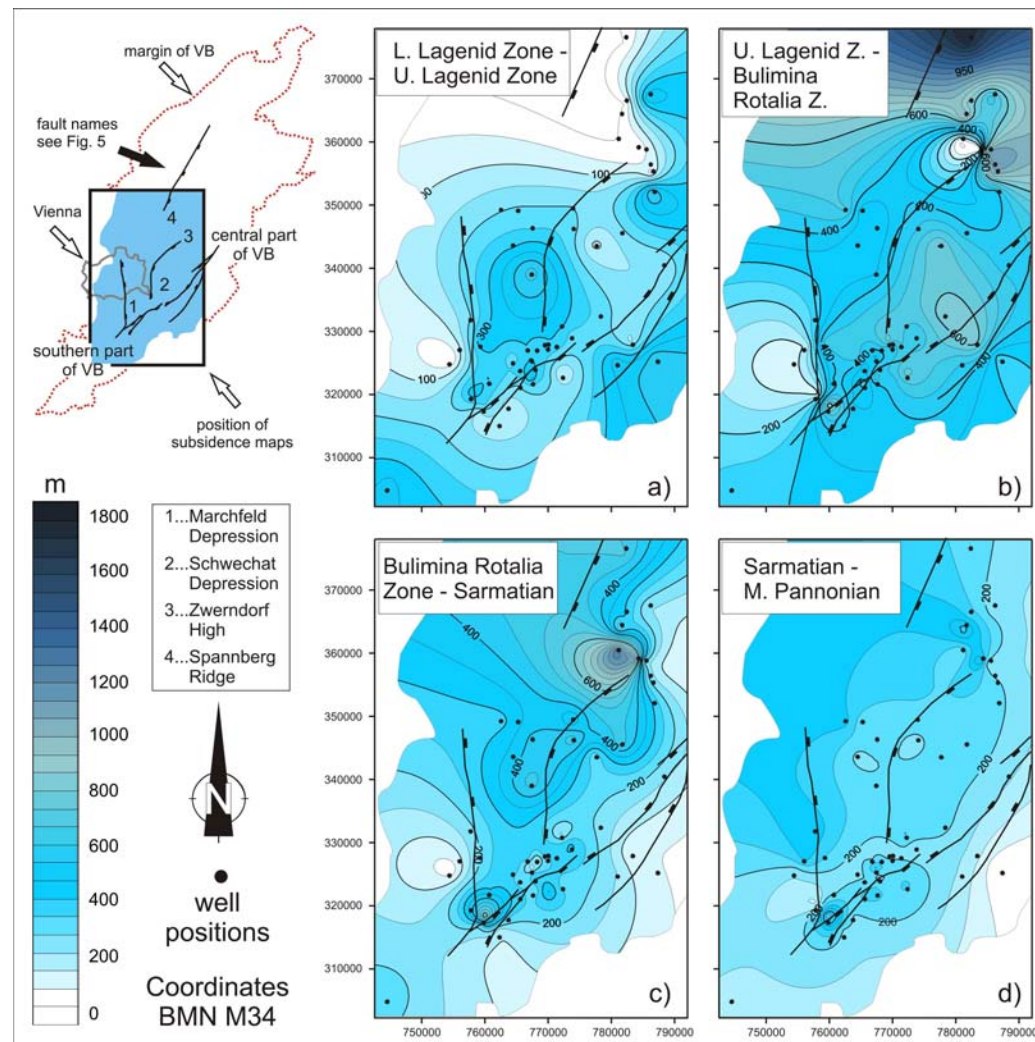


Fig. 2.9: Maps of tectonic subsidence of 4 stratigraphic intervals.

## 2.11 General Subsidence Trends

In general, the subsidence curves of the Vienna Basin display a typical pattern for strike-slip basins, with very high subsidence rates (up to  $> 1000$  m/Ma), but in only short phases, and a general “concave-up” shape (Allen and Allen, 2005).

The calculated TS rates are significant for interpreting the subsidence patterns and the tectonic driving forces of basin formation. To discriminate phases of increased subsidence, the TS-Rate curves were divided into 3 types based on their shapes (Fig. 2.10). There is one (*type A*) with high rates in the Badenian decaying continuously through the rest of the Miocene. The second type (*type B*) includes the Badenian signal but has an additional subsidence peak within the

Sarmatian. *Type C* has 3 peaks, with the Badenian and Sarmatian peaks followed by a weaker signal in the Middle Pannonian.

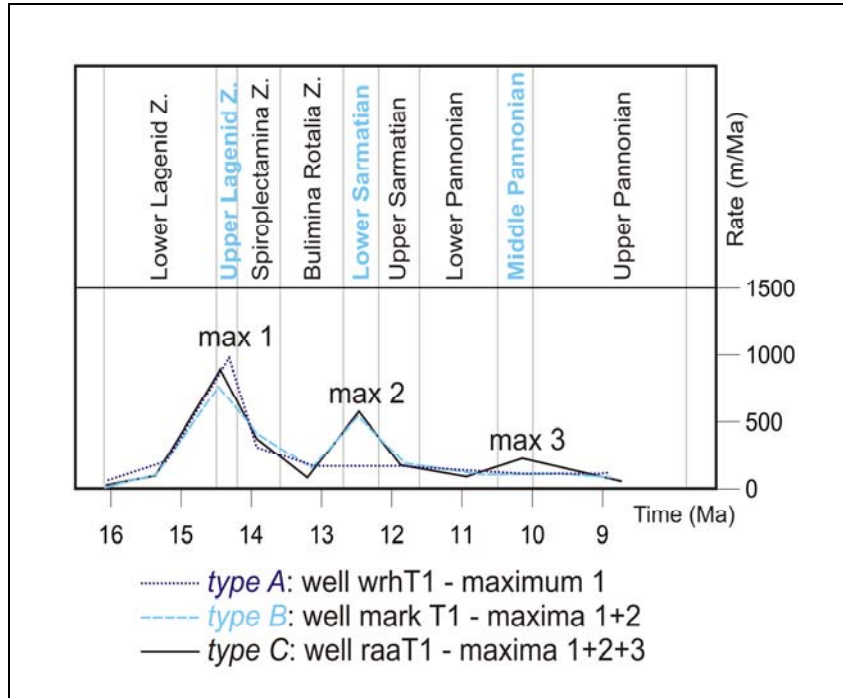


Fig. 2.10: Three different curve shapes of tectonic subsidence rates as base for the classification of subsidence phases.

*Type A*, with a major early Badenian subsidence event followed by decreasing subsidence, has been documented in previous investigations and conforms to the general pull-apart stretching model assumed for the Vienna Basin (Sclater et al., 1980; Lankreijer et al., 1995 and Baldi et al., 2001). Based on 2 boreholes, Baldi et al. (2001) calculated about 500 m of rapid subsidence in the Pannonian Basin during this time interval. In the early Badenian, uniform subsidence started and affected nearly the whole Carpatho-Pannonian area (Sclater et al., 1980). However, our results differ from others (e.g. Wagreich and Schmid, 2002) as the Karpatian was not included in the calculations, as different mechanisms for the Lower Miocene basin formation have been inferred. Large areas, which today lie outside the Vienna Basin, lay within the former Lower Miocene wedge-top zone. Subsidence occurred locally and was mainly governed by the synsedimentary thrusting of the underlying Alpine units. This basin phase essentially ended in the Middle Miocene, with the initiation of the pull-apart Vienna Basin. Therefore, the subsidence values presented here only include (Lower) Badenian data and strongly suggest a solely Badenian “rifting” event of strike-slip basin formation. The Sarmatian signal, which reaches to around half that of the Badenian subsidence rate, is comparable to a minor Sarmatian phase in the Styrian Basin (Sachsenhofer et al., 1997) with an estimated stretching factor of  $< 1.05$ . Minor extension is also implied by our data, as Sarmatian tectonic subsidence rates are always lower than Badenian subsidence rate maxima. This Sarmatian phase seems to reflect a

common development for the basins at the eastern margin of the Eastern Alps and might be a product of regional extensional tectonics related to a late phase of lateral extrusion.

The Pannonian subsidence phase shows maximum values of about half that of the Sarmatian subsidence. This can be correlated to the major basin-forming subsidence phase of the nearby Pannonian Basin, because of their co-eval occurrence and the position of the Vienna Basin, at the periphery of the Pannonian Basin System. This significant Pannonian subsidence was not recorded by previous workers, who proposed only subdued subsidence or subsidence termination in the Pannonian (e.g. Sclater et al., 1980; Royden, 1985).

Sclater et al. (1980) presumed a uniform stretching of a factor 2 with subsequent lithospheric cooling, which explains their rapid first subsidence phase (Badenian) and the slower linear second phase from the Sarmatian onward, ending during the Pannonian. However, their investigations were based on only one borehole from the centre of the Vienna Basin. Royden (1985) also indicated only one major extensional pull-apart phase, without a significant Pannonian subsidence pulse. Lankreijer et al. (1995) indicated more than one subsidence phase; in the Karpatian-Badenian, in the late Badenian to early Sarmatian and in Pontian to Pliocene times. This threefold subsidence path largely corresponds to our refined results, although the timing differs due recent improvements in the basin chronostratigraphy. However, this Pontian to Pliocene subsidence cannot be compared to the Middle Pannonian phase documented here, as Lankreijer et al. (1995) relied strongly on younger, Plio-Pleistocene subsidence, as recorded in the Mitterndorf subbasin, which is clearly separated in time from our Middle Pannonian pulse.

The subsidence modelling of Lankreijer et al. (1995) indicated that the Vienna Basin shows a trend from thin-skinned extension in the north-eastern part to whole lithospheric extension in the central-southern part. Stretching values between 1.04 and 1.30 for the crustal extension and between 1 in the northern part and 1.60 in the southern part for lithospheric extension were proposed. This modelling did not account for separate phases of subsidence, but relied on strong initial Karpatian and Badenian subsidence, followed by minor thermal subsidence. Such a model only accounts for our *type A*, with curves showing only one subsidence phase, followed by rapidly decaying values.

## **2.12 Conclusions**

The Vienna Basin is located at the transition between the Eastern Alps, the Carpathians and the Pannonian Basin System. In this special position, the basin underwent more than one phase of subsidence during the Miocene pull-apart tectonics. The general trends imply that the major phase of formation started in the Badenian (Upper Lagenidae Zone - Bulimina Rotalia Zone; Middle Miocene). Some of the backstripped wells show a decrease of subsidence throughout the Miocene, but, due to the intense internal segmentation of the basin, other wells display significant subsidence phases in the Sarmatian and Middle Pannonian also. These phases are comparable to events in the Styrian and Pannonian basins. As a result of chronostratigraphic refinements and the high density of boreholes, this study has shown that the interpretation of the overall subsidence pattern is not as simple as previously thought. Regionally or locally, the effects of at least three successive phases of extension, related to the late stage of Alpine-Carpathian orogeny and the ongoing lateral extrusion and Pannonian Basin formation, have been found in the Vienna Basin. This indicates that these tectonically related areas were influenced by each other during basin evolution and indicate that more than one extensional basin phase occurred during the Middle to Upper Miocene.



### **3 Error Quantification for Subsidence Analysis**

---

This chapter is based on:

Hölzel, M., Faber, R., Wagreich, M. (2008). DeCompactionTool: Software for subsidence analysis including statistical error quantification. *Computers and Geosciences*, 34, 1454-1460.



### **3.1 Abstract**

Subsidence analysis based on decompaction of the sedimentary record is a standard method for reconstructing the evolution of sedimentary basins. For such an analysis, data on strata thickness, lithology, age constraints, lithological properties, porosity, palaeobathymetry, sea-level changes and heat flux, amongst others, are required. The uncertainties associated with this wide range of input parameters have a major effect on the shape of the resulting subsidence curve, particularly because errors at successive points are not independent. The programme DeCompactionTool (DCT) combines 1D-subsidence calculations, including backstripping, with error quantification, based on the principles of Monte Carlo Simulation (MCS). In this, the range of possible input values (minimum, maximum, most likely number) is assigned to each of the parameters used. The parameter age has been implemented for the first time. A random number generator chooses values within the defined intervals and calculates results for every combination. The probability that a number is selected by the generator may follow a uniform distribution, a power distribution, a symmetric normal distribution or an asymmetric normal distribution. The results are mean values with two extreme values quantifying the error range. To demonstrate the programme's capabilities, an example of subsidence calculation based on well-data from the Vienna Basin is presented.

### 3.2 Introduction

Sedimentary basins are regions of prolonged subsidence of the Earth's surface. Subsidence analysis of wells or sections based on decompaction of the sediment column (Van Hinte, 1978; Steckler and Watts, 1978; Sclater and Christie, 1980; Bond and Kominz, 1984) is a standard method for investigating sedimentary basins (Leeder, 1999; Miall, 1999; Einsele, 2000; Allen and Allen, 2005). The restored sediment thicknesses allow the construction of plots showing the sediment accumulation rate versus time and basement subsidence, both of which provide information about the tectonic and sedimentary evolution of a basin. Subsidence calculations can also provide basic data for further calculations, e.g. calculating the vertical displacement of faults (ten Veen and Kleinspehn, 2000; Wagreich and Schmid, 2002).

The uncertainties associated with the various input parameters can have a major effect on the shape of the subsidence curves and thus on the interpretation of basin formation and evolution. Although potential error ranges of single parameters can be measured or estimated individually, quantitative approaches to error estimation have rarely been undertaken and, even when made, have normally concentrated on specific dependent parameters (e.g. stratigraphic age and thickness, porosity and compaction: Gallagher, 1989).

In most cases, the software used for basin analysis does not include error quantification for subsidence (e.g. Basinworks<sup>1</sup>, BasinMod<sup>2</sup>, Sedpak<sup>3</sup>, 2DMove<sup>4</sup>, PetroMod<sup>5</sup>) and because the error calculations have to be done during the subsidence calculation process, a separate statistical software package cannot be used in tandem with a subsidence calculation programme.

Waltham et al. (2000) described an iterative error estimation programme based on a Monte Carlo Simulation (MCS) using 5 input parameters. This showed that error calculations at successive points on a subsidence curve are not independent. Since that programme has been lost (pers. comm. Waltham 2005), we have developed an extension of the method, integrating 10 parameters, which includes the parameter age for the first time, for iterative calculations based on different probability functions. The programme runs on Windows XP/NT and is a C++ version (Faber and Wagreich, 2002) of a former DOS-based subsidence software (Wagreich, 1991), to which we have added MCS. Templates of input files and a limited version of the programme can be downloaded from the homepage of the corresponding author<sup>6</sup>.

### 3.3 Subsidence calculations

The quantitative analysis of subsidence rates through time (geohistory analysis, subsidence analysis) relies primarily on palaeowaterdepth reconstructions and the stepwise decompaction of

---

<sup>1</sup> Basinworks. <http://www.petrodynamics.com/>

<sup>2</sup> BasinMod: <http://www.platte.com/>

<sup>3</sup> Sedpak. <http://sedpak.geol.sc.edu/>

<sup>4</sup> 2DMove. <http://www.mve.com/Home/Software/2DMove>

<sup>5</sup> IES PetroMod. <http://www.iesgmbh.eu/index.php>

<sup>6</sup> Homepage M. Hölzel. <http://homepage.univie.ac.at/monika.hoelzel/DCT.htm>

stratigraphic units to correct their thickness at the time of interest (Van Hinte, 1978; Bond and Kominz, 1984). This is based on the reduction of porosity with depth. Normally pressured sediments exhibit an exponential porosity-depth relationship, where  $\phi$  is the porosity at any given depth  $y$ ,  $\phi_0$  is the initial porosity and  $c$  is a lithology-dependent coefficient that describes the rate at which the exponential decrease in porosity takes place with depth (Steckler and Watts, 1978; Sclater and Christie, 1980):

$$\phi = \phi_0 e^{-cy} \quad (1)$$

The total subsidence is partitioned into two parts; one caused by the tectonic driving force and another related to the sediment load. The backstripping procedure removes the effect of sediment loading and compaction from the basement subsidence, allowing quantification of tectonic basin subsidence.

In the programme, the following parameters are incorporated: (1) thickness of stratigraphic layers, (2) age, (3) lithology, (4) sedimentation (palaeowater) depth, (5) decompaction parameters (initial porosity  $\phi_0$ , which is the porosity at the beginning; the decompaction coefficient  $c$  and the final porosity), (6) physical properties (final grain density, mantle density) and (7) the rate of tectonic shortening.

### 3.4 Programme description and work flow

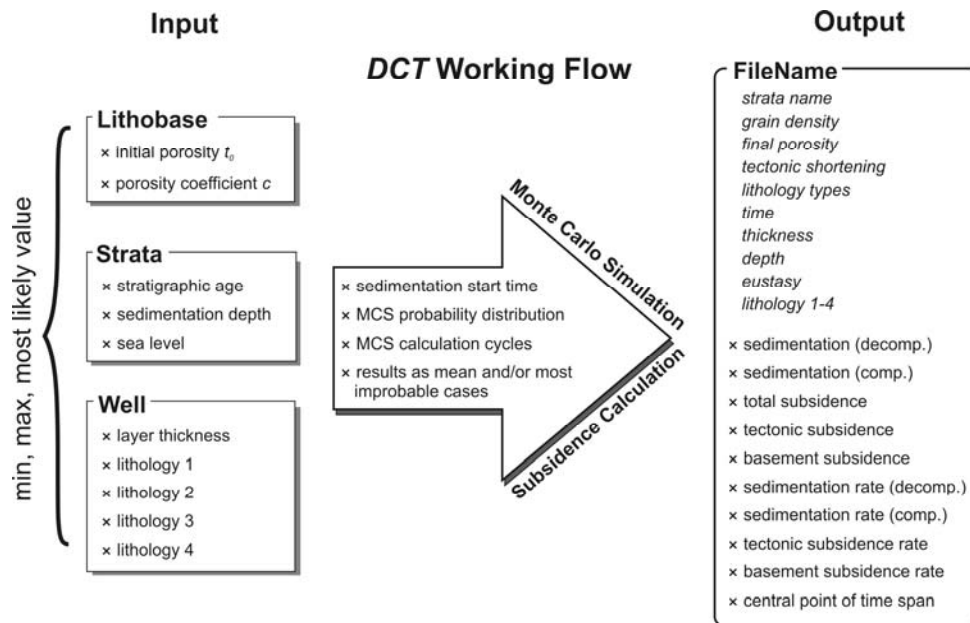


Fig. 3.1: Working flow model of DCT showing the 3 modules (*Input*) with all parameters; *Arrow*: Most important parameters which must be given in the programme directly when starting a calculation with or without MCS; *Output*: Text file with all feasible results as text data (*italics* mark the input parameters that are repeatedly listed for the reconstruction of a calculation in the output file).

The programme works with 3 modules for data input (programme structure Fig. 3.1):

- (1) *Lithobase*: This comprises lithology dependent values, including parameters for the decompaction exponential function, such as the initial porosity  $\phi_0$  and the porosity reduction coefficient  $c$ .
- (2) *Strata*: These are the general properties of the stratigraphic units, which are independent of the actual well (outcrop) location, such as sedimentation depth, age, sea level, name of a stratigraphic unit.
- (3) *Well*: This includes variable point data (well data, outcrop data), such as local thickness of strata and lithological composition, which consists of a percentage ratio of up to four lithologies, selected by the user.

ID-numbers connect properties of stratigraphic units and of lithologies between the three input modules (Fig. 3.1). Although the *Lithobase* and *Strata* datasets can remain the same during a suite of calculations (e.g. in the same area), the *Well*-files are different for every well.

To run the programme, the three input files (tab delimited data) have to be loaded. The following calculation steps include these parameters: sedimentation start time, tectonic shortening, final grain density, mantle density, final porosity, type of probability distribution, number of calculation steps for the MCS and for the text data export the floating point accuracy.

The MCS can be used with up to 10 input parameters and the user can choose the number of runs. When using 10 parameters, at least 10,000 iterations are recommended.

### 3.5 Method of error calculation

The sensitivity analysis of DCT is based on the principles of Monte Carlo Simulation (Metropolis and Ulam, 1949). In general, this means that the results are derived iteratively from calculations of randomly chosen values within defined intervals for the up to 10 input parameters. An interval for a parameter has a minimum, maximum and/or a most likely value. In the majority of cases, the most likely value would be a measured number, whereas minimal and maximal values would be mostly estimates.

The probability of a number being chosen (Fig. 3.2) can follow one of four continuous probability distributions: uniform probability distribution, asymmetric power distribution, symmetric normal distribution or asymmetric normal distribution. These distributions are characterised by a location parameter and a scale parameter, which are directly taken or calculated from the input values. Furthermore, the probability interval of both of the normal functions can be truncated in any order (see Fig. 3.2). A random number generator selects values within these intervals and calculates results for every combination. Therefore, the *pseudo-random number generator* of the computer is used to create sequences of values with constant probability within a given interval. The random number generator is initialised at the programme start, so that the possibility that several runs use exactly the same patterns is excluded. This is because between the programme start and calculation several user inputs are

required, which will take a certain, but not exactly predictable time. To adjust the value distribution to more common patterns, the user can choose from the functions listed in Fig. 3.1.

After  $n$  iterations, the results are expressed by the mean values and by the two extreme values. These are point-wise selections of the extreme values over all the results at a given time.

### 3.5.1 Uniform probability distribution

Within this probability distribution, all values between the minimum and the maximum values have the same probability to be chosen.

### 3.5.2 Asymmetric power distribution

A power distribution is mainly defined by  $p$  (*power parameter*;  $p > 0$ ), which is the shape-controlling coefficient of the function (for details, see Evans et al., 2000). The asymmetric power consists of two functions with a different stretching factor following two functions:

$$\text{left part} \quad f(x) = \left( \frac{x + \min}{\min} \right)^p \quad (2),$$

$$\text{right part} \quad f(x) = \left( \frac{\max - (x + \min)}{\max} \right)^p \quad (3),$$

where the borders of the functions are given by minimum ( $\min$ ) and maximum ( $\max$ ) parameters of the input interval, where the probability is zero. The position of the extremum the curve (highest probability) is derived from the most likely value ( $x$ ).

### 3.5.3 Symmetric normal distribution

The general formula for the probability density function of the normal distribution is:

$$f(x) = \frac{e^{-(x-\mu)^2/(2\sigma^2)}}{\sigma\sqrt{2\pi}} \quad (4),$$

where  $\sigma$  is the standard deviation and  $\mu$  the mean. The parameter  $\sigma$  is derived from minimum and maximum values. The user can specify the probability at  $x_{(\min)}$  and  $x_{(\max)}$ , which means that the curve can be truncated optionally (the default probability  $x_{(\min)}$  and  $x_{(\max)}$  is 0.001). In other words, values outside the  $x_{(\min)} - x_{(\max)}$  interval are ignored. For example, if 95 % of all chosen values should be within the  $x_{(\min)} - x_{(\max)}$  interval, the default probability at  $x_{(\min)}$  and  $x_{(\max)}$  is 0.025. The random number is then selected in relation to the generated curve. When a chosen value lies outside of the selected interval, it will be neglected and another random step for this parameter starts.

### 3.5.4 Asymmetric normal distribution

The shape of the asymmetric normal distribution follows the minimum, maximum and the most likely value. The probability curve itself is formed by two different normal distributions. The first one covers the interval from the minimum to the most likely value and the second one from there to the maximum value. The borders of the curve can be set by the user, so the probability function is truncated and does not go to infinity.

In the case of a truncated normal distribution, the area under the graph is 1 minus the two equal areas  $([-\infty, x_{(min)}])$  and  $[x_{(max)}, +\infty])$  outside the interval. If the area under right interval is not equal to the area of the left interval, the probability at the most likely value is not the same for both curves, which would lead to a discontinuity in the resulting shape of the curve. To avoid this discontinuity a scaling factor ( $sf$ ) is used and therefore the left and right curves do not enclose the same area. To find the scaling factor ( $sf$ ) for each curve, the following equation is applied, where  $y$  is the probability at  $x_{(min)}$  or  $x_{(max)}$  shifted so that the most likely value is at  $x = 0$ .

$$sf = \frac{\log(y)}{-x^2} \quad (5).$$

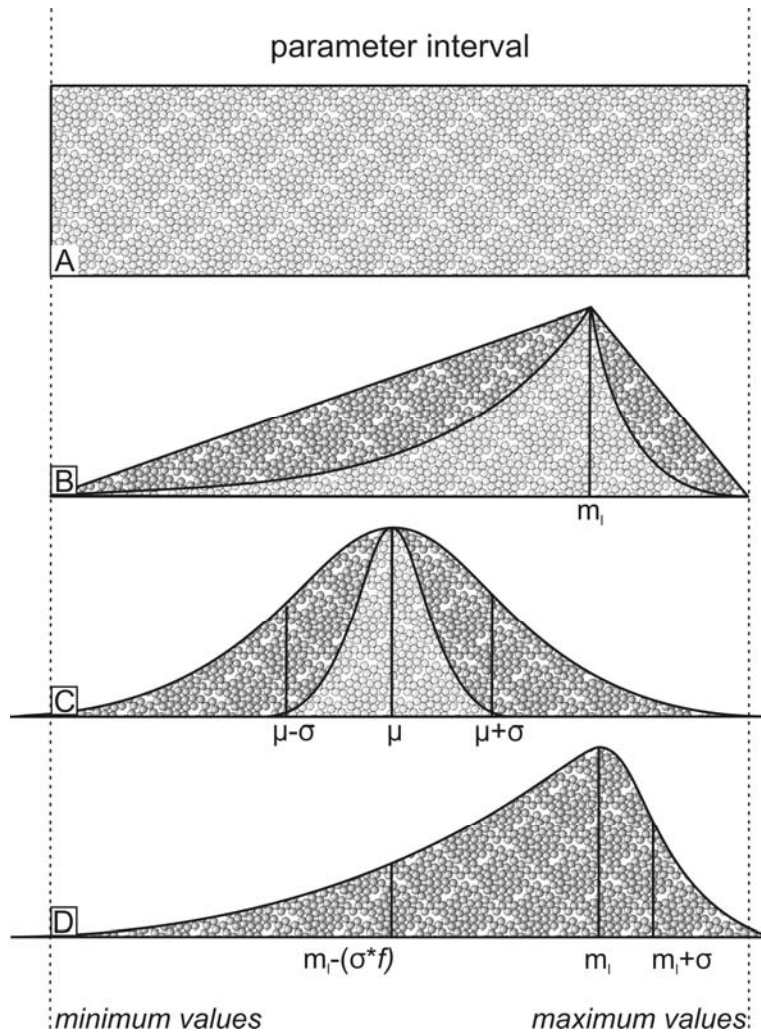


Fig. 3.2: Sketch of probability functions for numbers to be randomised: A) uniform probability distribution; B) asymmetric power distribution defined by  $p$  = most likely value; dark filling  $p = 1$ , light filling  $p = 2$ ; C) symmetric normal distribution defined by *mean*  $\mu$  = most likely value and truncated  $x_{(min)}$  and  $x_{(max)}$ ; D) asymmetric normal distribution defined by *mean*  $\mu$  = most likely value, scaling factor  $sf$ , truncated at  $x_{(min)}$  and  $x_{(max)}$ .

### 3.6 Error sources

Normally, *layer thickness* is derived from well data or outcrops (e.g. stratigraphic sections). Uncertainty derives from the unknown amount of erosion or from an erroneous stratigraphic classification. This leads to insecurity in *age*, which is based on either biostratigraphy, or chronostratigraphic correlations or geochronology.

*Sedimentation depth* (uncertainties in palaeobathymetry: e.g. Bertram and Milton, 1989) often has a wide error interval, especially in deep-water settings. However, if sedimentation (= palaeowater) depth is the most significant uncertainty then the nonlinear decompaction curve is not affected (Waltham et al., 2000).

*Sea-level* or eustatic corrections are mostly assigned to curves of eustatic changes, but regional sea-level histories often differ considerably from global curves. Thus, whether or not eustatic corrections are necessary has to be considered from case to case.

Quantification of *lithological parameters* (e.g. lithology, porosity) is often derived from geochemical and sedimentological analyses or from geophysical well logs. Thus, these factors are dependent on the quality of the analysis or measurements.

Decompaction of each strata interval utilises porosity versus depth curves (*initial porosity*  $\phi_0$ ; decompaction *coefficient*  $c$ ) for each lithology based on empirical subsurface porosity data from regional (Sclater and Christie, 1980) or global data sets (Magara, 1980; Bond and Kominz, 1984; Baldwin and Butler, 1985). From these spectra of curves, estimates for the best fitting curve should be determined.

### 3.7 Application

For testing, published data from Wagreeich and Schmid (2002) have been used (Fig. 3.3). In their paper, basement subsidence curves for the central Vienna Basin (Austria) were calculated in order to estimate the rate of vertical fault movement. This was used to reconstruct the complex Miocene history of this pull-apart basin, from 17 – 7 Ma. Data from well *raaT2* (courtesy of OMV AG) includes strata thickness and lithological information derived from SP (Self Potential) and resistivity logs. The lithologies comprise sandstone, shale and siltstone, with carbonate rocks being virtually absent. Age constraints are based on the new stratigraphic table of the Neogene of Austria (Piller et al., 2004). Relative sea-level changes have not been incorporated, since the basin was separated from the world ocean after 10.5 Ma (Steininger et al., 1999). Palaeobathymetric data (sedimentation depths) were based on sedimentological and palaeontological investigations (Kreutzer, 1993; Seifert, 1996).

**Input - Module 1: Lithobase**

Litho ID <sup>a</sup>	Lithology	$\phi$	$\phi_{min}$	$\phi_{max}$	c	c min	c max
0	Sand	0.49	0.40	0.49	0.00027	0.00027	0.000567
1	Quartz Sandstone	0.62	0.62	0.62	0.00036	0.00036	0.00036
2	Shaly Sandstone	0.56	0.56	0.56	0.00039	0.00039	0.00039
3	Shale	0.63	0.50	0.70	0.00051	0.00040	0.00051
4	Chalk	0.68	0.68	0.70	0.00047	0.00047	0.00071
5	Carbonate/Dolomite	0.24	0.24	0.24	0.00016	0.00016	0.00016
6	Carbonate/Calcite	0.24	0.24	0.24	0.00054	0.00054	0.00054

**Input - Module 2: Strata**

ID <sup>b</sup>	Strata Name	Top Age	Top Age min	Top Age max	Sedimentation depth	Sedimentation depth min	Sedimentation depth max	Sea level	Sea level min	Sea level max
4	Aderklaa Formation	16.3	16.3	16.4	0	0	0	0	0	0
5	Aderklaa Conglomerate	16.1	16.1	16.1	150	100	200	0	0	0
6	Lower Lagenidae Zone	14.5	14.5	15.1	150	100	200	0	0	0
7	Upper Lagenidae Zone	14.2	14.2	14.9	200	50	200	0	0	0
8	Spiroplectamina Zone	13.6	13.6	13.6	200	150	250	0	0	0
9	Bulimina Rot. Zone	12.7	12.7	13.0	100	50	150	0	0	0
10	Lower Sarmatian	12.2	12.2	12.3	100	50	150	0	0	0
11	Upper Sarmatian	11.6	11.5	11.6	100	50	150	0	0	0
12	Lower Pannonian	10.5	10.2	10.5	100	50	150	0	0	0
13	Middle Pannonian	10.0	9.8	10.0	100	50	150	0	0	0
14	Upper Pannonian	7.8	7.1	7.8	0	0	0	0	0	0

**Input - Module 3: Well**

ID <sup>b</sup>	Thickness	Thickness min	Thickness max	Litho1 ID <sup>c</sup>	Litho1	Litho1 min	Litho1 max	Litho2 ID <sup>d</sup>	Litho2	Litho2 min	Litho2 max	Litho3 ID	Litho3	Litho3 min	Litho3 max	Litho4 ID	Litho4	Litho4 min	Litho4 max
4	474	400	500	0	0.1519	0.1500	0.1750	3	0.3481	0.3250	0.3500	0	0	0	0	0	0	0	0
5	220	200	240	0	0.5000	0.5000	0.5000	3	0.0000	0.0000	0.0000	0	0	0	0	0	0	0	0
6	75	55	95	0	0.0400	0.0000	0.0400	3	0.4600	0.4600	0.5000	0	0	0	0	0	0	0	0
7	215	200	250	0	0.1512	0.1500	0.1512	3	0.3488	0.3488	0.3500	0	0	0	0	0	0	0	0
8	236	216	256	0	0.0000	0.0000	0.0000	3	0.5000	0.5000	0.5000	0	0	0	0	0	0	0	0
9	84	64	104	0	0.0357	0.0357	0.0357	3	0.4643	0.4643	0.4643	0	0	0	0	0	0	0	0
10	465	400	485	0	0.1505	0.1505	0.1505	3	0.3495	0.3495	0.3495	0	0	0	0	0	0	0	0
11	200	180	220	0	0.2450	0.2450	0.2450	3	0.2550	0.2550	0.2550	0	0	0	0	0	0	0	0
12	204	184	230	0	0.1275	0.1275	0.1275	3	0.3725	0.3725	0.3725	0	0	0	0	0	0	0	0
13	219	200	239	0	0.2009	0.2009	0.2009	3	0.2991	0.2991	0.2991	0	0	0	0	0	0	0	0
14	364	344	384	0	0.3407	0.3407	0.3407	3	0.1593	0.1593	0.1593	0	0	0	0	0	0	0	0

Fig. 3.3: Input parameters for subsidence calculations of well *raa72*. Initial porosity ( $\phi_0$ ) and decompaction coefficients (c) are compiled from Steckler and Watts (1978); Royden and Keen, 1980; Sclater and Christie (1980); Sawyer et al. (1983); Bond and Kominz (1984). <sup>a</sup>Litho ID connects properties from Module 1 with lithologies in Module 3. <sup>b</sup>Strata ID connects properties from stratigraphic horizons in Module 2 with data in Module 3. <sup>c</sup>Lithology ID = 0, which means sand. <sup>d</sup>Lithology ID = 3, which means shale.

In Fig. 3.4A, the mean results of well *raaT2* are displayed for total basement subsidence and in Fig. 3.4B for basement subsidence rates. All parameters were taken into account for the MCS. The results using symmetric normal- and uniform distributions for the MCS give a more continuous subsidence curve compared to the stepwise curve of Wagreich and Schmid (2002). Minor steps in the case study involved may result from the omission of eustatic corrections. These relatively continuous mean subsidence curves compare better with theoretical subsidence curves from numerical basin models (McKenzie, 1978; Pitman and Andrews, 1985; Allen and Allen, 2005). The graph in Fig. 3.4C displays the unequal error bars of a mean curve of the total basement subsidence of well *raaT2* calculated with a symmetric normal distribution. Error bars indicate different error ranges in the +x, -x, +y and -y directions. In previously available programmes, errors were only symmetrically indicated and were calculated separately for each input parameter.

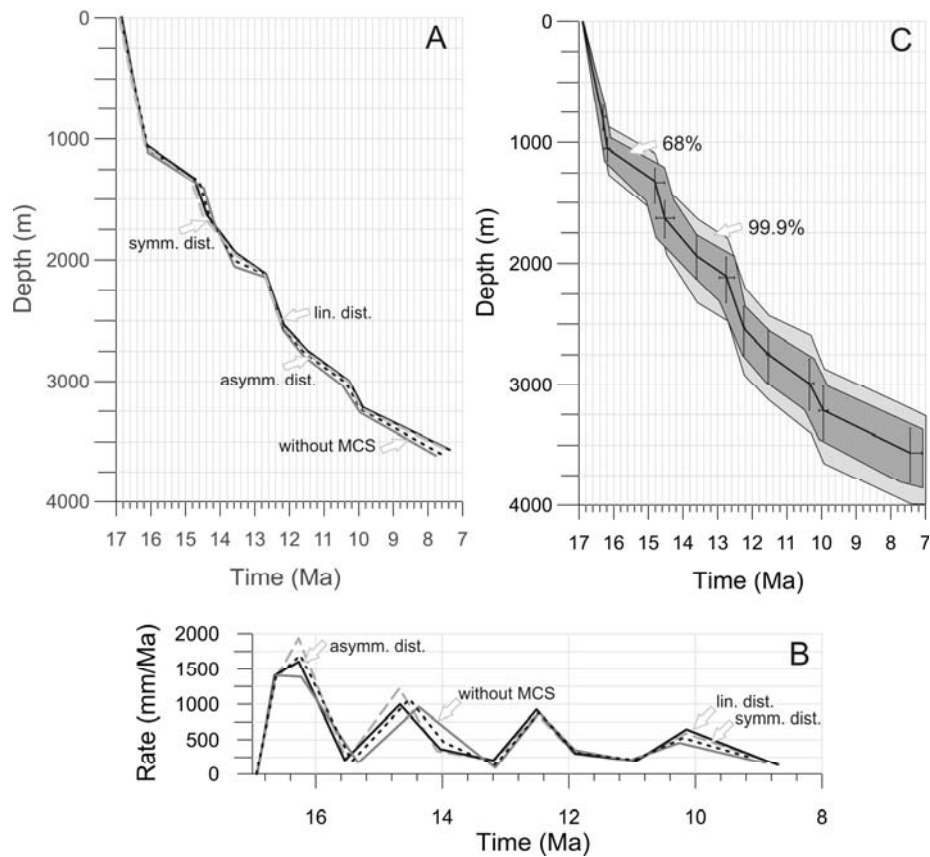


Fig. 3.4: A) Mean results of well *raaT2*, showing the total basement subsidence and B) basement subsidence rates. Calculations were undertaken without the Monte Carlo algorithm and with MCS using 3 probability distributions. As the results of the power and symmetric normal distribution are very similar, the power distribution has not been shown. Settings: 10,000 iterations, final porosity 10 %. C) Total basement subsidence of well *raaT2*, calculated with MCS with a symmetric normal distribution. One case (light grey) covers a probability area of 99.9 % and one case (dark grey) 68 %.

### 3.8 Discussion and Conclusion

Evaluations of error sources and the impact of different factors on the accuracy of subsidence calculations have been published for quite some time. The majority of the parameters applied (e.g. final porosity, sedimentation depth, decompaction parameters dependent on lithology) have an influence on variations in the subsidence curve in the y-direction (depth). Changes in the values have different impacts on a shape of a curve, because of their diverse units; for example, a change of only 5 % in final porosity has more effect on the final subsidence curve than a change of 100 m of the sedimentation depth.

Previously, errors have only been given for certain parameters influencing the variance in the y-direction (depth). Age uncertainties, which result in variations of the x-direction and therefore influence the gradient of curves, are, for the first time, also taken into account with the DCT software. As the age constraints have a strong impact on the results and to make applications realistic, the overstepping of age boundaries are permitted.

Different probability functions have been implemented, to test their impact on the final results. For the mean results, the curves lie in three groups (Fig. 3.4), based on the number of parameters defining the probability area; three parameters - asymmetric power and asymmetric normal distribution; two parameters - uniform and symmetric normal distribution; one parameter - without MC runs.

The number of parameters used influences the number of iterations of the MCS necessary to get essentially constant results; that is, the point at which further iterations cause no marked changes in the subsidence curve. Waltham et al. (2000) showed that when using five parameters there are only marginal variations after 1,000 iterations. In our case, using 10 parameters, calculations have shown that starting from 10,000 iterations onward, error variations appear to be negligible.

All the input data within the three modules is variable. Input data has to be tabulated in text files with unique column IDs, which are provided together with the programme. As an example, the initial porosity ( $\phi_0$ ) and the decompaction coefficients ( $c$ ) can be defined by the user, because this data is not implemented in the software directly, as it is in other programmes. The greater flexibility allows the programme to be better adjusted to answer a particular question. The output as text files represents a base for further processing and graphic presentation of the results, using other programmes.

The programme can be applied to basins where exponential porosity-depth relations are assumed (e.g. normally pressured basins, rift basins, pull-apart basins), because linear or power-law equations or other types of assumptions are not integrated. The programme is not applicable for overpressured basins (Magara, 1980) or shallower basins (Allen and Allen, 2005).

The change of one single parameter does not significantly influence the errors; it is the bulk of the parameters. As a result, the programme provides an extension to the full backstripping process proposed by Waltham et al. (2000), especially as a base for further work. In general, the MCS-method results in a mean that can be better compared to numerical basin models.

## **4 Sedimentary Fault Backstripping**

---

This chapter is based on:

Hölzel, Monika and Wagreich Michael (submitted 2009). Sedimentary fault backstripping of a complex fault system – Results and limitations of a case study in the southern Vienna Basin (Austria). *Marine and Petroleum Geology*.



#### **4.1 Abstract**

To quantify the vertical displacement of a structural complex fault array in the southern Vienna Basin, we applied sedimentary fault backstripping. The method is based on the calculation of basement subsidence by backstripping the stratigraphic records of footwall and hanging wall blocks that belong to a single normal fault surface. The analysed faults were synsedimentary active during the Middle to late Miocene (16.3 – 7.8 Ma). Displacement along single large normal fault surfaces shows constant normal slip through time of up to 700 m/my, but no regular distribution of slip magnitudes along strike. Converging fault surfaces are influencing each other with either alternating phases of normal activity or reverse faulting due to kinematic linkage which results in a complex pattern of slip rates versus stratigraphy.

## 4.2 Introduction

Various methods discriminate and analyse fault displacement through time with the aim to either get information about the regional geological history or about fault surface development in general (Walsh and Watterson, 1988; Nicol et al., 1997; Cartwright et al., 1998; Childs et al., 2003). In respect of the deformation of sedimentary strata and sedimentary basin fills, the incorporation of compaction of the sediment pile during faulting was disregarded for a long time. We present an application of a method introduced as *fault backstripping* by ten Veen and Kleinspehn (2000) and Waggreich and Schmid (2002) for the calculation of vertical fault displacement (throw) in sediments. Based on the calculation of basement subsidence, the timing and sense of fault movement can be determined accurately. In the ideal case, a complete sedimentary record of the hanging wall and footwall blocks of a fault is analysed.

The method can only be applied to *synsedimentary faults*, where sedimentation rates exceed fault displacement rates and fault scarps are rapidly blanketed by sediment, so that the fault displacement history is preserved as thickness and displacement changes in the synfaulting sedimentary succession (Childs et al., 2003). This type of geometry is also referred to as *growth fault* with thicker sediments in the hanging wall than in the footwall (O'Connell, 1961). It implies that, during sedimentation, the fault was active and cut the former top ground surface.

Unfortunately, the term *fault backstripping* or *displacement backstripping* is also used for a different technique for the reconstruction of fault displacement (Walsh and Watterson, 1988; Nicol et al., 1997; Rowan et al., 1998; Childs et al., 2003). This method addresses to the tip line behaviour of fault surfaces during fault movement. Tip lines are the borders of a fault surface, where displacement dies out to zero (Boyer and Elliott, 1982). To clearly differentiate, in the following, we (re-)name the method described here as *sedimentary fault backstripping*.

This paper emphasises on the method of *sedimentary fault backstripping* and in its application and geological interpretation in a case study in the Vienna Basin (Austria), a prolific mature oil basin exploited since nearly one century (Hamilton et al., 2000). We include a review of the sensibility of the method, because applications in the past sometimes seemed to be not backed-up quite well.

Fault features are named according to "The glossary of normal faults" (Peacock et al., 2000).

## 4.3 Sedimentary fault backstripping

### 4.3.1 Basement subsidence

The method for reconstructing vertical fault displacement over time (ten Veen and Kleinspehn, 2000; Waggreich and Schmid, 2002; Chevalier et al., 2003) is primarily based on subsidence calculations on both blocks belonging to a fault surface (hanging wall and footwall block).

The quantitative analysis of subsidence (Steckler and Watts, 1978; Van Hinte, 1978; Bond and Kominz, 1984) through time (*geohistory analysis*, *subsidence analysis*) relies on the stepwise decompaction of stratigraphic units to correct their thickness at the time of interest, and includes

also corrections for palaeowater depth. Decompaction calculations are based on the reduction of porosity with depth. Normally pressured sediments have an exponential relationship  $\phi = \phi_0 e^{-cy}$ , where  $\phi$  is the porosity at any depth  $y$ ,  $\phi_0$  is the surface porosity and  $c$  is a coefficient that is dependent on lithology and describes the rate at which the exponential decrease in porosity takes place with depth (Steckler and Watts, 1978; Sclater et al., 1980).

For the calculation of subsidence, the following parameters are incorporated: thickness of stratigraphic layers, stratigraphic age, lithology, sedimentation (palaeowater) depth, sea level, decompaction parameters (porosity for  $t_0$  = porosity at the beginning, decompaction coefficient  $c$ , final porosity).

For the calculation of subsidence, a computer programme has been developed at the Department of Geodynamic and Sedimentology, University Vienna. It combines subsidence analysis with integrated error quantification, which is very important, because input variables influence each other and errors of each input value cannot be quantified separately (Waltham et al., 2000; Hölzel et al., 2008a). Subsidence maps for the southern and central part of the Vienna Basin based on that method were published by Hölzel et al. (2008b).

#### 4.3.2 Vertical displacement

For the second part of the analysis, the total basement subsidence of the footwall- and the hanging wall blocks of a synsedimentary fault are compared and divided through time. Segments of convergence or divergence ( $\Delta s_i$ ) record times with vertical activity along the fault. Inactivity or strike-slip movement is reflected in parallel segments. The relative sense of fault movement can be determined by the calculations, resulting in “negative” rates for normal and “positive” rates for reverse faulting.

The most accurate form to present results is a step plot of throw rates vs. time. Rates are calculated by subtracting  $\Delta s_{i-1}$  from  $\Delta s_i$ , and dividing by the duration of the stratigraphic interval. So the results are rates, time averaged over intervals (Fig. 4.1).

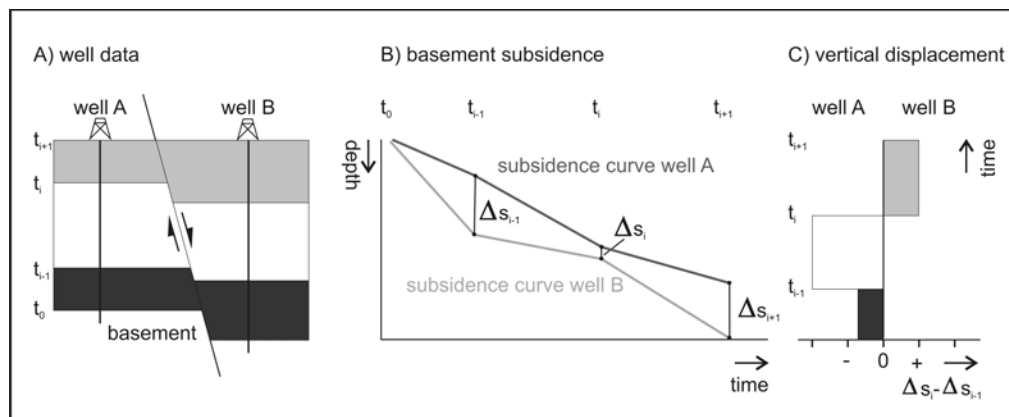


Fig. 4.1: The Sedimentary Fault Backstripping method: Quantification of vertical displacement, based on the analysis of basement subsidence of the footwall and hanging wall blocks along a fault surface (modified from Wagreich and Schmid, 2002).

#### 4.4 Application in the southern Vienna Basin

##### 4.4.1 Geological overview of the Vienna Basin

The Vienna Basin is a complex, but due to the occurrence of hydrocarbons a very intensively investigated pull-apart structure (Royden, 1985; Wessely, 1988; Wessely, 2006) between the Eastern Alps and the Western Carpathians, covered by parts of Austria, Slovakia, and the Czech Republic (Fig. 4.2).

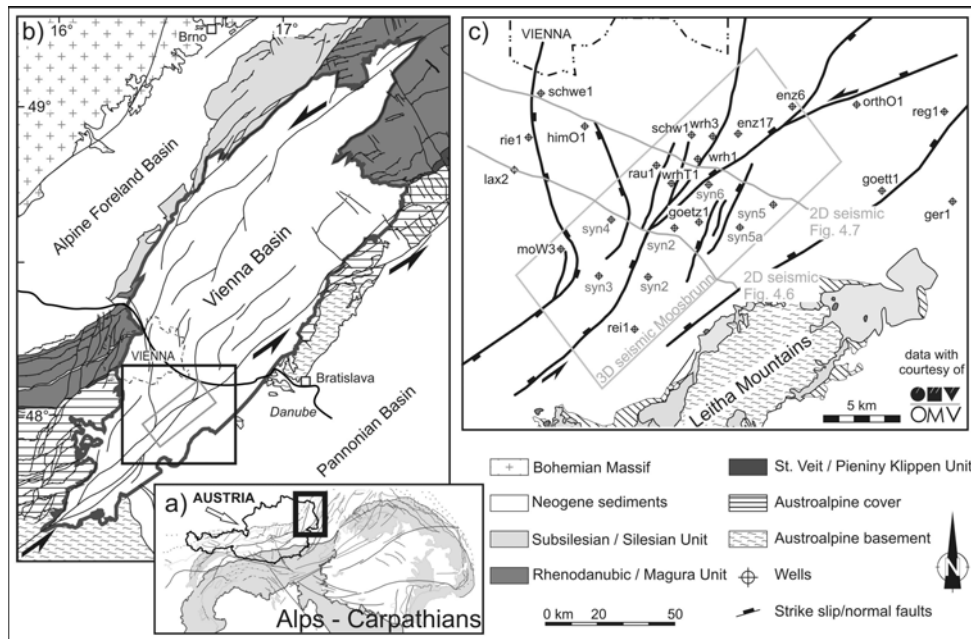


Fig. 4.2a and 4.2b: Position of the Vienna Basin within the geological units of the Eastern Alps and western Carpathians (modified from Decker et al., 2005).

Fig. 4.2c shows the southern part with the 3D seismic cube Moosbrunn (rectangle) and the coverage of boreholes used for subsidence analysis. The locations of the 2 seismic lines of Fig. 4.6. and Fig. 4.7 are displayed by grey lines.

A complex fault system divides the basin into high zones and deep depocentres filled with up to 5.5 km of Miocene sediments. The tectonic history started with a piggy-back basin type (wedge top basins, Lower Miocene, c. 18.5 – 16.3 Ma), where sediments were syntectonically deposited on top of the NW-thrusting Alpine nappes. In the Middle and Upper Miocene (c. 16.3 – 7.8 Ma) NNE-oriented duplexes evolved during the rapid subsidence triggered by pull-apart mechanisms (Decker, 1996). Growth strata along normal faults indicate that horizontal extension took place from the base of the Badenian (Middle Miocene; above Aderklaa conglomerate of Fig. 4.3) to the end of the Pannonian (Upper Miocene; Fig. 4.3). The pull-apart phase was terminated by a late Miocene stage of E-W directed shortening (Decker, 1996).

Our investigations concern the Middle to Upper Miocene pull-apart evolution. During that time span structural styles were dominated by extensional strike-slip duplexes and by en-echelon normal faults connected to strike-slip faults (Decker et al., 2005).

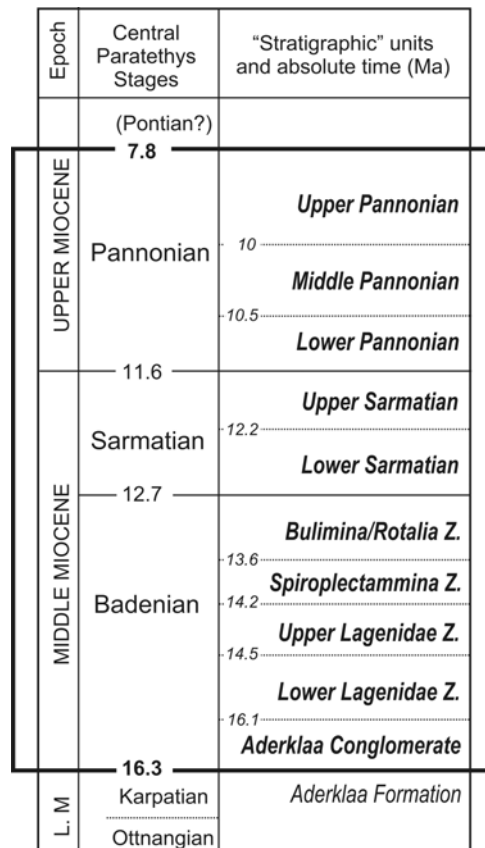


Fig. 4.3: Timeframe of investigation in the Middle to Upper Miocene (not to scale). The chronostratigraphic chart is compiled from Piller et al. (2004) and Strauss et al. (2006).

#### 4.4.2 Data collection and integration

The data comes from 25 selected boreholes drilled in the southern part of the Vienna Basin. With courtesy of OMV-Austria, information about the stratigraphic record of wells, coordinates, and Self-Potential logs (SP-logs) was available. For selecting wells, following criteria based on seismic mapping of the underground were applied: 1.) Wells in undisturbed blocks were favoured to get undisturbed thicknesses of the sedimentary layers. 2.) There should be at least one well in each fault block. 3.) For a complete stratigraphic record, wells, which reach great depth or the basement, should be taken. With these criteria it was possible to minimise errors derived from well data.

Sediment layer thicknesses were achieved from the depth of formation tops. The thickness had to be dip corrected (Chevalier et al., 2003), because some blocks are slightly tilted. Log data also contain information on the porosity of the layers. For that purpose, mainly self potential logs (SP-logs) and resistivity logs were used to differentiate between porous and non-porous lithologies (sand vs. shale).

Measurements were crosschecked with well cuttings. The lithology does not vary very much, because in the investigated area, sediments are only composed of sand, sandstone, siltstone or shale with minor occurrence of carbonates. Palaeobathymetric data (sedimentation depth) was taken from a compilation (Wagreich and Schmid, 2002), which is based on various sedimentological and palaeontological investigations (Kreutzer, 1993; Seifert, 1996). Relative sea level changes are not incorporated, since the basin has been separated from the world ocean after 10.5 Ma (Steininger and Wessely, 1999).

Time units are based on the stratigraphic time scale for the Neogene of Austria (Piller et al., 2004) and on personal communication with M. Harzhauser. Terms for stratigraphic units are taken from the central Paratethys stages nomenclature and from the local eco- and biostratigraphic zonation of the Vienna Basin (Rögl, 1998; Strauss et al., 2006). As the absolute time scale of the Paratethyan zonations is still under discussion (Hohenegger et al., 2008), we used a more robust averaged scale by including units with inferred unusual short durations into longer-ranging stratigraphic units, e.g., combining the Lower and Upper Lagenidae Zones of Fig. 4.3.

#### 4.4.3 Seismic mapping and 3D visualisation

In the southern part of the Vienna Basin, OMV-Austria provided a 3D seismic cube (*Moosbrunn*), which was used to establish the structural framework for our study. The data set covers an area of 192 km<sup>2</sup> and reaches a depth of 3 s TWT (Two-Way-Traveltime; ~4700 m). The maximal depth of the top of the underlying Austroalpine basement nappes in the study area is at 2600 m, so the overlying sedimentary fill is fully covered by seismic data.

For detecting the sedimentary development and the geometry of horizons in relation to the fault arrays, 8 stratigraphic horizons have been mapped. Stratigraphic bounding is tied on over 25 wells and is based on Strauss et al. (2006), who have undertaken detailed seismic stratigraphic investigations in parts of the cube.

Hinsch et al. (2005a; 2005b) already did extensive fault mapping and modelling within the block *Moosbrunn*. Their fault arrays were modified and extended by additional structural mapping within the cube. Thus, the investigated area could be enlarged, and is covered by 2D lines with a better resolution in- and outside the cube.

Afterwards, the mapped spurs have been exported to the 3D modelling software Gocad to establish a geo-referenced relationship between fault geometry, well positions and stratigraphic horizons (Fig. 4.4). The time to depth conversion formula and the background of the modelling work flow follows the method described in Hinsch et al. (2005a; pp. 50, Appendix). In areas, which are not covered by seismic lines, faults were modelled based on digitised versions of the pre-Neogene basement map of the Vienna Basin (1:200000 by Kröll and Wessely, 1993) and a horizon (Aderklaa Conglomerate; Top 16.1 Ma) compiled by OMV-Austria geologists.

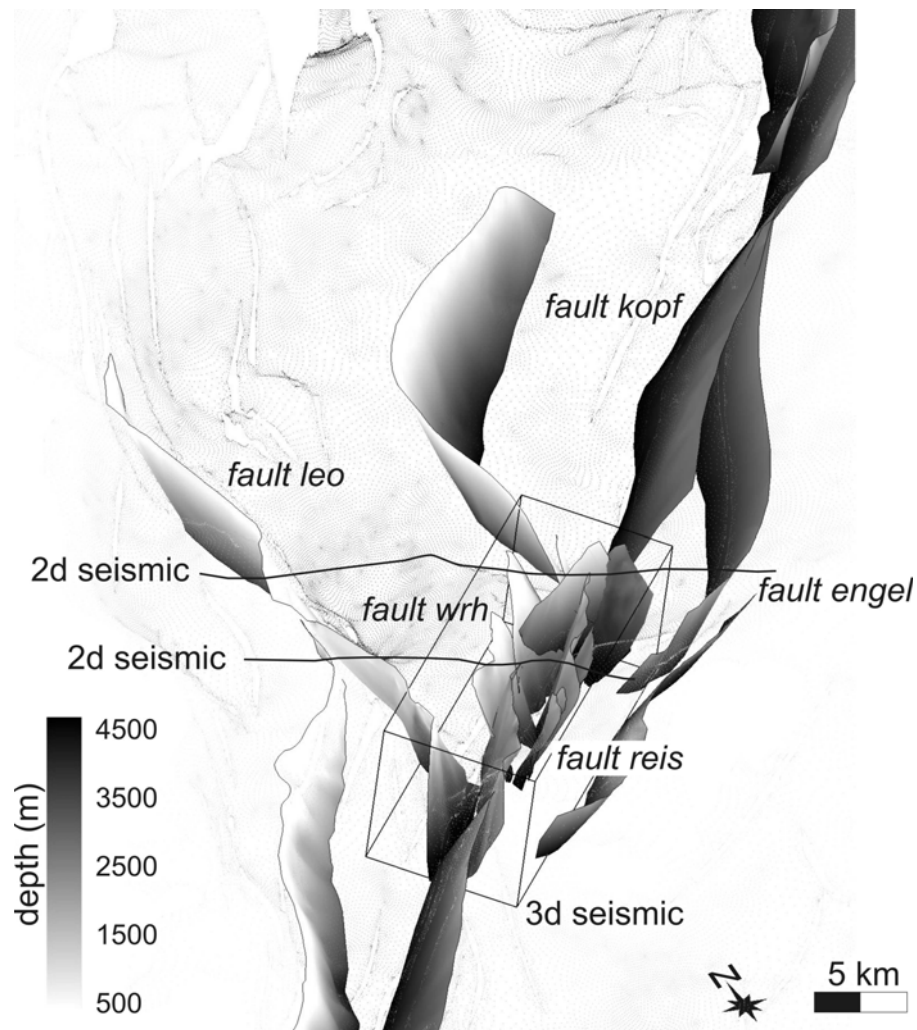


Fig. 4.4: Modelling in 3D (software Gocad) of the most important fault surfaces in the southern part of the Vienna Basin. The dotted surface represents the pre-Neogene relief.

Because of the irregular spatial distribution of the available drill data, 9 synthetic wells within the seismic dataset were constructed. These pseudo-wells provide information about layer thickness, which were measured from the seismic record and converted to depth. If an existing well necessary for a fault block does not contain the whole stratigraphic record, it was extended to depth in the same way. We have also used wells, which obviously were drilled through minor faults with a vertical displacement smaller than 20 m, but for which we could reconstruct the real layer thickness by the back-up of seismic images.

Along transects perpendicular to fault surfaces strike direction the comparison of the calculated displacement rates and the underground architecture was undertaken.

#### 4.4.4 Fault pattern and fault block model

A fault block model has been established reduced to major faults, which show a vertical displacement of more than c. 20 m. The model covers mainly the area south of the river Danube (Fig. 4.2). According to existing data (Hinsch and Decker, 2003; Hinsch et al., 2005a; Hinsch et al., 2005b) and additional structural interpretation, the area was divided into 8 major fault compartments (Fig. 4.5).

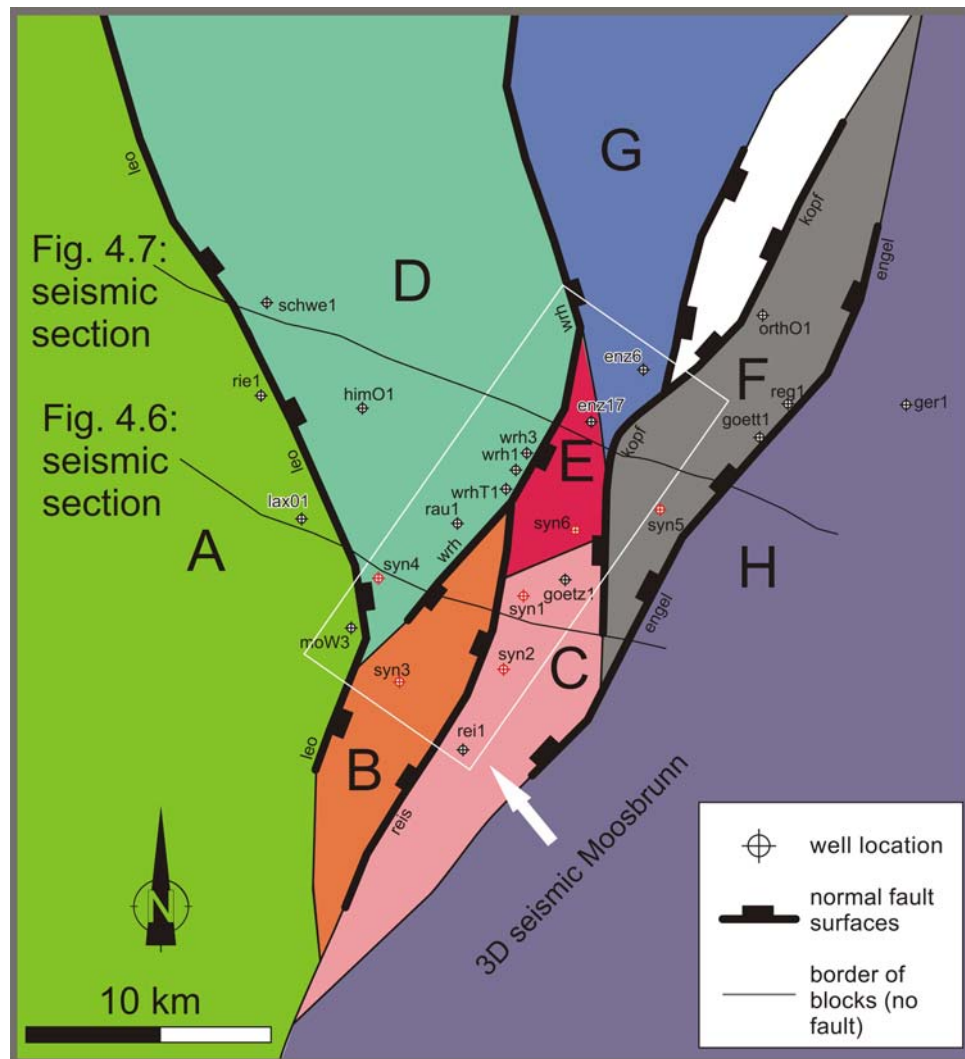


Fig. 4.5: Sketch map of the fault block model.

The structural build-up comprises one of the basin forming major faults, the SW-NE striking *Leopoldsdorf Fault*. It is a sinistral strike-slip feature with a very large normal slip component due to bending with an overall vertical displacement of 4000 m.

In the south of the 3D seismic cube, a branch of the *Leopoldsdorf Fault* is part of a *negative flower structure* (Brix and Schultz, 1993; Decker et al., 2005; Hinsch et al., 2005a; Hinsch et al.,

2005b). In most cases, these fault surfaces reach the underlying Alpine nappe system or at least the base of the Middle Miocene and converge with depth.

The interaction between the major *Leopoldsdorf Fault* and the *negative flower structure* formed also relay ramps, which have been taken into account during the interpretation.

Faults of both of these major structural elements show for most of the stratigraphic units different sediment thickness of the hanging wall and the footwall, which refers them as being synsedimentary active. Seismic profiles (Fig. 4.6 and Fig. 4.7) have been used for first predictions of the timing and amount of fault displacement, based on the layer and fault architecture. The challenge is, to keep in mind that in this complex fault system, a hanging wall block for one fault surface is contemporaneous a footwall block for another parallel striking fault. Hinsch et al. (2003) have also proposed that fault geometries depicted in the Neogene sediments and the pre-Miocene basement topography indicate a kinematical linkage of both faults rather than a cross cutting relation.

**Block A** (footwall) and Block D (hanging wall) border the Leopoldsdorf Fault (*leo*, Fig. 4.4 and Fig. 4.5). **Block B** is the hanging wall block of both branches of the negative flower structure (*leo*, *reis*, *wrh*) and is vertically displaced for up to 1 s TWT with respect to the boundaries of the faults (Hinsch et al., 2005a). Hanging wall strata (from Top Aderklaa Conglomerate to Top Upper Pannonian; c. 16.1 – 7.1 Ma) is tilted to the SE (~13°). This implies that slip motion at the eastern fault branch (*reis*) has been higher than at the western border fault (*leo*). Thickness variation shows accelerated activity of the hanging wall in the Badenian, which decreased with time deduced from smaller offsets of younger horizons in relation to older ones. These thickness variations indicate major fault activity during the Lower Badenian and from the Lower Pannonian to the Upper Pannonian. **Block C** forms the footwall for fault surface *reis*. Stratigraphic horizons are more or less horizontal and at the same depth as in fault block A, the footwall of the Leopoldsdorf Fault. **Block D** is additionally the hanging wall block along the fault (*wrh*), where the duplexes of the negative flower structure are becoming narrow. **Block E** builds up the hanging wall block of the converging fault splays (*wrh*, *kopf*), but the overall normal offset in this area is smaller than of that in the southern part (block B). The blocks E and C form a relay ramp, because of overstepping fault segments, which are interacting with each other. **Block F** acts as hanging wall for fault *engel* and at the same time as footwall for fault *kopf*.

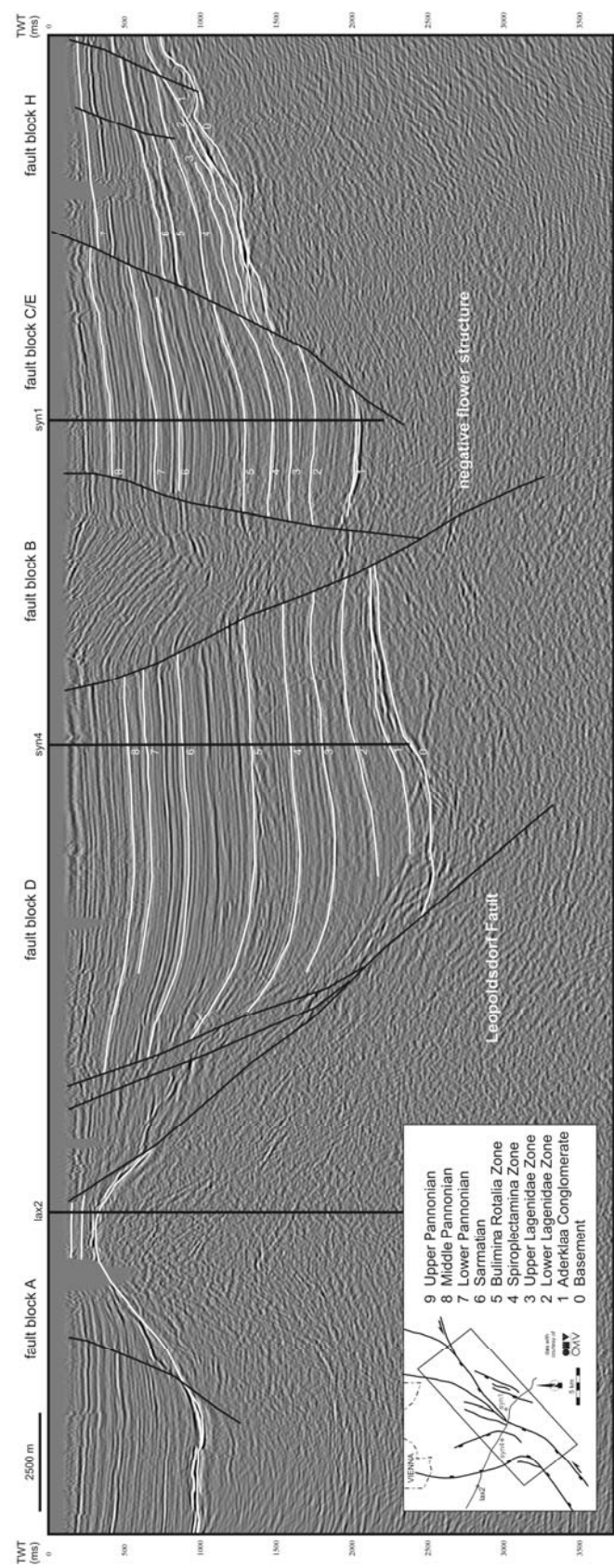


Fig. 4.6: Seismic cross section (published as supplement in Brix and Schultz, 1993) through the basin with wells from G1 and G4 (Fig. 4.1 and Fig. 4.5).

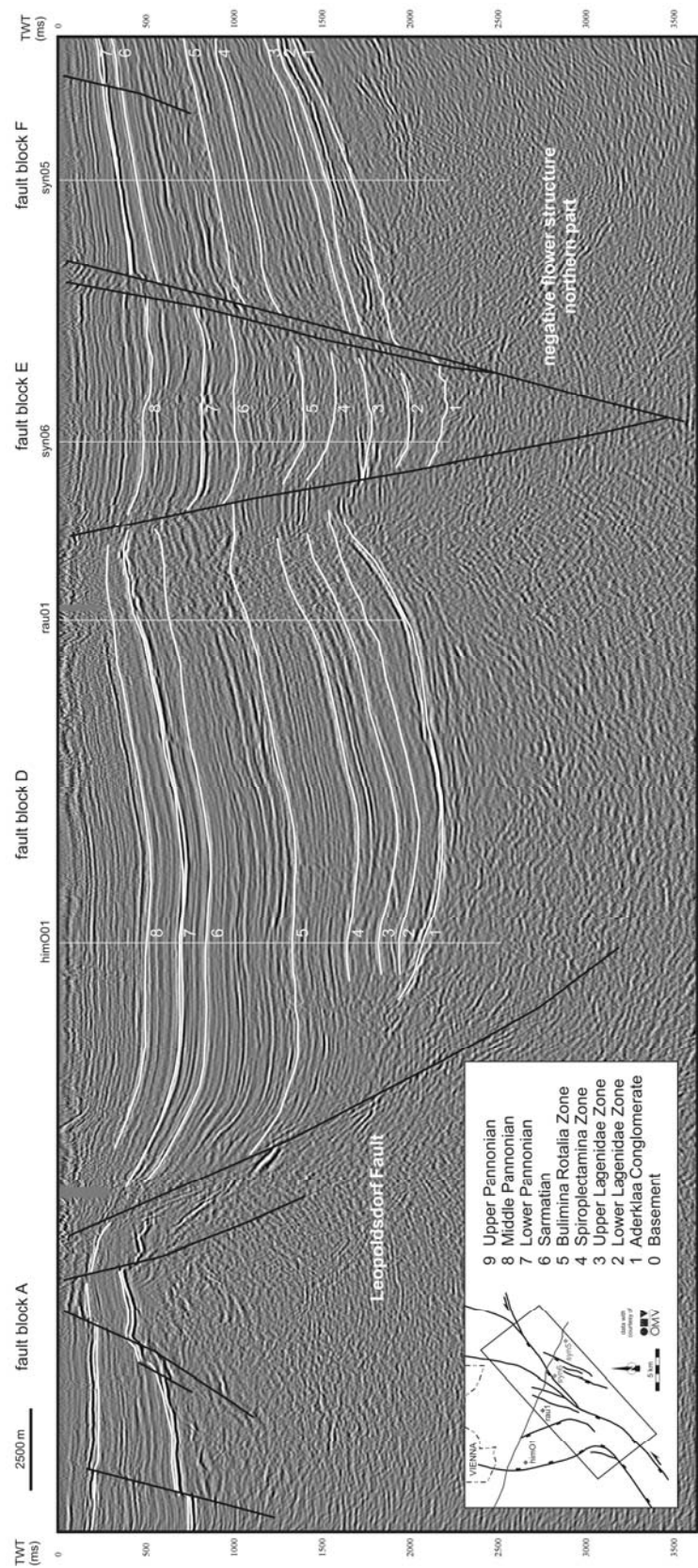


Fig. 4.7: Seismic cross section showing wells from G2 and G4 (Fig. 4.1 and Fig. 4.5).

### 4.5 Results

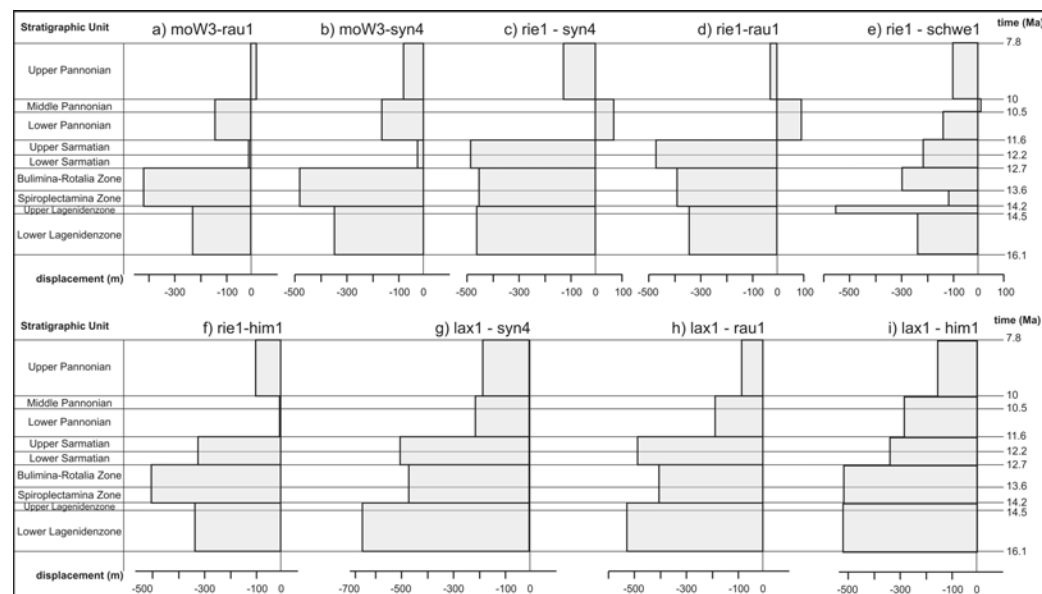


Fig. 4.8: Rates of vertical displacement for well pairs along the Leopoldsdorf Fault (*leo* in Fig. 4.4 and Fig. 4.5) in the according fault blocks A and D. Note scale differences of displacement axes.

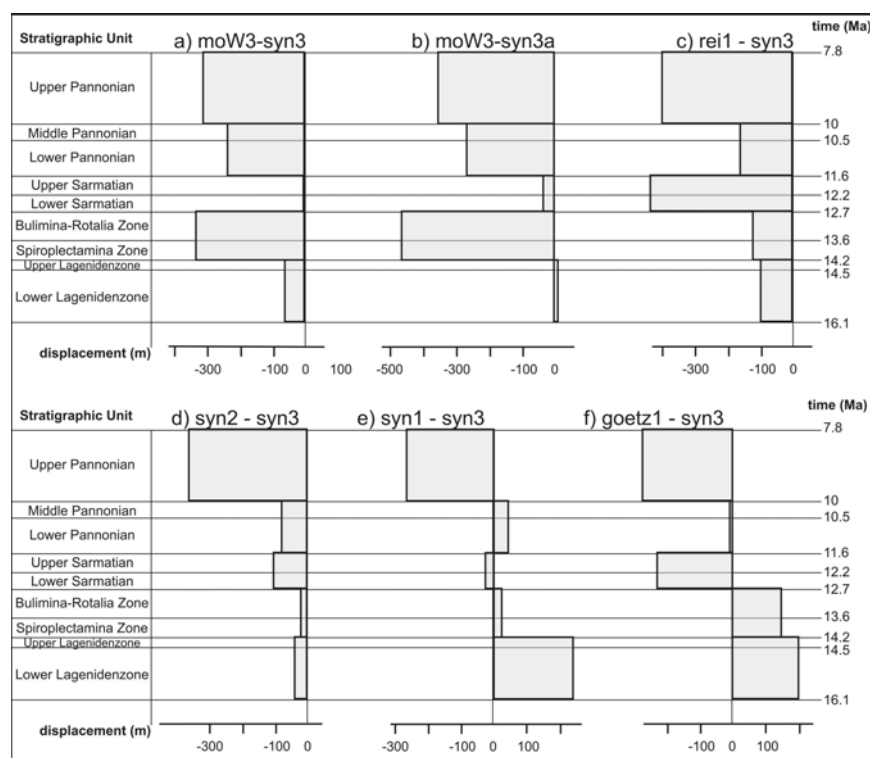


Fig. 4.9: Rates of vertical displacement of the southern part of the negative flower structure bordered by fault blocks A-B and C-B. The well pairs are across both fault branches with block B being the hanging wall of both fault surfaces (for well positions see Fig. 4.5). Note scale differences of displacement axes.

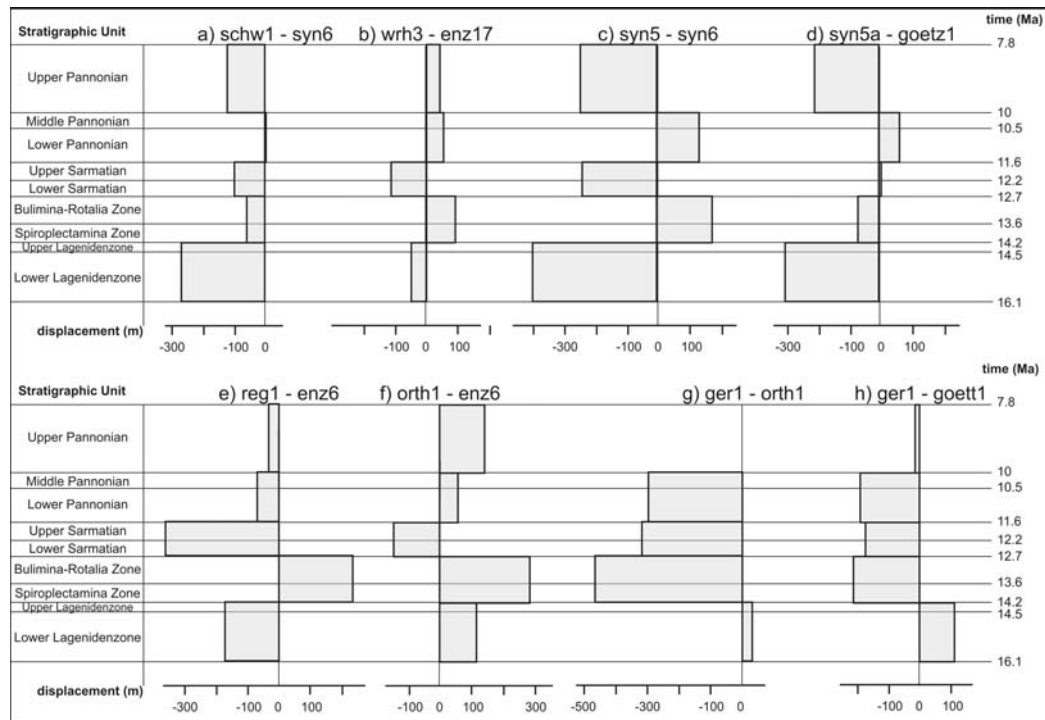


Fig. 4.10: Rates of vertical displacement for the northern segments of the negative flower structure (for well and fault positions see Fig. 4.5). Note scale differences of displacement axes.

Fig. 4.10a and b includes faults *wrh* (footwall D and hanging wall E), fault *kopf* (footwall F and hanging wall C and E).

Fig. 4.10c and d show fault *kopf* with footwall F and hanging wall C and E.

Fig. 4.10e and f are plots from the northern continuation along the fault surface *kopf* (footwall block F and hanging wall block G).

Fig. 4.10g and h show rates of vertical displacement for fault *engel* with footwall H and hanging wall F.

The basement subsidence data base for the comparison of well pairs (footwall and hanging wall) was already published in Hölzel et al. (2008b). In general, our data on fault slip indicate different slip histories for different faults with strongly varying rates from Badenian to Pannonian times. No uniform picture can be drawn for this complex fault system as suggested for the central Vienna Basin by Wagreich and Schmid (2002).

Fig. 4.8 shows the vertical displacement rates along the Leopoldsdorf Fault from well pairs from south to north, starting where the Leopoldsdorf Fault is no longer part of the negative flower structure. Well pairs show normal offset up to 500 m/my for the Badenian and the Sarmatian with a decrease in the Pannonian with a maximum of 200 m/my.

The results of the southern most part of the negative flower structure are displayed in Fig. 4.9. Comparing the fault surfaces *leo* (Fig. 4.9a; b) and *reis* (Fig. 4.9c-f) it is obvious that displacement alternates at the two segments of the negative flower structure. The plots of Fig. 4.9c-f highlight along-strike fault dynamics from the highly active centre zone of the fault

surface to parts with decreasing fault movement towards the tip lines (Fig. 4.9f). All plots show strong activity during the Upper Pannonian.

The results from the northern segments of the negative flower structure are very inhomogeneous (Fig. 4.10). Along fault surface *wrh* in northern direction (Fig. 4.10a, b), displacement varies through time. In the early Badenian vertical displacement ranges from 50 m/my up to 270 m/my. During the late Badenian normal as well as reverse slip can be identified. Sarmatian activity shows rates up to 300 m/my. Then, in the Pannonian, the activity decreases to nearly no movement (or pure strike-slip), ending with moderate slip rates in the Upper Pannonian (0-120 m/my).

The fault *kopf* is a converging fault surface to the northern parts of fault surface *wrh*. The related fault pairs (Fig. 4.10c,d) display similar slip distributions through time as Fig. 4.10 a, b, with high vertical displacement in the early Badenian, incoherent slip directions for the late Badenian, normal offset up to 300 m/my in the Sarmatian, reverse movement during the early to middle Pannonian, but slightly high rates for the late Pannonian with 250 m/my.

Well pairs of Fig. 4.10e, f with footwall F and hanging wall G are the continuation along the fault surface *kopf*. The block G belongs to the northern most duplex of the investigated area.

Along the fault *engel* (Fig. 4.10g, h) the uppermost record of the Pannonian is missing. The rates display high amounts of normal slip during the Middle and late Miocene with up to 550 m/my. In the lowermost Badenian reverse slip is obvious.

#### 4.6 Discussion

Displacements on normal faults are rarely accommodated on a single well-defined surface, but are partitioned between interacting fault segments (Imber et al., 2004). Consequently, the southern Vienna Basin area is built up by a very complex fault system with normal slip and strike-slip components and vertical and horizontal (?) block rotations (Marton et al., 2000). Data derived from sedimentary fault backstripping show the inhomogeneity in normal slip rates of the system. Plots show normal movement as well as reverse slip. There exist also intervening times of no activity or purely strike slip activity, which cannot be distinguished by our method.

Our data show **no linear slip distribution** along fault surfaces such as a slip maximum in the central part and decreasing slip to the tip lines. Numerical models have shown that slip distributions on normal faults are indeed often asymmetric and display local and often irregular maxima (Maerten et al., 1999). This can be caused by mechanical interaction between intersecting faults or through the transfer of displacement from one fault segment to another one, which most often occurs in relay zones (Imber et al., 2004).

Faults are **soft linked** when they interact through their stress field and no linkage by faults is visible at the scale of observation (Walsh and Watterson, 1991). Then the geometries of the fault surfaces do not change significantly. Fault lengths are established rapidly and subsequent interaction between faults retards the lateral propagation producing essentially constant lengths for much of the duration of faulting (Imber et al., 2004). In contrast to that is hard linkage with

faults segments that are physically linked to each other, which changes of the geometry of the fault plane.

Zones where faults are connected to each other with a sharp angle are zones with the lowest slip rates through time (Fig. 4.10a-d). The transect through the southern part of the *negative flower structure* (Fig. 4.9) shows fault slip activity over the whole investigation time frame, but remarkable are the maxima in the late Pannonian. They correlate with the rest of the fault surfaces very well. Where the fault splays are combining in the northern part of the investigated area, vertical fault slip in the pre-Pannonian has been minor or not existent. That implies that probably there has been no activity or just strike slip events.

Data indicates also periods of **reverse faulting**. The stratigraphic record of boreholes where reversals occur was checked in seismic sections and gaps due to erosion can be excluded. Le Guerroue and Cobbold (2006) found out in their analogue models of strike-slip systems that in all negative flower structures faults had reverse components of slip and that parts with reverse slip direction are normal and widespread. In the northern parts of block *Moosbrunn* fault block rotation could be a reason for the reverse slip activity (Fig. 4.10c-f). The alternating activity of fault branches shows (Fig. 4.10a, b) that along one fault displacement goes downward and as a reason of space problems layers have to be uplifted at the connected fault surface. Cartwright et al. (1998) investigated the cyclicity of growth faults and came to one conclusion that individual faults do not share identical development, and that some are in phase with their neighbours and some are out of phase.

#### **4.7 Errors, limitations, and requirements for sedimentary fault backstripping**

The following paragraph provides a review about requirements and error sources of the sedimentary fault backstripping method adopted for this study, which are inevitable for the sensitivity of the method.

One main prerequisite of the method is that the stratigraphic record used for subsidence calculations has to be complete. Before applying the method one has to make sure that there are no gaps in the record and that wells are deep enough to penetrate all layers of interest.

If stratigraphic information is derived from subsurface seismic data, uncertainties could occur during the conversion of seismic data from time to depth. In our special case, when we measured missing stratigraphic information at a location (*synthetic well*), formation tops had to be converted into depth and therefore the *synthetic well* results have to be interpreted with care.

The lithology was measured from SP and resistivity logs. Some of the layers had to be dip-corrected so lithology information along the well path is differing from the real thickness of the layers, but were applied as measured.

To minimise errors of the subsidence calculation, which are the basis for further displacement calculations and therefore are very sensitive, we have applied error quantification into our subsidence calculation programme based on Monte Carlo Simulation (Hölzel et al., 2008a). The

accuracy of chronostratigraphic age estimates of mapped horizons remains a major influencing factor, as rates are time averaged over stratigraphic intervals.

The definition of fault blocks is a very crucial issue. We have only incorporated fault surfaces which have a vertical offset of at least 20 m, because the amount of slip along smaller faults lies within the overall error of the calculations. It is very important to clearly define the relationships between blocks, because what is the hanging wall for one fault surface can be the footwall for a parallel fault. The internal structure of a block has also influence on the subsidence behaviour. For example, a depression zone or erosional features in the hanging wall of a normal fault could lead to positive rates, which erroneously indicate reverse faulting or a reverse period during normal fault movement. Therefore, from each block more than one stratigraphic section is required to have control over hidden erosional events which could not have been detected in the seismic record or in the field.

Well data is often restricted due to ongoing exploration and/or outcrops are not evenly distributed over an area. Results are optimal, if the stratigraphic record comes from the nearest point as possible to the fault surface, especially if blocks are tilted. With the support of subsurface (i.e. seismic) data the stratigraphic record could be “shifted” to a position nearer to the fault surface. Deformed strata around a fault plane (fault drag) also distorts the results with apparent more or less displacement than undeformed fault contacts. So without subsurface images the nearest position of well is not automatically the optimum choice for sedimentary fault backstripping.

During the interpretation of the slip rates it should be kept in mind that different mechanisms of fault surface developments are possible and that the calculations are just approximations normalised over a time period. Surfaces of synsedimentary faults may be propagating, stationary, or have retreating tip-lines (Childs et al., 2003).

### **4.8 Conclusion**

The southern Vienna Basin area is built up by a highly complex fault system of a flower structure with normal and reverse slip and strike-slip components and vertical block rotations. We tested the method of sedimentary fault backstripping on such a complex fault system. The method, which is based on backstripped subsidence analysis, shows a strong **inhomogeneity** in normal slip rates of the system. Individual faults display strong varieties in timing and magnitude of fault movements. Times of high slip rates along faults alternate with times of inactivity or strike slip movement. Mapping and visualisation provides a necessary basis for the exact definition of the fault arrays and the relation between stratigraphic data and geometry of faults surfaces. One essential base for application of sedimentary fault backstripping to a fault system is the knowledge of how fault surfaces are connected and the definition of the total time span, in which a fault has been active, e.g. by using seismic sections. The largest fault surface in the investigated southern Vienna Basin, the Leopoldsdorf Fault, shows normal slip through the Middle to the Upper Miocene. Slip rates as high as 700 m/my have been reconstructed. The

partly connected negative flower structure shows parts, which were active in alternating sense in the same time intervals.

Other fault segments show different character with reverse movement. Because of kinematic linkage no continuous slip over fault surfaces could be detected.

As a stand-alone method *sedimentary fault backstripping* is not suited for the quantification of vertical fault movement, especially in complex fault systems. But using supporting methods like remote sensing for the detection of fault lineaments, seismic interpretation, and/or 3D visualisation of surface and subsurface data, the careful selection before and the quality check after the calculations, it is an alternative to other methods discriminating vertical fault displacement. Thus it can provide detailed insights into fault histories in time and gives a tool for comparison and correlation along and between individual faults.



## **5    Synthesis I - Wedge Top Phase**

---

This chapter is based on: Hölzel, M., Decker, K., Zámolyi, A., Strauss, P., Wagneich M. (submitted 2008). Lower Miocene structural evolution of the central Vienna Basin (Austria). Marine and Petroleum Geology.



### **5.1 Abstract**

The tectonic evolution of the Vienna Basin overlying the Alpine-Carpathian fold and thrust belt includes two stages of distinct basin subsidence and deformation. The earlier phase contemporaneous with thrusting of the Alpine-Carpathian floor thrust is related to the formation of a wedge-top basin (“piggy-back”), which was connected to the evolving foreland basin (Lower Miocene; c. 18.5 – 16 Ma). This stage is followed by the formation of a pull-apart basin (Middle to Upper Miocene; c. 16 – 8 Ma). Sediments of the latter unconformably overly wedge-top basin strata and protected them against erosion.

Analyses of subcrop data from the central part of the basin focus on the complex stratal geometries and tectonics of the Lower Miocene wedge-top basin. During that period the overriding allochthon is characterised by syntectonic subsidence and sedimentation, out-of-sequence fold-thrusting, normal faulting and sinistral wrenching. All types of faults are dated as Lower Miocene by the occurrence of growth strata and the age of overlying post-tectonic sediments related to the pull-apart basin stage. Faults mapped in 3D seismic are compared to faults along the SW margin of the Vienna Basin. They prove that complex Lower Miocene deformation occurred in large parts of the Austroalpine overriding nappes concurrent with thrusting at the Alpine floor thrust and in the Molasse unit.

The structural analysis of 3D seismic data shows that Lower Miocene sediments of the Ottnangian and Karpatian stage unconformably overly the Alpine-Carpathian thrust nappes with a thickness of up to 1500 m. Geometries include onlaps to the basin floor, internal unconformities and toplaps to the overlying Middle Miocene sediments. These toplaps are the results of tilting and subsequent erosion of the sediment pile by out-of-sequence thrusting in the central part at the Karpatian-Badenian transition (c. 16.3 Ma) prior to the onset of pull-apart deformation.

## 5.2 Introduction

The Vienna Basin is interpreted as a thin-skinned pull-apart structure on top of the thrust sheets of the Eastern Alps and Western Carpathians (Royden, 1985; Wessely, 1988; Brix and Schultz, 1993; Lankreijer et al., 1995; Decker, 1996; Decker and Peresson, 1996), which developed as a result of lateral escape of the Eastern Alps along the Vienna Basin Transfer Fault (Fig. 5.1; Fig. 5.2; Ratschbacher et al., 1991; Peresson and Decker, 1997). It covers an area of some 5000 km<sup>2</sup> and includes up to 5.5 km thick Miocene sediments.

Tectonics, subsidence and sedimentation in the basin are characterised by two distinct stages, which are referred to as a Lower Miocene piggy-back stage (Seifert, 1992; Peresson and Decker, 1997) and a subsequent Middle to Upper Miocene stage of pull-apart basin formation at the sinistral Vienna Basin Transfer Fault. Basin subsidence and sedimentation terminated during a compressional phase in the Upper Miocene (Decker and Peresson, 1996).

Lower Miocene sedimentation in the Vienna Basin and the half grabens NW of it (Fig. 5.3) occurred contemporaneously with both, the development of a foreland basin system in the Molasse unit north of the Alpine-Carpathian orogen (Kapounek et al., 1965) and N- to NW-directed thrusting of the Alpine-Carpathian allochthon over the European foreland (Linzer et al. 2002; Zámolyi et al., 2008). In the Vienna Basin, Lower Miocene sedimentation (Eggenburgian to Lower Badenian, c. 18 - 16 Ma) post-dates Cretaceous to Palaeogene folding and thrusting of the Penninic and Austroalpine units. Strata overly older rocks with a marked angular unconformity. Fluvatile, deltaic and other shallow-marine sediments reach up to 1.5 km thickness. Facies distribution and paleogeographic reconstructions (Seifert, 1992) indicate that the area of Lower Miocene exceeded the present limits of the Vienna Basin. North-West of the Vienna Basin other remnants of the wedge-top deposition zone, which now are separated from the pull-apart, occur in several halfgrabens. The oldest sediment infill there has Karpatian age (Harzhauser and Wessely, 2003). The halfgrabens are bordered by Middle to Upper Miocene normal faults in the NW.

Isolated occurrences of Oligocene and Lower Miocene deposits indicate that sediments of that age may have been deposited on large parts of the Austroalpine thrust sheets (Frisch et al., 1998). Due to post-Lower Miocene uplift and erosion, however, remnants are only locally preserved in so-called intramontaneous basins (Sachsenhofer et al., 2000; Strauss et al., 2001; Sachsenhofer et al., 2003; Gruber et al., 2004; Hölzel and Wägrich, 2004). These basins are all located at releasing segments of major strike-slip faults (Ratschbacher et al., 1991) giving rise to a continuing discussion as whether these basins are small fault-controlled structures, or being remnants of a much larger wedge-top basin, which survived erosion due to Middle Miocene divergent strike-slip faulting.

Preservation of Lower Miocene strata in the Vienna Basin is due to the formation of the Middle to Upper Miocene (Badenian to Pannonian; c. 16 – 7 Ma) pull-apart basin, which is superimposed on the older basin. Fault patterns in the pull-apart and at the basin margin depict NNE-oriented extensional duplexes (Decker and Peresson, 1996) associated with substantial horizontal extension and normal faulting on NNE-striking faults, which lead to rapid basement

subsidence of up to 1500 mm/Ma (Lankreijer et al., 1995; Hölzel et al., 2008b) . The Lower Miocene strata underlie a huge part of this younger basin extending over some 3300 km<sup>2</sup> (Fig. 5.3). This situation provides a unique opportunity to identify and analyse Lower Miocene tectonic structures, which displace the strata of the wedge-top basin but terminate upwards below the Middle Miocene growth strata of the pull-apart. Such detailed investigations of the Lower Miocene deformation within the overriding Alpine thrust units are not possible in other parts of the Eastern Alps. The current study therefore focuses on analysing Lower Miocene kinematics and determining fault ages from growth strata, stratigraphic ages of deformed sediments and cross-cutting relations. The resulting structural data are finally compared to outcrop data from the basin margin. Data allows a precise assessment of the deformation of the overriding Penninic-Austroalpine thrust sheets, which occurred contemporaneously with thrusting over the foreland basin and the European margin.

### ***5.3 Techniques and working area***

The presented work integrates structural data from seismic, surface outcrops, facies analyses and well data. The main database is a 3D seismic cube covering 1175 km<sup>2</sup> (Seyring-Matzen-Dürnkrot, SB1), including the oil- and gas fields Aderklaa, Schönkirchen and Matzen explored by OMV-Austria (Kreutzer, 1986; Fuchs and Hamilton, 2006). It covers the area between the northern city limits of Vienna and the Austrian-Slovak-Czech border with a recording time of 4000 ms TWT (Two-Way-Traveltime; corresponding to about 7 km depth). This dataset is supplemented by 2D seismic lines in the Marchfeld area SE of SB1 (in the following referred to as SB2). About 40 boreholes are used in the seismic projects. Four Lower Miocene horizons have been picked and interpolated, which supplement four horizons available from OMV Austria. Horizons were selected because of their significant high amplitudes or because they mark a stratigraphic unconformity. About 40 faults were mapped as fault surfaces along inlines, crosslines and random lines with a spacing of 125 m. A covariance data set of the 3D cube allowed better detection and spatial reconstruction of fault traces in timelines (horizontal slices with a spacing 20 ms TWT), which could not be located just in vertical sections.

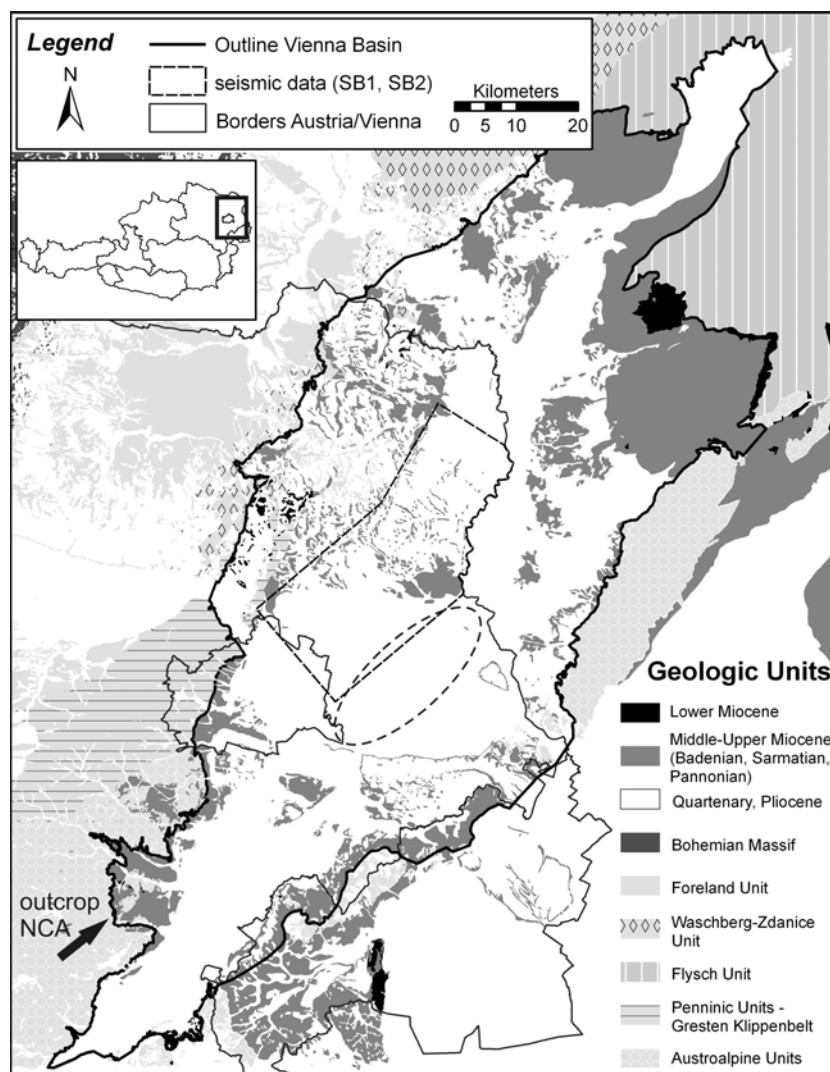


Fig. 5.1: Position of the Vienna Basin at the transition of the Eastern Alps to the Western Carpathians. The rectangle marks the 3D seismic data set (SB1) and the ellipse surrounds the area covered by 2D seismic data (SB2). The arrow points to the surface outcrops presented in this chapter.

The resulting precise data allows distinguishing the pre-Neogene basin floor, which is mainly built up by lithified carbonates of the Austroalpine units. Due to the lithological properties of these rocks seismic images from the pre-Neogene basin floor are rather bad and noisy. The basal unconformity of the basin fill above these Austroalpine rocks (top basin floor) is mapped in seismic due to the very high impedance contrast associated with that surface. The paleorelief and structural features deforming the basin floor therefore could be reconstructed. The main feature, an uplifted basement high, lies in the centre of SB1 and is locally referred to as Spannberg Ridge (Fig. 5.1; Fig. 5.2). The Middle to Upper Miocene growth faults of the Seyring-Bockfliess and Steinberg Faults are dominating the area in the SW to NW part of SB1. Southeast of the Steinberg Fault, SW-dipping layers have been tilted by Middle Miocene

rollover in the hanging wall of the Steinberg Fault. The sediments of the wedge-top zone are deposited at the flanks of the Spannberg Ridge. They are cut by the Upper Miocene Markgrafneusiedl Fault (Fig. 5.2), which is a very young and still active element in the Vienna Basin (Chwatal et al., 2005; Beidinger et al., 2008). Fault interpretations derived from the subcrop are supplemented with kinematic data obtained from outcrops at the SW margin of the Vienna Basin (Fig. 5.1).

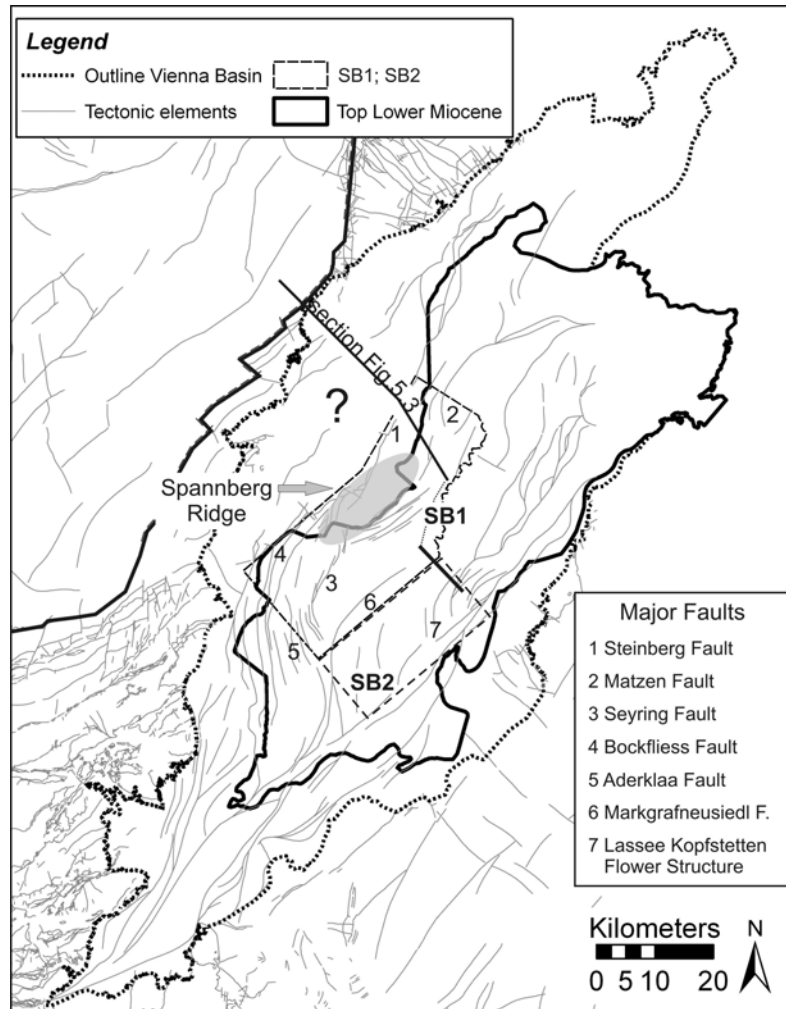


Fig. 5.2: Distribution of Lower Miocene strata. Data has been compiled from the map of the pre-Neogene top of the basin floor (Kröll and Wessely, 1993), from the isopach map of the distribution of the Bockfliess Member in the part of former Czechoslovakia (Spicka, 1967), from cross sections through the basin in the Czech part (Picha et al., 2006), from seismic data in the Austrian part based on own interpretations along with data compiled by OMV, and information from literature (Jiricek and Tomek, 1981; Harzhauser et al., 2002; Harzhauser and Wessely, 2003; Kovac et al., 2004).

### 5.4 Stratigraphy, marker horizons and time constraints

The investigations concentrate on the Lower Miocene sediments of the wedge-top basin below the Middle Miocene fill of the pull-apart basin (Fig. 5.3). The oldest sediments occur in isolated basins and form onlaps on the pre-Neogene topography. These deposits are not well dated. In the Austrian part of the central Vienna Basin they are of Ottnangian age (Bockfliess Mb., c. 18 Ma). Eggenburgian stratigraphic ages are recorded from other parts of the wedge-top basin such as the Korneuburg Basin (Harzhauser et al., 2002; Harzhauser and Wessely, 2003; Wessely, 2006) or the Slovak part of the Vienna Basin (Kovac et al., 2004).

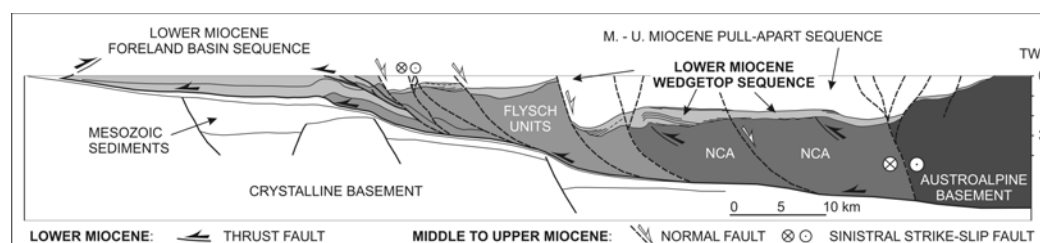


Fig. 5.3: Cross section through the Vienna Basin indicating the distribution of Lower Miocene wedge-top basins at the thrust sheets of the Eastern Alps. They are covered by Middle- to Upper Miocene sediments of the pull-apart of the Vienna Basin.

The top boundary of the Lower Miocene wedge-top sediments corresponds to an erosional unconformity easily mapped in seismic (horizon UK4 TK, Fig. 5.5). Seismic reflectors at this boundary show a very high impedance contrast (Fig. 5.4)

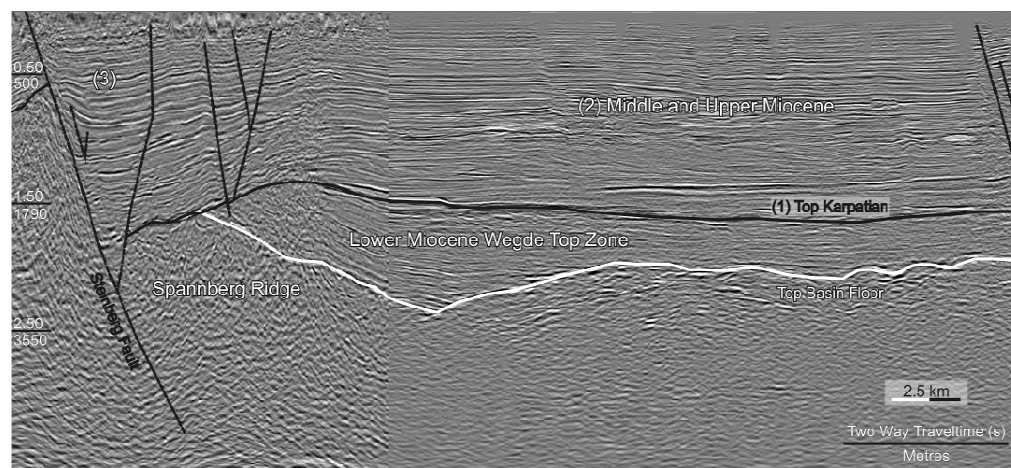


Fig. 5.4: Seismic section across the central Vienna Basin. Lower Miocene sediments overlie pre-Neogene basement with an angular unconformity. (1) The top of the Lower Miocene panel is marked by an erosional unconformity (2) separating it from Middle to Upper Miocene pull-apart basin fill. (3) Growth strata at the Steinberg fault are related to Badenian-Pannonian normal faulting.

Eight Lower Miocene horizon surfaces in the 3D seismic data are mapped, either within stratigraphic units or at formation tops. This procedure results in a detailed lithostratigraphic resolution of the studied time interval of about 2 Ma, which is used to put time constraints on the tectonic activity concurrent with wedge-top basin sedimentation. Tectonic analyses of the

structures in the underlying Austroalpine nappes and the Lower Miocene sediments are discussed in detail in the chapter 4. The formations deposited between c. 18 - 16 Ma are the Bockfliess Member, the Gänserndorf Member, the Aderklaa Formation and the Aderklaa Conglomerate Member (Fig. 5.5). They comprise deltaic, fluvial, braided river and limnic clastic sediments (Kreutzer, 1993; Weissenböck, 1996; Kovac et al., 2004), including mud- and sandstones up to conglomerates or breccias. Figure 4 shows the timeframe of sediment deposition and tectonic activity of the wedge-top basins for area SB1 in detail.

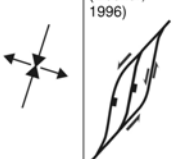
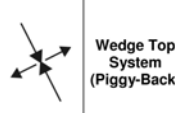
Time of Tops (Ma)	Classical Stages	Central Paratethys Stages	Reference horizons (SB1)	Central Vienna Basin			Regional stress field	
				Unit - Name	Lithology	Environment		
7.8	Tortonian	Upper Pannonian					→←	<b>Compressive</b> (Peresson & Decker, 1997)  Decker, 1996; Fodor, 1995
10		Middle Pannonian					↔	
10.5		Lower Pannonian					↔	
11.6	Serravallian	Upper Sarmatian						<b>Pull-Apart</b> (Decker, 1996) 
12.2		Lower Sarmatian						
12.7	Langhian	Bulimina-Rotalia Zone						
13.6		Spiroplectamina Zone						
14.2		Upper Lagenidae Zone						
14.5		Lower Lagenidae Zone						
16.1	Burdigalian	Aderklaa Conglomerate	B1-TAC	<b>Aderklaa Conglomerate Mb.</b>	gravel, cobble, conglomerate, no fossils	braided river system		
16.3		Upper Karpatian	UK4-TK UK3 UK2 UK1	<b>Aderklaa Fm.</b>	sandstone	meandering river, delta		<b>Wedge Top System (Piggy-Back)</b> 
16.9		Lower Karpatian	LK1-GF	<b>Gänserndorf Mb.</b>	sandstone, mudstone, conglomerate, breccias	meandering river system		
17.2			O3-TB	<b>Bockfliess Mb.</b>	sandstone, mudstone	meandering river system		
(17.2)			O2					
17.5		Oltangian	O1	?				
18.3		Eggenburgian		?				
	Aquitainian							

Fig. 5.5: Stratigraphic overview of the Vienna Basin fill. Time axis not to scale. Compilation of: (Kreutzer, 1993; Weissenböck, 1996; Gradstein and Ogg., 2004; Kovac et al., 2004; Piller et al., 2004)

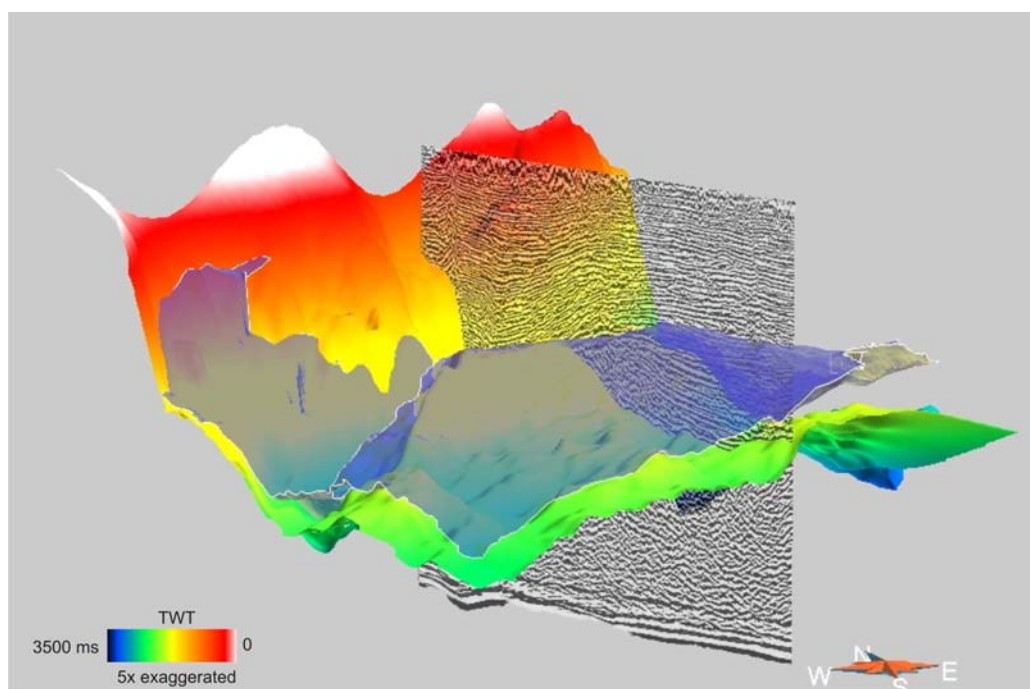


Fig. 5.6: 3D image of the basement high Spannberg Ridge including part of section Fig. 5.4. The lower surface correlates to the top basin floor, the upper one to the top of the Karpatian (UK4-TK; Fig. 5.5).

#### 5.4.1 Ottnangian: Bockfliess Formation (horizons O1, O2, O3-TB)

Eggenburgian (?) to Ottnangian sediments (O1, O2) fill up the pre-Neogene palaeo-relief and terminate with onlaps at the borders of small-scale subbasins in the area SE of the Spannberg Ridge. The upper parts of the Ottnangian are eroded due to the uplift of the Spannberg Ridge (Fig. 5.4; Fig. 5.6). The Bockfliess Member is part of the Ottnangian succession. The top of the member approximately coincides with the Ottnangian-Karpatian stage boundary (c. 17.5 Ma; Fuchs, 1990, unpublished results). The Bockfliess Mb. includes progradational prodelta and delta front sediments (Sauer and Kuffner, 1997; unpublished results) deposited in a regressive regime related to the uplift of the Alpine units (Weissenböck, 1996).

The horizon O3-TB, which represents the top of the Bockfliess Mb., extends significantly further to the SE than older horizons. It covers both flanks of the Spannberg Ridge and only shows onlaps on the basin floor in the southern part of SB1. The layer continues concordantly to the former relief. In the SE part of SB2 the horizon is cut by the Middle to Upper Miocene negative flower structure of the Lasse-Kopfstetten strike-slip fault. In the SW part of SB1 the horizon terminates at the NW dipping Bockfliess Fault (Fig. 5.2). The sharp linear contact SE of the Spannberg Ridge is the result of erosion at the top of the ridge. The cut-off trends parallel to the ridge crest. An angular unconformity between the Ottnangian and Karpatian sediments (top of the Bockfliess Mb.) as proposed by Weissenböck (1996) could not be confirmed in SB1.

#### 5.4.2 Lower Karpatian: Gänserndorf Formation (horizon LK1-GF)

The Gänserndorf Formation is dated to the Lower Karpatian stage (17.5 – 16.9 Ma). Mapped strata are concordant with the underlying horizons and show very similar internal geometry to horizon O3-TB. The formation consists of sandstones, conglomerates, claystones and evaporitic layers deposited in a fluvial and delta plain environment of rivers flowing from N to S (Jiricek and Seifert, 1990). Strata geometries within SB1 accordingly show a sediment migration direction from NE to SW (Fig. 5.7).

#### 5.4.3 Upper Karpatian: Aderklaa Formation (horizons UK 1, UK2, UK3, UK4-TK)

The Upper Karpatian Aderklaa Formation includes sandstones and shale successions from delta complexes with intercalated terrestrial sediments (Jiricek and Seifert, 1990). Upper Karpatian strata are difficult to correlate along the strike of the Spannberg Ridge, because layers are truncated by erosion at the top of the ridge. Horizons NE of the ridge are concordant to layers of the Lower Karpatian and show toplaps to the top Karpatian surface (UK4-TK). Several horizons within the Aderklaa Fm. show both onlaps on deeper horizons and toplap features to the top Karpatian.

SW of the Spannberg Ridge an additional Upper Karpatian horizon has been interpreted (UK2). Strata reach the borders of the SB1 and probably continue into the SB2 area. To the north, strata also form an erosional contact towards the base of the Aderklaa Conglomerate, but in map view the border shows an oblique strike with respect to the trend of the Spannberg Ridge crest (Fig. 5.7).

#### 5.4.4 Karpatian/Lower Badenian: Aderklaa Conglomerate Member (horizon B1-TAC)

The uppermost part of the Lower Miocene is partly marked by an angular unconformity, which is covered by coarse-grained fluvial clastic material with components from the Northern Calcareous Alps (Aderklaa Conglomerate Mb., Jiricek and Seifert, 1990; Rothneusiedl Conglomerate in the southern part of the basin; Wessely, personal communication, 2008). Both the unconformity and the overlying fluvial conglomerates are widespread occurring nearly in the whole Vienna Basin. The angular unconformity is restricted to those parts of the basin, which were subjected to erosion due to the tectonic uplift of basement features and tilting of the sediment pile such as the area adjacent to the Spannberg Ridge.

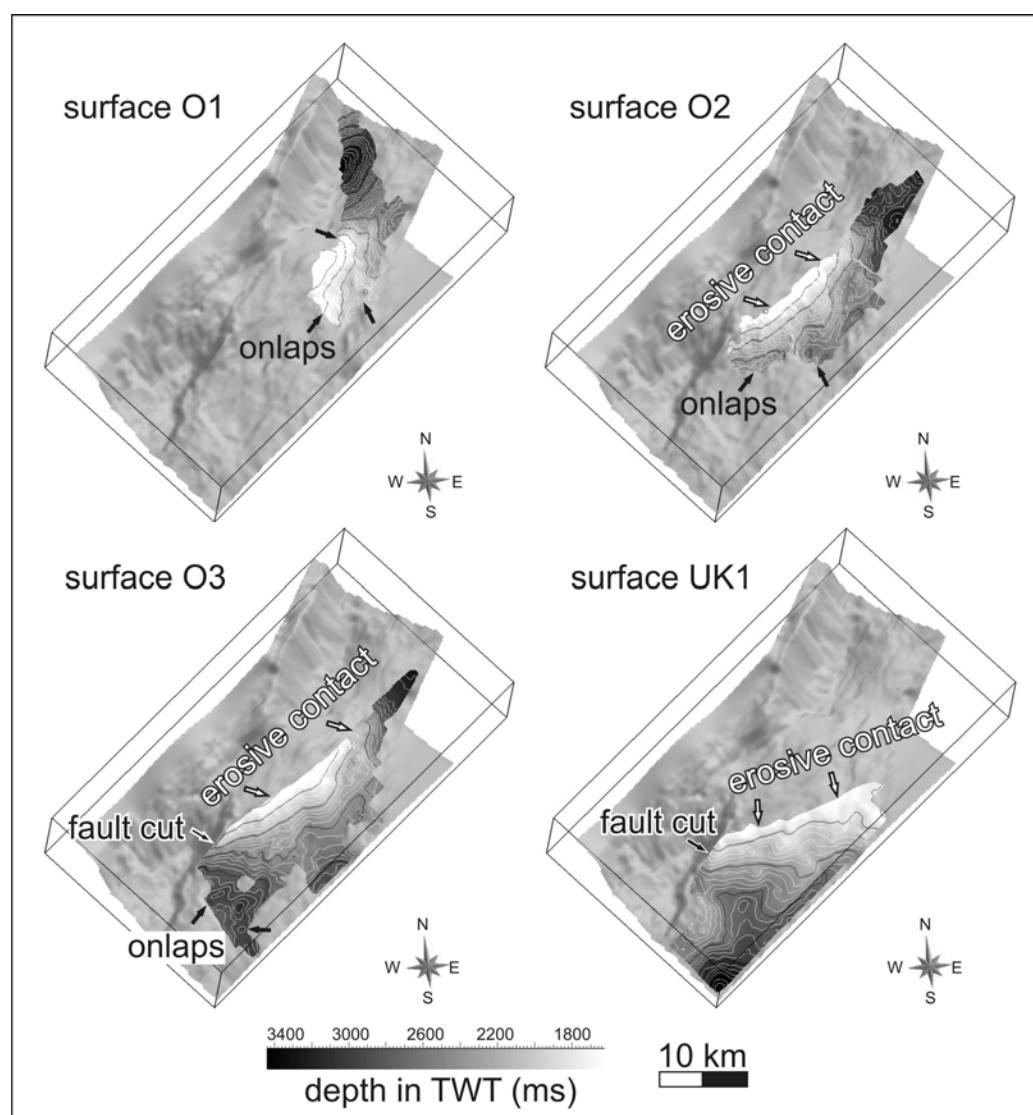


Fig. 5.7: Lower Miocene reference horizons from the 3D seismic cube SB1. Contacts to the underlying basin floor are sedimentary onlaps, contacts to the overlying Middle Miocene unconformity are erosive or fault related.

### 5.5 Tectonic structures in the subcrop

Detailed fault mapping in the 3D seismic volume SB1 revealed 11 major faults with proven Lower Miocene deformation ages (Fig. 5.8; Fig. 5.9). The structural inventory comprises (1) ENE and WSW dipping normal faults with and without growth strata; (2) SE- to ESE-dipping thrust faults with associated fault-propagation folds; and (3) NW-SE-striking sinistral strike-slip faults. All faults displace Lower Miocene sediments and terminate at or shortly above the top Karpatian unconformity (UK4-TK). Several faults are cut by Middle to Upper Miocene faults such as the Aderklaa fault system (Fig. 5.2). Lower Miocene faults are not limited to the central part of the Vienna Basin (Hamilton et al., 1980) although this paper focuses on examples

mapped in the SB1 area. Similar structures also occur in the SB2 area and the Slovak part of the Vienna Basin (Kováč et al., 1989; Marko et al., 1991; Strauss et al., 2006).

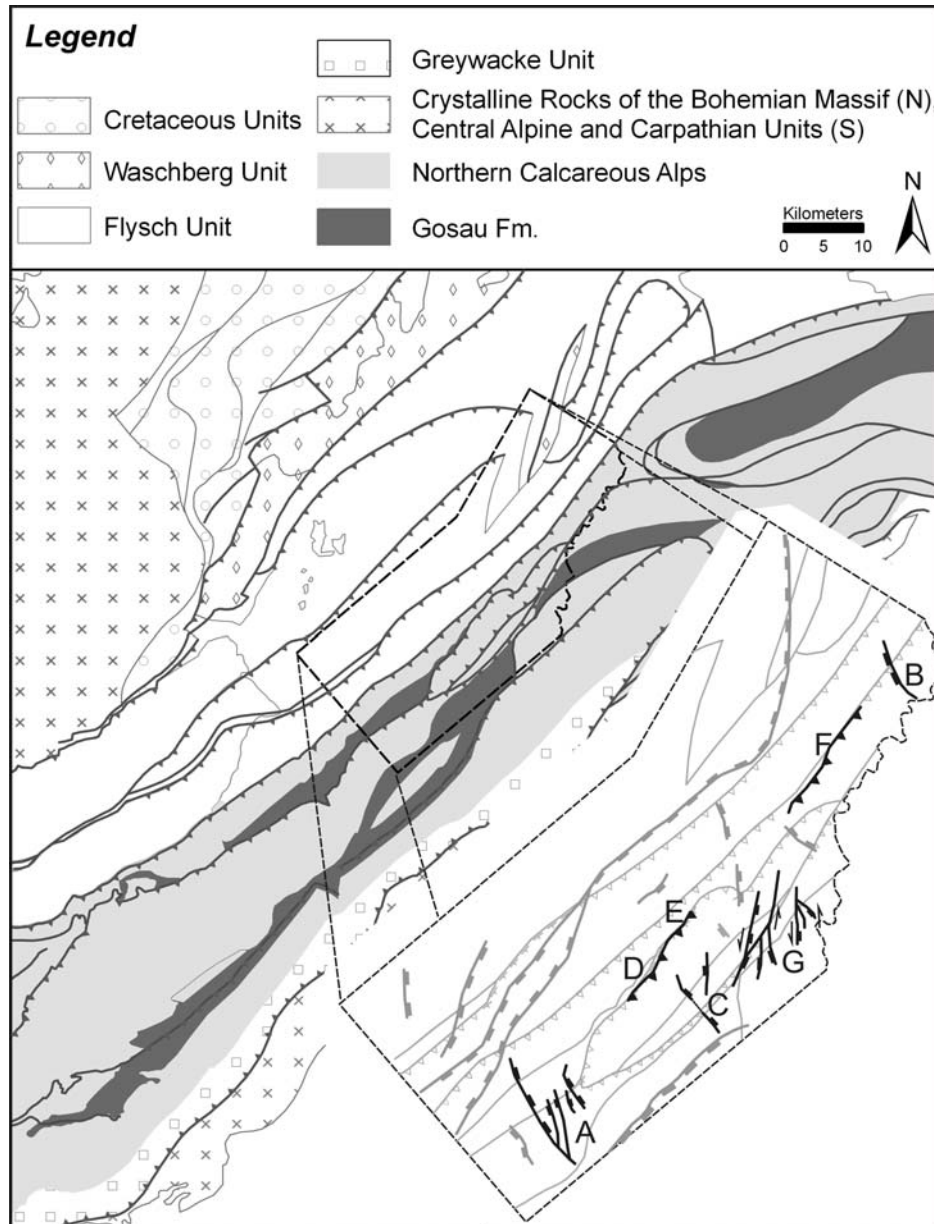


Fig. 5.8: Geological sketch map of the basin floor (Miocene sediments of the Vienna Basin stripped off) modified from the compilation by Kröll and Wessely (1993). The enlarged polygon shows Lower Miocene faults (black, A to G., compare fault list in Fig. 5.9) and Middle to Upper Miocene faults (grey) within the 3D seismic volume SB1. Grey lines with triangles denote pre-Neogene thrusts in the Flysch unit and the NCA.

fault names/groups	fault type	active during/until			displacement of	dip dir/strike dir
		Ottnangian	Karpatian	Middle, Upper Miocene		
A	normal	+	+	Badenian	+	dip dir ENE
B	normal	?	+	Badenian	+	dip dir SW
C	normal	+			+	dip dir NW, E
D	reverse, fault propagation folds	+	+		+	dip dir SE
E	reverse, fault propagation folds	+	+		+	dip dir SE
F	reverse, fault propagation folds	+	+	reactivated as normal fault	+	dip dir SE
G	sinistral strike-slip	+			+	strike dir NW-SE

Fig. 5.9: Summary of Lower Miocene faults within SB1. Their positions are indicated in Fig. 5.8.

#### 5.5.1 Normal faults

Lower Miocene normal faults are ENE- and WSW-directed growth faults delimiting major half grabens filled with Lower Miocene growth strata (Faults A, B and C; Fig. 5.9). Faults have vertical displacements of up to 400 ms TWT (Two-Way-Traveltime; c. 780 m). Growth strata are identified from different thicknesses of stratigraphic horizons in the footwall and hanging wall. They mainly occur in the Gänserndorf and Aderklaa Fm. (Fig. 5.10) providing evidence for a Karpatian age of main fault activity, with additional evidence for Ottnangian normal faulting obtained from fault C.

Along fault A Lower to Middle Badenian strata unconformably overlying the Lower Miocene growth strata are of constant thickness providing no evidence for normal faulting during that time interval. The fault, however, apparently was reactivated during the Upper Badenian as shown by hanging wall growth strata. The fault is cut by the Upper Pannonian Aderklaa Fault System (Fig. 5.10).

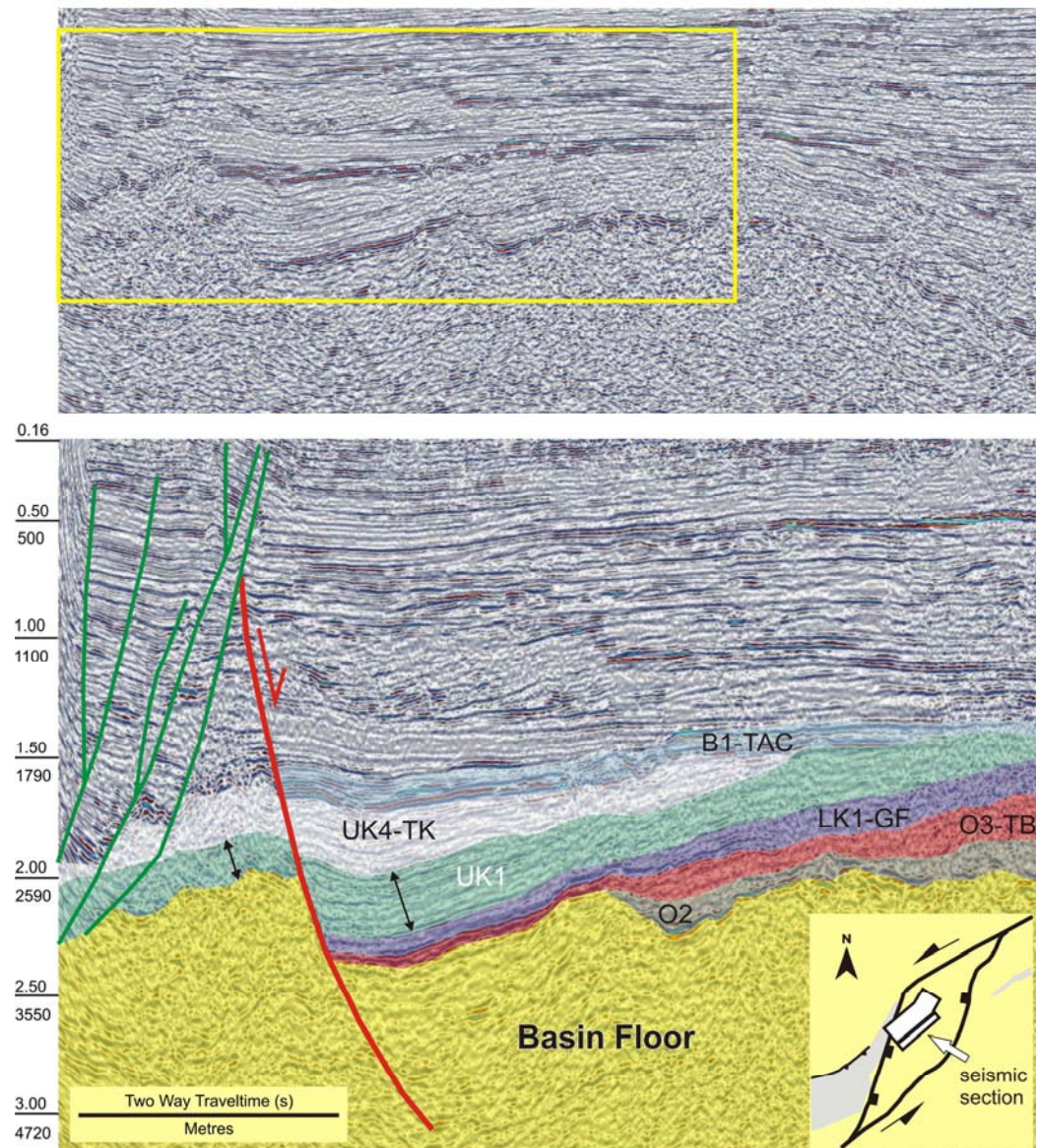


Fig. 5.10: Lower Miocene NE-directed normal growth fault. Note tilting of strata in the hanging wall of the listric fault and growth strata (Gänsersdorf and Aderklaa Fm., arrows) date normal faulting to the Karpatian stage. The fault was re-activated during the Middle Miocene. It is cut by Middle to Late Miocene normal faults of the Aderklaa fault system.

#### 5.5.2 Thrust faults and fault propagation folds

Seismic data highlight Lower Miocene thrust faults at the front of and within the Austroalpine units (Faults D, E and F; Fig. 5.9). Thrusts are striking SW-NE with a thrust direction to NW and are traced over several kilometres each. Otnangian to Karpatian (c. 18 - 16 Ma) sediments overlying these thrusts are folded into fault propagation folds. The end of the thrust event is constrained by the erosional truncation and the transgressive Lower Badenian, which is not affected by folding (c. 16.1 Ma). Thrust fault F marks the floor thrust of the Austroalpine units

over the Flysch Nappes. Data further show that Upper Miocene (Upper Pannonian) normal faults of the Matzen Fault System root in this thrust surface and reactivated it as a normal fault. The thrust faults D and E are associated with the floor thrust of the Göller Nappe within the Austroalpine units (Fig. 5.11).

The existence of another Karpatian thrust fault within the Flysch units is suggested by the geometry of the Spannberg Ridge and by Karpatian growth strata overlying the SE flank of the ridge. Strata are tilted towards the SE and thicken away from the ridge crest (Fig. 5.11). These growth strata are deformed by the fault propagation fold at faults D and E providing local evidence for a back-breaking thrust sequence in the Lower Miocene.

Middle to Upper Miocene strata covering the antiform of the Spannberg Ridge act as an additional time constraint for dating thrusting in front of the ridge. Figure 12 shows a strike line cutting the NW flank of the Spannberg Ridge. The Middle Miocene sediments (Badenian to Sarmatian; c. 16.1 to c. 12 Ma) overlying basement rocks and Karpatian strata mimic growth strata with sediment thicknesses increasing at both flanks of the ridge. The orientations of the axial surfaces of the Miocene anticline overlying the ridge, however, clearly define these sediments as drape sequence post-dating the formation of the Spannberg ridge. Axial surfaces within sediments draping the pre-existing topographic feature dip away from it. In contrast, axial surfaces of growth strata should dip towards the structural high (Shaw et al., 2005). The Middle Miocene sediments therefore form a drape sequence over the Spannberg Ridge. It is consequently deduced that the timing of ridge formation by out-of-sequence thrusting pre-dates the Karpatian/Badenian boundary (16.3 Ma).

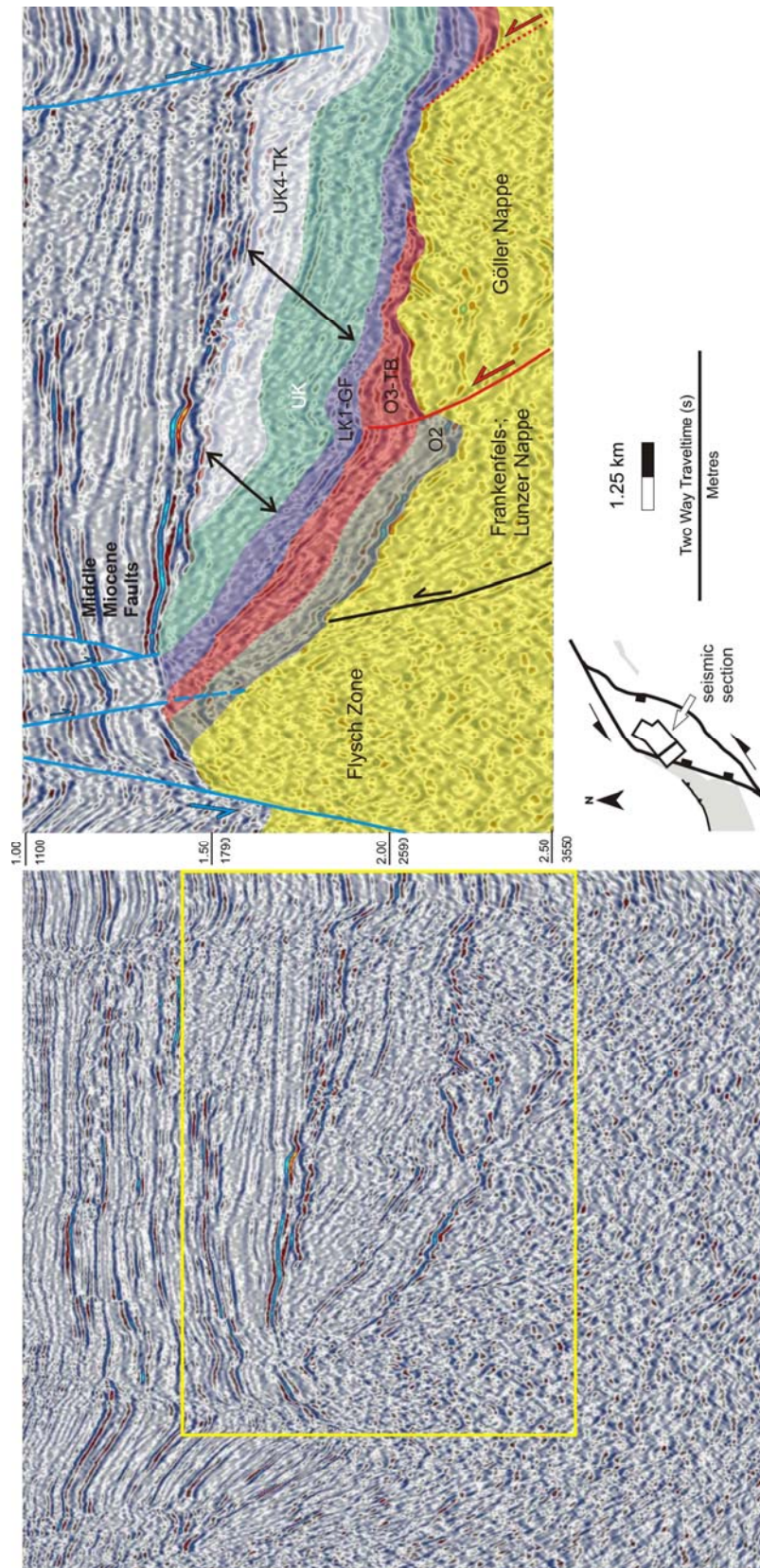


Fig. 5.11: Seismic section across the Spannberg ridge, central Vienna Basin. The tilted Lower Miocene growth strata at the SE flank of the basement high thicken away from the ridge. Strata show toplaps onto the Middle Miocene unconformity.

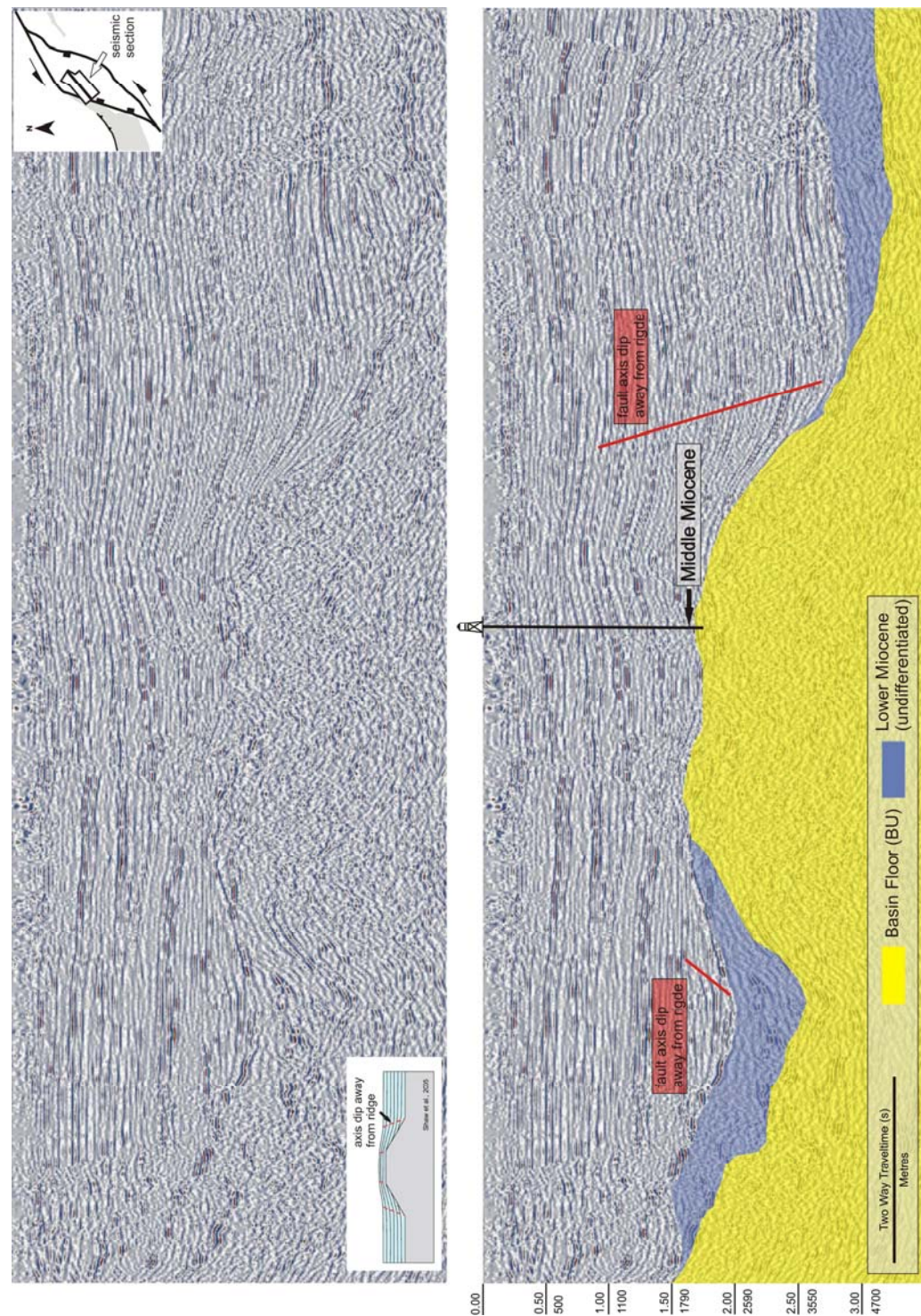


Fig. 5.12: Seismic line paralleling the strike of the Spannberg Ridge showing a drape sequence of Middle and Upper Miocene sediments over the basement high. Axial surfaces of the drape sequence dip away from the basement high. This helps to distinguish the succession from growth strata and indicates that the ridge formed prior to the Middle Miocene.

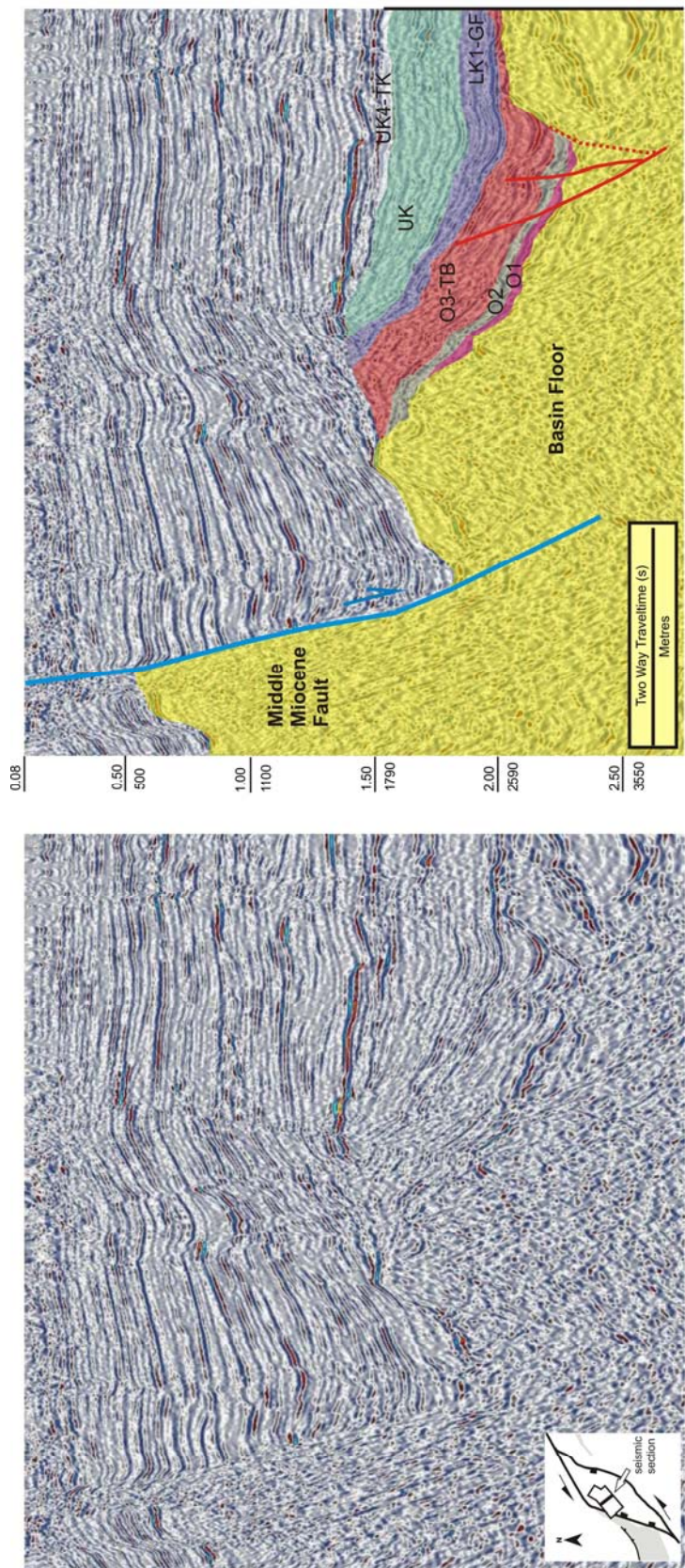


Fig. 5.13: Seismic cross line cutting the Spannberg Ridge, in the middle of SB1. Sediment is dissected by strike-slip faults of a sinistral flower structure with a length of c. 9 km.

### *5.5.3 Strike-slip faults*

Thrusting occurred contemporaneously with strike-slip faulting in the Northern Calcareous Alps (Göller Nappe) south of the thrust surfaces D and E. Seismic data depict fault zone G with numerous NNE-striking en-echelon fault splays, which root in a common NE-striking master fault. The fault zone is traced over a distance of 9 km along strike (Fig. 5.8). Fault geometries in 3D and cross sections resembling typical flower structures strongly suggest sinistral strike-slip faulting.

This kinematic interpretation is corroborated by fault mapping in the Northern Calcareous Alps SW of the Vienna Basin showing several major ENE-striking sinistral wrench faults. In the outcrops these faults are dated pre-Middle Miocene as they are cut by the boundary faults of the Vienna pull-apart basin, which formed during the Middle to Upper Miocene (< 16.1 Ma).

### **5.6 Early Miocene fault kinematics derived from outcrop data**

Fault kinematic data can be derived from the Northern Calcareous Alps (NCA) exposed at the SW margin (Fig. 5.1; Fig. 5.14). Outcrops are located in the same tectonic units, which form the pre-Neogene basin floor of the Vienna Basin. Analyses focus on outcrop analogues of the floor thrust of the Göller Nappe, which proved a Lower Miocene out-of-sequence thrust by seismic interpretation (Faults D, E; Fig. 5.9). Data from the contact indicate complex Lower Miocene deformation history with older NW-directed shortening overprinted by younger sinistral wrenching. Evidence for out-of-sequence thrusting at the outcropping thrust comes from contacts with younger sediments overlying older ones and by strata derived from tectonic units in the footwall of the NCA (Wessely, 2006). The youngest deformed sediments date the contact as post-Late Eocene (Peresson and Decker, 1997). The upper time constraint is given by crosscutting Badenian to Pannonian strike-slip faults, which correlate to the pull-apart formation of the Vienna Basin.

Lower Miocene ENE- to NE-striking sinistral faults mapped in outcrops S of the Göller Nappe occur at the same structural position as the sinistral wrench fault G mapped from seismic (Fig. 5.8). Outcrop faults include convergent strike-slip duplexes of about 1 to 5 km length. Branch faults display convex-up geometries and oblique-reverse slip typical for convergent flower structures. Cross-cutting relations date these faults as pre-Middle Miocene as well (Fig. 5.14).

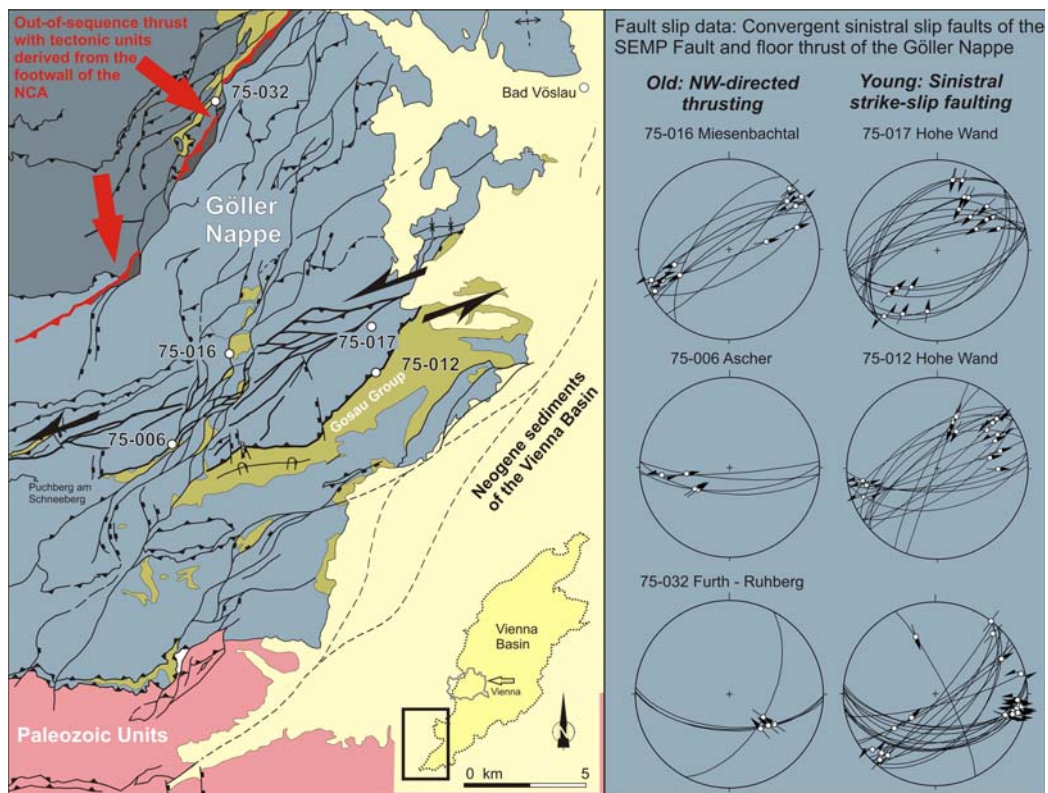


Fig. 5.14: Tectonic sketch map of the NCA adjacent to the Vienna Basin highlighting the Lower Miocene faults. Arrows indicate out-of-sequence thrusting at the floor thrust of the Göller Nappe, which is inferred from young-over-old contacts and the occurrence of tectonic units derived from the footwall of the NCA. Lower Miocene ENE-striking sinistral wrench faults are dissected by NNE-striking Middle to Upper Miocene faults. Fault data plots are Schmidt's net lower hemisphere projections.

### 5.7 Evolution of the Lower Miocene wedge-top zone

Seismic mapping of Lower Miocene strata and faults in the central part of the Vienna Basin in Austria show wedge-top basins filled up with sediments, which unconformably overlie the Alpine-Carpathian thrust nappes. They comprise Ottnangian to Karpatian strata including the Bockfliess-, Gänserndorf- and Aderklaa Fm. The sediment pile reaches a maximum thickness up to 1500 m and tapers towards the hinterland. It is characterised by predominantly fluvial sediments deposited during and progressive deformation. In the northern part of the Vienna Basin (Slovakia, Czech Republic) the succession contains several unconformities (Kovac et al., 2004), which could not be found in the Austrian part. The Lower Miocene basins underwent significant erosion due to tilting at the end of the Karpatian (c. 16.3 Ma), and later tectonic dissection by the major Middle to Upper Miocene normal faults. Figure 15 summarises tectonic activity and sedimentation for the Lower Miocene in the central Vienna Basin.

Time (Ma)	Paratethys stages		Reference horizons from seismic	Lithostrati- graphic Units	Sedimentary Structures	Tectonic Structures		Development in relation to the uplift of the Spann- berg Ridge
	Badenian			Aderklaa Conglomerate	Drape			post
16.3	Karpatian	Upper Karpatian	UK4-TK	Aderklaa Fm.	Drape ?	Fault Propagation Folds		syn
					Erosion of Lower Miocene sediments			
					Growth folds in tilted sediments	NE-directed extensional growth faulting	Sinistral strike-slip faulting	
					Growth strata related to faulting			
16.9		Lower Karpatian	LK1-GF	Gänsersdorf Mb./Fm.			prae	
17.2	O3-TB							
(17.2)	O2		Bockfliess Mb.					
17.5		O1			within SE subbasins			

Fig. 5.15: Summary table indicating the timing of Lower Miocene deformation in the Vienna Basin. Syntectonic deformation of the wedge-top strata in parts of the basin occurred throughout the Karpatian stage. Note the evidence for different timing of out-of-sequence thrusting in front of the Spannberg Ridge (right column) and thrusting in the NCA southeast of it.

There is no regularity within the wedge-top basin shapes or types of borders. It has been generally accepted that basins have preferred axes trending WSW-ENE, bordered by strike-slip faults or oriented along normal faults. We propose that the wedge-top basins show no preferred orientation, in deeper parts they seem to be isolated, but depocentres merge with time. The controlling factors are erosion of thrust units building up an initial palaeo-relief, thrusts within these units concerning parts of the Lower Miocene sediment pile and syntectonic normal faults with preferred dips to SW and NE.

Structural subcrop data from the basin centre and outcrop data from the SW margin prove significant deformation of the Austroalpine overriding nappes during the Lower Miocene.

Structural features mapped in seismic include ENE- and WSW-directed normal faults. Their fault blocks show growth strata reflecting the main phase of activity in the Karpatian.

Thrust surfaces were mapped within the basin floor. Lower Miocene sediments are overlying the thrusts, which are folded into fault propagation folds. Thrusting occurred during the Karpatian as constrained by the age of deformed sediments and the undeformed Aderklaa Conglomerate (Lower Badenian, base at c. 16.3 Ma). Data from the eastern parts of SB2, however, indicates that fault propagation folding also affected Lower Badenian strata. Thrusts provide evidence for the reactivation of major thrust contacts and for out-of-sequence thrusting of the Austroalpine units contemporaneous with thrusting in the foreland Molasse basin. We suggest that a major out-of-sequence thrust in the Waschberg- or Flysch units in front of the Austroalpine units resulted in tilting of the wedge-top strata and their partial erosion adjacent to the Spannberg Ridge. A distinct thrust surface responsible for these motions, however, could not be detected in seismic so far.

Thrusting occurred contemporaneously with strike-slip faulting south of the front of the NCA. Seismic data depict a fault zone with numerous NNE-striking en-echelon splay faults, which root in a common NE-striking master fault with 9 km length. Fault geometries and cross sections resemble flower structures and suggest sinistral movement. This kinematic interpretation is corroborated by fault mapping within the NCA at the SW margin with major ENE-striking sinistral wrench faults. They are dated pre-Middle Miocene as they are cut by the boundary faults of the pull-apart basin, which evolved from the Badenian on.

The Lower Miocene succession of the Vienna Basin is classified as a wedge-top depozone (DeCelles and Giles, 1996), which overlies the frontal parts of the Alpine-Carpathian orogenic wedge. This wedge-top (“piggy-back”) basin together with the Molasse foredeep formed the Alpine foreland basin system. The Vienna Basin wedge-top succession shows typical characteristics of wedge-top basins such as sediment received from the eroding orogenic wedge, dominance of fluvial or deltaic rocks, tapering of the zone and progressive syndepositional deformation (Ori and Friend, 1984; DeCelles and Giles, 1996; Chiang et al., 2004; Clevis et al., 2004).



## **6     Synthesis II - Pull-Apart Phase**



The internal fault surface behaviour during the pull-apart opening of the Vienna Basin was studied in the southern part of the Vienna Basin. Relations can be drawn to the study of Wagreich and Schmid (2002) from the central part.

The combination of subsidence analysis in the southern and central part of the Vienna Basin and the quantification of vertical fault displacement in the southern part showed that distinct phases of fault activity are rare or limited to single fault surfaces.

The southern Vienna Basin area is built up by a highly complex fault system with normal and reverse slip and strike-slip components and vertical block rotations. Individual faults display strong varieties in timing and magnitude of fault movements. Times of high slip rates along faults alternate with times of inactivity or strike slip movement. Mapping and visualisation provides a necessary basis for the exact definition of the fault arrays and the relation between stratigraphic data and geometry of faults surfaces. One essential base for application of sedimentary fault backstripping to a fault system is the knowledge of how fault surfaces are connected and the definition of the total time span, in which a fault has been active, e.g. by using seismic sections.

The largest fault surface in the investigated southern Vienna Basin, the Leopoldsdorf Fault, shows normal slip through Middle to Late Miocene times. Slip rates as high as 700 m/my have been reconstructed. The partly connected negative flower structure shows parts, which were active in alternating sense in the same time intervals. Other fault segments show different character with reverse movement. Because of kinematic linkage no continuous slip over fault surfaces could be detected.

Wagreich and Schmid (2002) could show that fault senses are also changing through time at a transect through major faults of the central Vienna Basin. For the Middle to Late Miocene rates are also up to 700 m/my, but show no significant peaks. Only in the Sarmatian a zone of higher tectonic activity could be detected. This is in coherence with the additional subsidence data from my study area (Chapter 2). A relation to the Styrian Basin and or regional extensional events may be the explanation. The general trends imply that the major phase of formation started in the Badenian (Upper Lagenidae Zone - Bulimina Rotalia Zone; Middle Miocene).

Some of the backstripped wells show a decrease of subsidence throughout the Miocene, but, due to the intense internal segmentation of the basin, other wells display significant subsidence phases in the Sarmatian and Middle Pannonian also. Regionally or locally, the effects of at least three successive phases of extension, related to the late stage of Alpine-Carpathian orogeny and the ongoing lateral extrusion and Pannonian Basin formation, have been found in the Vienna Basin. This indicates that these tectonically related areas were influenced by each other during basin evolution and indicate that more than one extensional basin phase occurred during the Middle to Late Miocene.

At this point it would be a challenging task to extend the knowledge base to synsedimentary faults, like the Steinberg Fault (normal offset: 5000 m) in the northern part with the awareness that *sedimentary fault backstripping* as a stand-alone method is not suited for the quantification of vertical fault movement. But using supporting methods like remote sensing for the detection

of fault lineaments, seismic interpretation, and/or 3D visualisation of surface and subsurface data, the careful selection before and the quality check after the calculations, it is an alternative to other methods discriminating vertical fault displacement. Thus it can provide detailed insights into fault histories in time and gives a tool for comparison and correlation along and between individual faults.

## **7   References**



- Aydin, A., Schultz, R. A. (1990). Effect of mechanical interaction on the development of strike-slip faults with echelon patterns. *Journal of Structural Geology* 12, 123-129.
- Allen, P. A., Allen, J. R. L. (2005). *Basin Analysis*. Blackwell Scientific Publications, Oxford, 549 pp.
- Baldi, K., Benkovics, L., Sztano, O. (2001). Badenian (Middle Miocene) basin development in SW-Hungary: subsidence history based on quantitative paleobathymetry of foraminifera. *International Journal of Earth Sciences*, 91, 490-504.
- Baldwin, B., Butler, C.O. (1985). Compaction curves. *Bulletin of the American Association of Petroleum Geologists* 69 (4), 622-626.
- Bates, R. L., Jackson, J. A. (1987). *Glossary of Geology*. Alexandria, VA, American Geological Institute.
- Beidinger, A., Decker, K. Roch, K. H. (2008). Combined Geophysical, Geomorphological and Geological Studies at the active Lassee Segment of the Vienna Basin Fault System. YORSGET - International Meeting of Young Researchers in Structural Geology and Tectonics, Oviedo, Spain, *Trabajos de Geologia*, 14.
- Bertram, G.T., Milton, N.J. (1989). Reconstructing basin evolution from sedimentary thickness; the importance of palaeobathymetric control, with reference to the North Sea. *Basin Research* 1, 247-257.
- Billings, M. P. (1942). *Structural Geology*. New York, Prentice-Hall.
- Bond, G. C., Kominz, M. A. (1984). Construction of tectonic subsidence curves for the early Paleozoic miogeocline, southern Canadian Rocky Mountains: Implications for subsidence mechanisms, age of breakup, and crustal thinning. *Geological Society of America Bulletin*, 95, 155-173.
- Boyer, S. E., Elliott, D. (1982). Thrust systems. *AAPG Bulletin*, 66, 1196-1230.
- Brix, F., Schultz, O. (Eds; 1993). *Erdöl und Erdgas in Österreich*. Naturhistorisches Museum, Vienna.
- Bürgmann, R., Pollard, D. D., Martel, S. J. (1994). Slip distributions on faults: effects of stress gradients, inelastic deformation, heterogeneous host-rock stiffness, and fault interaction. *Journal of Structural Geology* 16, 1675-1690.
- Bus, Z., Greneczy, G., Toth, L., Monus, P. (in press.). Active crustal deformation in two seismogenic zones of the Pannonian region - GPS versus seismological observations. *Tectonophysics*.
- Cartwright, J., Bouroulec, R., James, D., Johnson, H. (1998). Polycyclic motion history of some Gulf Coast growth faults from high-resolution displacement analysis. *Geology*, 26, 819-822.
- Chevalier, F., Guiraud, M., Garcia, J.-P., Dommergues, J.-L., Quesne, D., Allemand, P., Dumont, T. (2003). Calculating the long-term displacement rates of a normal fault from the high-resolution stratigraphic record (early Tethyan rifting, French Alps). *Terra Nova*, 15, 410-416.

- Chiang, C.-C., Yu, H.-S., Chou, Y.-W. (2004). Characteristics of the wedge-top depozone of the southern Taiwan foreland basin system. *Basin Research*, 16, 65-78.
- Childs, C., Nicol, A., Walsh, J. J., Watterson, J. (2003). The growth and propagation of synsedimentary faults. *Journal of Structural Geology*, 25, 633-648.
- Clevis, Q., de Jager, G., Nijman, W., de Boer, P. L. (2004). Stratigraphic signatures of translation of thrust-sheet top basins over low-angle detachment faults. *Basin Research*, 16, 145-163.
- Chwatal, W., Decker, K., Roch, K.-H. (2005). Mapping of active capable faults by high-resolution geophysical methods: examples from the central Vienna Basin. *Austrian Journal of Earth Sciences*, 97, 52- 59.
- DeCelles, P. G., Giles, K. A. (1996). Foreland basin systems. *Basin Research*, 8, 105-123.
- Decker, K., Peresson, H., Hinsch, R. (2005). Active tectonics and Quaternary basin formation along the Vienna Basin Transform fault. *Quaternary Science Reviews*, 24, 305-320.
- Decker, K., Peresson, H. (1996). Tertiary kinematics in the Alpine-Carpathian-Pannonian system: links between thrusting, transform faulting und crustal extension. In: Wessely, G. and Liebl, W. (eds.), *Oil and Gas in Alpidic Thrustbelts and Basins of Central and Eastern Europe*. EAGE Special Publication, pp. 69-77.
- Decker, K. (1996). Miocene tectonics at the Alpine-Carpathian junction and the evolution of the Vienna Basin. *Mitteilungen der Gesellschaft der Geologie und Bergbaustudenten in Österreich*, 41, 33-44.
- Decker, K., Peresson, H. (1996). Tertiary kinematics in the Alpine-Carpathian-Pannonian system: links between thrusting, transform faulting und crustal extension. *Oil and Gas in Alpidic Thrustbelts and Basins of Central and Eastern Europe*. in: Wessely, G., Liebl, W., EAGE Special Publication. 5 69-77.
- Einsele, G. (2000). *Sedimentary Basins - Evolution, Facies, and Sediment Budget*. Springer, Berlin, 792 pp.
- Evans, M., Hastings, N., Peacock, B. (2000). *Statistical Distributions*. John Wiley and Sons, 248pp.
- Faber, R., Wagreich, M. (2005). Modelling of topography and sedimentation along synsedimentary faults: WinGeol/SedTec. *Austrian Journal of Earth Sciences* 97, 60-66.
- Flügel, H. W., Walitzi, E. M. (1968). Regelung und Porosität in Tonmergeln des Wiener Beckens. *Neues Jahrbuch für Geologie und Paläontologie, Monatshefte*, 1968, 1-11.
- Fodor, L. (1995). From transpression to transtension: Oligocene-Miocene structural evolution of the Vienna Basin and the East-Alpine-Western Carpathian junction. *Tectonophysics*, 242, 151-182.
- Friedl, K. (1927). Über die jüngsten Erdölforschungen im Wiener Becken. *Zeitschrift Petroleum* 6.
- Friedl, K. (1929). Zur Frage der im Wiener Becken vorhandenen großen Verwerfungen. *Mitteilungen der Österreichischen Geologischen Gesellschaft* 22, 125-132.

- Frisch, W., Kuhlemann, J., Dunkl, I., Brügel, A. (1998). Palinspastic reconstruction and topographic evolution of the Eastern Alps during late Tertiary tectonic extrusion. *Tectonophysics*, 29, 1-15.
- Fuchs, R., Hamilton, W. (2006). New Depositional Architecture for an Old Giant: The Matzen Filed, Austria. in: Golonka, J., Picha, F. J. (Eds.), *The Carpathians and their foreland: Geology and hydrocarbon resources*. AAPG Memoir, pp. 205-219.
- Gallagher, K. (1989). An examination of some uncertainties associated with estimates of sedimentation rates and tectonic subsidence. *Basin Research* 2, 97-114.
- Geiki, A. (1882). *Text-Book of Geology*. London, Macmillan.
- Genser, J., Cloetingh, S. A. P. L., Neubauer, F. (2007). Late orogenic rebound and oblique Alpine convergence: New constraints from subsidence analysis of the Austrian Molasse basin. *Global and Planetary Change*, 58, 214-223.
- Gradstein, F., Ogg, J. (2004). Geologic Time Scale 2004 - why, how, and where next! *Lethaia*, 37, 175-181.
- Gruber, W., Sachsenhofer, R. F., Kofler, N., Decker, K. (2004). The architecture of the Trofaiach pull-apart basin (Eastern Alps); an integrated geophysical and structural study. *Geologica Carpathica*, 55, 281-298.
- Hamilton, W., Wagner, L., Wessely, G. (2000). Oil and gas in Austria. *Mitteilungen der Österreichischen Geologischen Gesellschaft*, 92, 235-262.
- Hamilton, W., Jiricek, R., Wessely, G. (1980). The alpine-carpathian floor of the Vienna Basin in Austria and CSSR. in: Minarikova, D., Lobitzer, H. (Eds.), *Thirty Years of Geological Cooperation Between Austria and Czechoslovakia*. Geologische Bundesanstalt, pp. 45-56.
- Harzhauser, M., Böhme, M., Mandic, O., Hofmann, C.-C. (2002). The Karpatian (Late Burdigalian) of the Korneuburg Basin. A Palaeoecological and Biostratigraphical Synthesis. *Beitr. Paläont.*, 27, 441-456.
- Harzhauser, M., Daxner-Höck, G., Piller, W. (2002). An integrated stratigraphy of the Pannonian (Late Miocene) in the Vienna Basin. *Austrian Journal of Earth Sciences*, 95/96, 6-19.
- Harzhauser, M., Wessely, G. (2003). The Karpatian of the Korneuburg Basin. in: Brzobohaty, R., Cicha, I., Kovac, M., Rögl, R. (Eds.), *The Karpatian - A Lower Miocene Stage of the Central Paratethys*. Masaryk University, pp. 107-109.
- Harzhauser, M., Piller, W. E. (2004). The Early Sarmatian - hidden seesaw changes. *Courier Forschungs-Institut Senckenberg*, 246, 89-111.
- Hills, E. S. (1949). *Outlines of Structural Geology*. London, Methuen.
- Hinsch, R., Decker, K. (2003). Do seismic slip deficits indicate underestimated seismic potential along the Vienna Basin Transform Fault System? *Terra Nova* 15, 343-349.
- Hinsch, R., Decker, K., Peresson, H. (2005a). 3-D seismic interpretation and structural modeling in the Vienna Basin: implications for Miocene to recent kinematics. *Austrian Journal of Earth Sciences* 97, 38-51.

- Hinsch, R., Decker, K., Wagneich, M. (2005b). 3-D mapping of segmented active faults in the southern Vienna Basin. *Quaternary Science Reviews*, 24, 321-336.
- Hohenegger, J., Coric, S., Khatun, M., Rögl, F., Rupp, C., Selge, A., Uchman, A., Wagneich, M. (2008). Cyclostratigraphic dating in the Lower Badenian (Middle Miocene) of the Vienna Basin (Austria): the Baden-Soos core. *International Journal of Earth Sciences*, DOI 10.1007/s00531-007-0287-7.
- Hölzel, M., Wagneich, M. (2004). Sedimentology of a Miocene Delta Complex: The Type Section of the Ingering Formation (Fohnsdorf Basin, Austria). *Austrian Journal of Earth Sciences*, 95/96, 80-86.
- Hölzel, M., Wagneich, M. (2006). Miocene fault activity in the southern Vienna Basin based on fault backstripping. *EGU 2006, Vienna, Geophysical Research Abstracts*, 8, EGU06-A-06999.
- Hölzel, M., Decker, K., Zámolyi, A., Strauss, P., Wagneich, M. (2008). The transition from piggy back to pull-apart in the Vienna Basin (Austria-Slovakia-Czech Republic). *EGU Geophysical Research Abstracts*, 10, EGU2008-A-04689.
- Hölzel, M., Faber, R., Wagneich, M. (2008a). DeCompactionTool: Software for subsidence analysis including statistical error quantification. *Computers & Geosciences*, 34, 1454-14960.
- Hölzel, M., Wagneich, M., Faber, R., Strauss, P. (2008b). Regional subsidence analysis in the Vienna Basin (Austria). *Austrian Journal of Earth Sciences*, 101, 89-98.
- Imber, J., Tuckwell, G. W., Childs, C., Walsh, J. J., Manzonocchi, T., Heath, A. E., Bonson, C. G., Strand, J. (2004). Three-dimensional distinct element modelling of relay growth and breaching along normal faults. *Journal of Structural Geology*, 26, 1897-1911.
- Janoschek, R. (1942). Die bisherigen Ergebnisse der erdölgeologischen Untersuchungen im inneralpinen Wiener Becken. *Oel und Kohle*, 38 (125), 125-149.
- Jiricek, R., Tomek, C. (1981). Sedimentary and Structural Evolution of the Vienna Basin. *Earth Evolution Sciences*, 1, 195-206.
- Jiricek, R., Seifert, P. (1990). Paleogeography of the Neogene in the Vienna Basin and the adjacent part of the foredeep. In: Minarikova, D., Lobitzer, H. (Eds.), *Thirty Years of Geological Cooperation between Austria and Czechoslovakia*. Geologische Bundesanstalt; pp. 89-105.
- Kapounek, J., Koelbl, L., Weinberger, F. (1963). Results of new exploration in the basement of the Vienna Basin. *Sixth WPC, Frankfurt/Main*.
- Keferstein, C. (1828). *Beobachtungen und Ansichten über die geognostischen Verhältnisse der nördlichen Kalkalpenkette in Österreich und Bayern*. Deutschland geognostisch-geologisch dargestellt.
- Kováč, M., Barath, I., Harzhauser, M., Hlavaty, I., Hudackova, N. (2004). Miocene depositional systems and sequence stratigraphy of the Vienna Basin. *Courier Forschungs-Institut Senckenberg*, 246, 187-212.

- Kreutzer, N. (1993). Das Neogen des Wiener Beckens. In: Brix, F., Schultz, O. (Eds), Erdöl und Erdgas in Österreich. Naturhistorisches Museum and Fa. Berger, Vienna, pp. 232-248.
- Lankreijer, A., Kovac, M., Cloetingh, S., Pitonak, P., Hloska, P., Biermann, C. (1995). Quantitative subsidence analysis and forward modelling of the Vienna and Danube basins: thin-skinned versus thick-skinned extension. *Tectonophysics*, 252, 433-451.
- Lankreijer, A. C. (1998). Rheology and basement control on extensional basin evolution in Central and Eastern Europe: Variscan and Alpine-Carpathian-Pannonian tectonics. Amsterdam, Vrije Universiteit 158.
- Leeder, M.R. (1999). *Sedimentology and Sedimentary Basins*. Blackwell Scientific Publications, Oxford, 620pp.
- Le Guerroue, E., Cobbold, P. R. (2006). Influence of erosion and sedimentation on strike-slip fault systems: insights from analogue models. *Journal of Structural Geology*, 28, 421-430.
- Linzer, H.G., Decker, K., Peresson, H., Dell'Mour, R., Frisch, W. (2002). Balancing lateral orogenic float of the Eastern Alps. *Tectonophysics*, 354, 211-237.
- Kapounek, J., Kröll, A., Papp, A., Turnovsky, K. (1965). Die Verbreitung von Oligozän, Unter- und Mittelmiozän in Niederösterreich. *Erdöl-Erdgas-Kohle*, 81, 109-116.
- Kováč, M., Baráth, I., Holicky, I., Marko, F., Tunyi, I. (1989). Basin opening in the Lower Miocene strike-slip zone in the SW part of the Western Carpathians. *Geologica Carpathica*, 40, 37-62.
- Kovac, M., Barath, I., Harzhauser, M., Hlavaty, I., Hudackova, N. (2004). Miocene depositional systems and sequence stratigraphy of the Vienna Basin. *Courier Forschungs-Institut Senckenberg*, 246, 187-212.
- Kreutzer, N. (1986). Die Ablagerungssequenzen der miozänen Badener Serie im Feld Matzen und im zentralen Wiener Becken. *Erdöl-Erdgas-Kohle*, 102, 492-502.
- Kreutzer, N. (1993). Das Neogen des Wiener Beckens. in: Brix, F., Schultz, O. (Eds.), *Erdöl und Erdgas in Österreich*. Naturhistorisches Museum, pp. 232-248.
- Kröll, A., Wessely, G. (1973). Neue Ergebnisse beim Tiefenaufschluß im Wiener Becken. *Erdöl-Erdgas-Zeitschrift* 89, 400-413.
- Kröll, A., Wessely, G. (1993). Wiener Becken und angrenzende Gebiete - Strukturkarte-Basis der tertiären Beckenfüllung. *Geologische Themenkarte der Republik Österreich 1:200 000*.
- Larsen, P.-H. (1988). Relay structures in a Lower Permian basement involved extension system, East Greenland. *Journal of Structural Geology* 10, 3-8.
- Maerten, L., Willemse, E. J. M., Pollard, D. D., Rawnsley, K. (1999). Slip distributions on intersecting normal faults. *Journal of Structural Geology* 21, 259-271.
- Magara, K. (1980). Comparison of porosity-depth relationships of shale and sandstone. *Journal of Petroleum Geology* 3 (2), 175-185.
- Marko, F., Fodor, L., Kovac, M. (1991). Miocene strike-slip faulting and block rotation in Brezovske Karpaty Mts. (Western Carpathians). *Mineralia Slovaca*, 23, 189-200.

- Marton, E., Kuhlemann, J., Frisch, W., Dunkl, I. (2000). Miocene rotations in the Eastern Alps - palaeomagnetic results from intramontane basin sediments. *Tectonophysics*, 323, 163-182.
- McKenzie, D. (1978). Some remarks on the development of sedimentary basins. *Earth Planetary Science Letters* 40, 25-32.
- Metropolis, N., Ulam, S. (1949). The Monte Carlo Method. *Journal of the American Statistical Association* 44, 335-341.
- Miall, A.D. (1999). *Principles of Sedimentary Basin Analysis*. Springer, Berlin, 616pp.
- Morley, C. K. (1995). Developements in the Structural Geology of rifts over the last decade and their impact on hydrocarbon exploration. *Hydrocarbon Habitat in Rift Basins*. in: Lambiase, J. J., Geological Society of London. 80 1-32.
- Nicol, A., Walsh, J. J., Watterson, J., Underhill, J. R. (1997). Displacement rates of normal faults. *Nature*, 390, 157-159.
- Ocamb, R. D. (1961). Growth faults of south Louisiana. *Gulf Coast Association of Geological Societies Transactions*, 11, 139-175.
- Ori, G. G., Friend, P. F. (1984). Sedimentary basins formed and carried piggyback on active thrust sheets. *Geology*, 12, 475-478.
- Peacock, D. C. P., Knipe, R. J., Sanderson, D. J. (2000). Glossary of normal faults. *Journal of Structural Geology*, 22, 291-305.
- Piller, W., Egger, H., Gross, M., Harzhauser, M., Hubmann, B., van Husen, D., Krenmayr, H.-G., Krystyn, L., Lein, R., Mandl, G., Rögl, F., Roetzel, R., Rupp, C., Schnabel, W., Schönlaub, H. P., Summesberger, H., Wagreich, M. (2004). Die Stratigraphische Tabelle von Österreich 2004 (Sedimentäre Schichtfolgen). *Berichte des Instituts für Erdwissenschaften K.-F.-Universität Graz*, 329-330.
- Pitman, W.C., Andrews, J.A. (1985). Subsidence and thermal history of small pull-apart basins. In: Biddle, K. T. and Christie-Blick, N. (Eds.), *Strike-Slip Deformation, Basin Formation, and Sedimentation*. Society of Economic Paleontologists and Mineralogists Special Publication 37, pp. 45-77.
- Peresson, H., Decker, K. (1997). The Tertiary dynamics of the northern Eastern Alps (Austria): changing palaeostresses in a collisional plate boundary. *Tectonophysics*, 1997, 125-157.
- Petraschek, W. (1922). Der geologische Bau des Wiener Beckens. *Berg- und Hüttenmännisches Jahrbuch* 69/70 (H. 4).
- Picha, F. J., Stranik, Z., Krejci, O. (2006). Geology and Hydrocarbon Resources of the Outer Western Carpathians and Their Foreland, Czech Republic. in: Golonka, J., Picha, F. J. (Eds.), *The Carpathians and their foreland: Geology and hydrocarbon resources*. AAPG Memoir, pp. 49-175.
- Ratschbacher, L., Frisch, W., Linzer, H.-G., Merle, O. (1991). Lateral extrusion in the Eastern Alps, 2. Structural analysis. *Tectonics*, 10, 257-271.
- Reid, H. F., Davis, W. M., Lawson, A. C., Ransome, F. L. (1913). Report on the Committee on the Nomenclature of Faults *Geological Society of America Bulletin* 24, 163-186.

- Rowan, M. G., Hart, B. S., Nelson, S., Flemings, P. B., Trudgill, B. C. (1998). Three-dimensional geometry and evolution of a salt-related growth-fault array: Eugene Island 330 field, offshore Louisiana, Gulf of Mexico. *Marine and Petroleum Geology* 15, 309-328.
- Royden, L., Keen, C. E. (1980). Rifting process and thermal evolution of the continental margin of eastern Canada determined from subsidence curves. *Earth and Planetary Science Letters*, 51, 343-361.
- Royden, L. H. (1985). The Vienna Basin: A thin-skinned pull-apart basin. in: Biddle, K., Christie-Blick, N. (Eds.), *Strike slip deformation, basin formation and sedimentation*, Society of Economic Paleontologists and Mineralogists Special Publication, pp. 319-338.
- Royden, L. H., Baldi, T. (1988). Late Cenozoic Tectonics of the Pannonian Basin System. The Pannonian Basin-A Study in basin evolution. in: Royden, L., Horvath, F., AAPG Memoir. 45 1-16.
- Rögl, F. (1996). Stratigraphic correlation of the Paratethys (Oligocene and Miocene). *Mitteilungen der Geologischen Gesellschaft österreichischer Bergbaustudenten*, 41, 65-73.
- Rögl, F. (1998). Palaeogeographic considerations for Mediterranean and Paratethys Seaways (Oligocene to Miocene). *Annalen des Naturhistorischen Museums in Wien*, 99, 279-310.
- Rögl, F., Spezzaferri, S., Coric, S. (2002). Micropaleontology and biostratigraphy of the Karpatian-Badenian transition (Early-Middle Miocene boundary) in Austria (Central Paratethys). *Courier Forschungs-Institut Senckenberg*, 237, 47-67.
- Sachsenhofer, R. F., Lankreijer, A., Cloetingh, S., Ebner, F. (1997). Subsidence analysis and quantitative basin modelling in the Styrian Basin (Pannonian Basin System, Austria). *Tectonophysics*, 272, 175-196.
- Sachsenhofer, R. F., Kogler, A., Polesny, H., Strauss, P., Wagreich, M. (2000). The Neogene Fohnsdorf Basin: Basin formation and basin inversion during lateral extrusion in the Eastern Alps (Austria). *International Journal of Earth Sciences*, 89, 415-430.
- Sachsenhofer, R. F., Bechtel, A., Reischenbacher, D., Weiss, A. (2003). Evolution of lacustrine systems along the Miocene Mur-Mürz fault system (Eastern Alps, Austria) and implications on source rocks in pull-apart basins. *Marine and Petroleum Geology*, 20, 83-110.
- Sawyer, D. S. (1983). Total tectonic subsidence and the mechanism of rifting at the U.S. Atlantic margin. *Eos, Transactions, American Geophysical Union*, 64, 851-852.
- Schopper, T. (1991). Strukturgeologische Untersuchungen als Hilfe für die tektonische Deutung des Bewegungsmechanismus des Wiener Beckens. *Mitteilungen der Österreichischen Geologischen Gesellschaft* 84, 101-134.
- Sclater, J. G., Christie, P. A. F. (1980). Continental stretching; an explanation of the post-Mid-Cretaceous subsidence of the central North Sea basin. *Journal of Geophysical Research*, 85, 3711-3739.

- Sclater, J. G., Royden, L., Horvath, F., Burchfiel, B. C., Semken, S., Stegena, L. (1980). The formation of the intra-Carpathian basins as determined from subsidence data. *Earth and Planetary Science Letters*, 51, 139-162.
- Segall, P., Pollard, D. D. (1980). Mechanics of discontinuous faults. *Journal of Geophysical Research* 85, 4337-4350.
- Seifert, P. (1992). Palinspastic reconstruction of the easternmost Alps between Upper Eocene and Miocene. *Geologica Carpathica*, 43, 327-331.
- Seifert, P. (1996). Sedimentary-tectonic development and Austrian hydrocarbon potential of the Vienna Basin. In: Wessely, G., Liebl, W. (Eds.), *Oil and gas in Alpidic thrustbelts and basins of central and eastern Europe*. EAGE Special Publications, 5, pp. 331-341.
- Shaw, J. H., Connors, C., Suppe, J. (Eds; 2005). *Seismic Interpretation of Contractional Fault-Related Faults*. AAPG Seismic Atlas - Studies in Geology. American Association of Petroleum Geologists, Tulsa, Oklahoma.
- Spicka, V. (1967). Paleografie a tektogenze Videnske panve a prispevek k Jeji naftove geologicke problematice. *Rozpr. CSAV*.
- Steckler, M. S., Watts, A. B. (1978). Subsidence of the Atlantic-type continental margin off New York. *Earth and Planetary Science Letters*, 41, 1-13.
- Steininger, F.F., Wessely, G. (1999). From the Tethyan Ocean to the Paratethys Sea: Oligocene to Neogene Stratigraphy, Paleogeography and Palaeobiogeography of the circum-Mediterranean region and the Oligocene to Neogene Basin evolution in Austria. *Mitteilungen der Österreichischen Geologischen Gesellschaft* 92, 95-116.
- Strauss, P., Harzhauser, M., Hinsch, R., Wagneich, M. (2006). Sequence stratigraphy in a classic pull-apart basin (Neogene, Vienna Basin) - A 3D seismic based integrated approach. *Geologica Carpathica*, 57, 185-197.
- Strauss, P., Wagneich, M., Decker, K., Sachsenhofer, R. F. (2001). Tectonics and sedimentation in the Fohnsdorf-Seckau basin (Miocene-Austria): from a pull-apart basin to a half-graben. *International Journal of Earth Sciences*, 90, 549-559.
- Stowasser, H. (1958). Einige Bausteine zur Tektogenese des Wiener Beckens. *Erdoel-Zeitschrift* 74, 395-400.
- Stowasser, H. (1966). Strukturbildung am Steinbergbruch im Wiener Becken. *Erdöl-Erdgas-Zeitschrift* 82, 188-191.
- ten Veen, J.H., Kleinspehn, K.L. (2000). Quantifying the timing and sense of fault dip slip: New application of biostratigraphy and geohistory analysis. *Geology* 28, 471-474.
- Tollmann, A. (1985). *Geologie von Österreich - Außeralpiner Anteil*. Wien, Deuticke.
- Van Hinte, J. E. (1978). Geohistory analysis - Application of micropaleontology in exploration geology. *AAPG Bulletin*, 62, 201-222.
- Wagneich, M. (1991). Subsidenzanalyse an kalkalpinen Oberkreideseerien der Gosau-Gruppe (Österreich). *Zentralblatt für Geologie und Paläontologie*, Teil 1, 1990, 1645-1657.

- Wagreich, M., Schmid, H.-P. (2002). Backstripping dip-slip fault histories: apparent slip rates for the Miocene of the Vienna Basin. *Terra Nova*, 14, 163-168.
- Walsh, J. J., Bailey, W. R., Childs, C., Nicol, A., Bonson, C. G. (2003). Formation of segmented normal faults: a 3-D perspective. *Journal of Structural Geology* 25, 1251-1262.
- Walsh, J. J., Watterson, J. (1991). Geometric and kinematic coherence and scale effects in normal fault systems. In: Roberts, A. M., Yielding, G., Freeman, B., (Eds.), *The Geometry of Normal Faults*. Geological Society of London Special Publication, 56, pp. 193-203.
- Walsh, J. J., Watterson, J. (1988). Analysis of the relationship between displacements and dimensions of faults. *Journal of Structural Geology*, 10, 239-247.
- Walsh, J. J., Watterson, J. (1987). Distributions of cumulative slip and seismic slip on a single normal fault. *Journal of Structural Geology* 9, 1039-1046.
- Waltham, D., Taberner, C., Docherty, C. (2000). Error Estimation in Decompacted Subsidence Curves. *Bulletin of the American Association of Petroleum Geologists* 84 (8), 1087-1094.
- Weissenböck, M. (1996). Lower to Middle Miocene sedimentation model of the central Vienna Basin. in: Wessely, G., Liebl, W. (Eds.), *Oil and Gas in Alpidic Thrustbelts and Basins of Central and Eastern Europe*. EAGE Special Publication, pp. 355-363.
- Wessely, G. (1992). The Calcareous Alps below the Vienna Basin in Austria and their structural and facial development in the Alpine-Carpathian border zone. *Geologica Carpathica*, 43, 347-353.
- Wessely, G. (1988). Structure and Development of the Vienna Basin in Austria. In: Royden, L. and Horvath, F. (eds.), *The Pannonian Basin-A Study in basin evolution*. AAPG Memoir, pp. 333-346.
- Wessely, G. (2006). *Niederösterreich*. Geologische Bundesanstalt, Vienna.
- Zámolyi, A., Decker, K., Hölzel, M., Strauss, P., Wagreich, M. (2008). Kinematics and timing of deformation at the front of the Alpine-Carpathian wedge (Waschberg-Zdanice unit, Austria-Czech Republic). *Geophysical Research Abstracts*, 10, 04297.



## **8     Appendix 1**

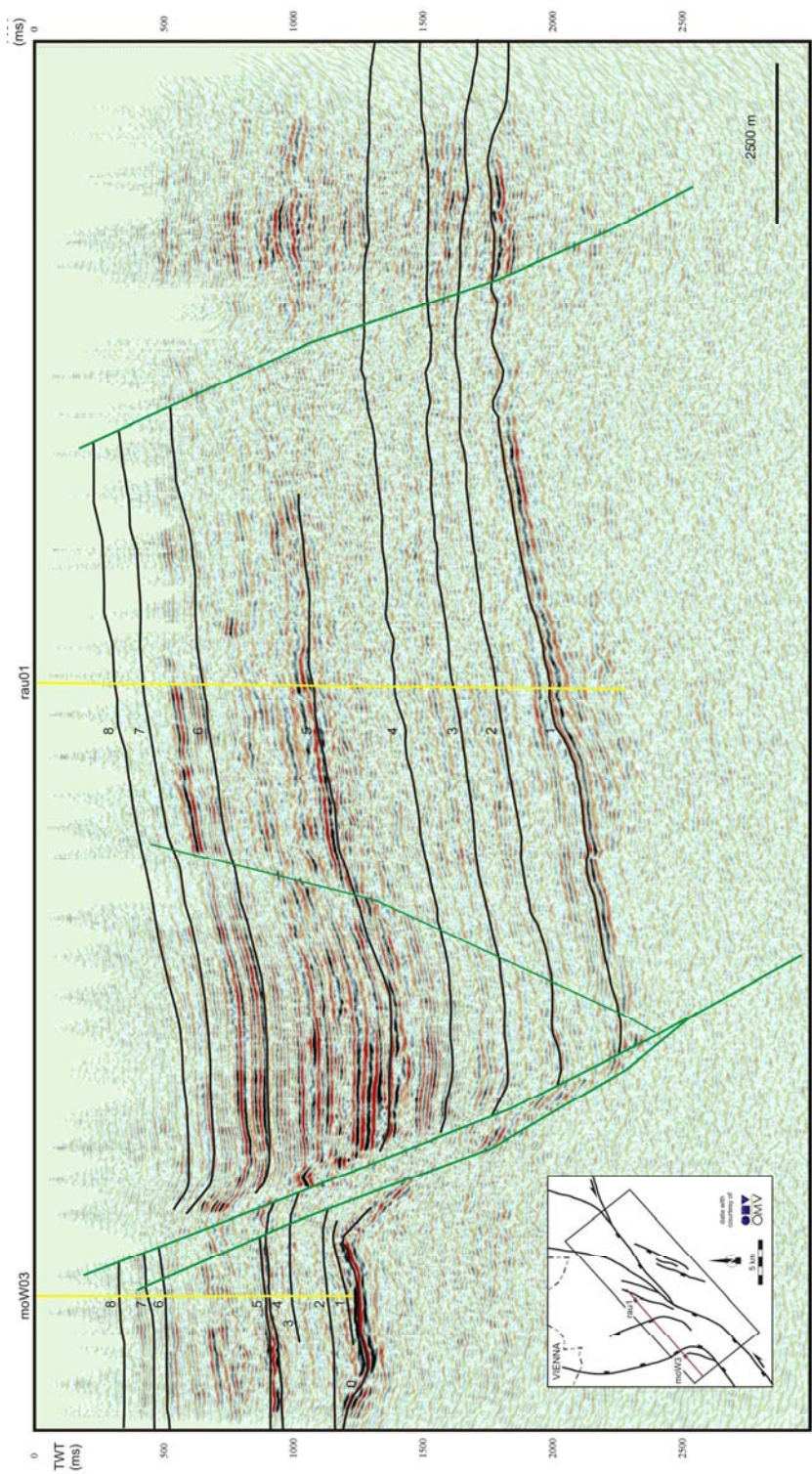
**8.1     *Seismic sections***

**8.2     *Displacement Plots***

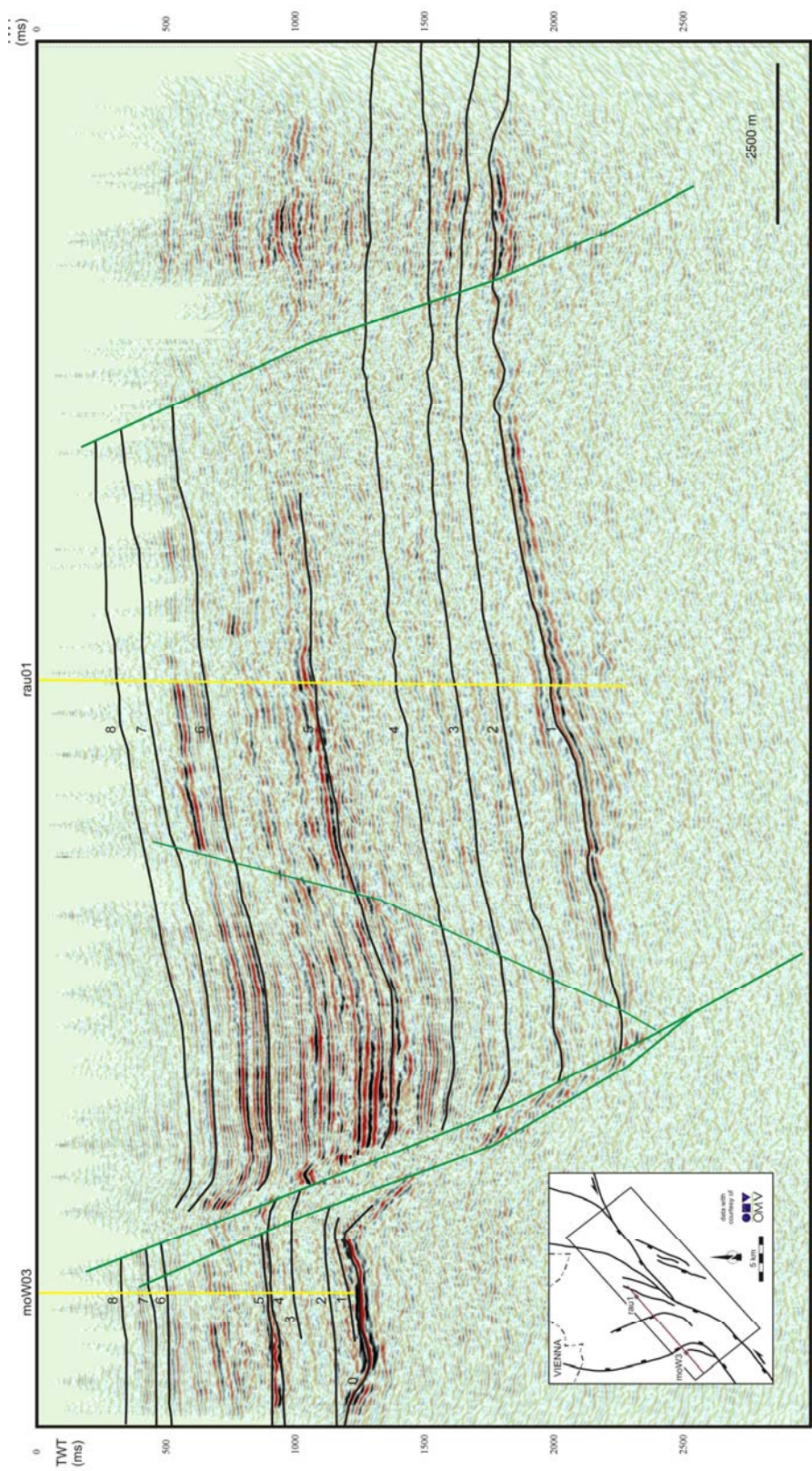
**8.3     *Input Data for Subsidence Analysis***



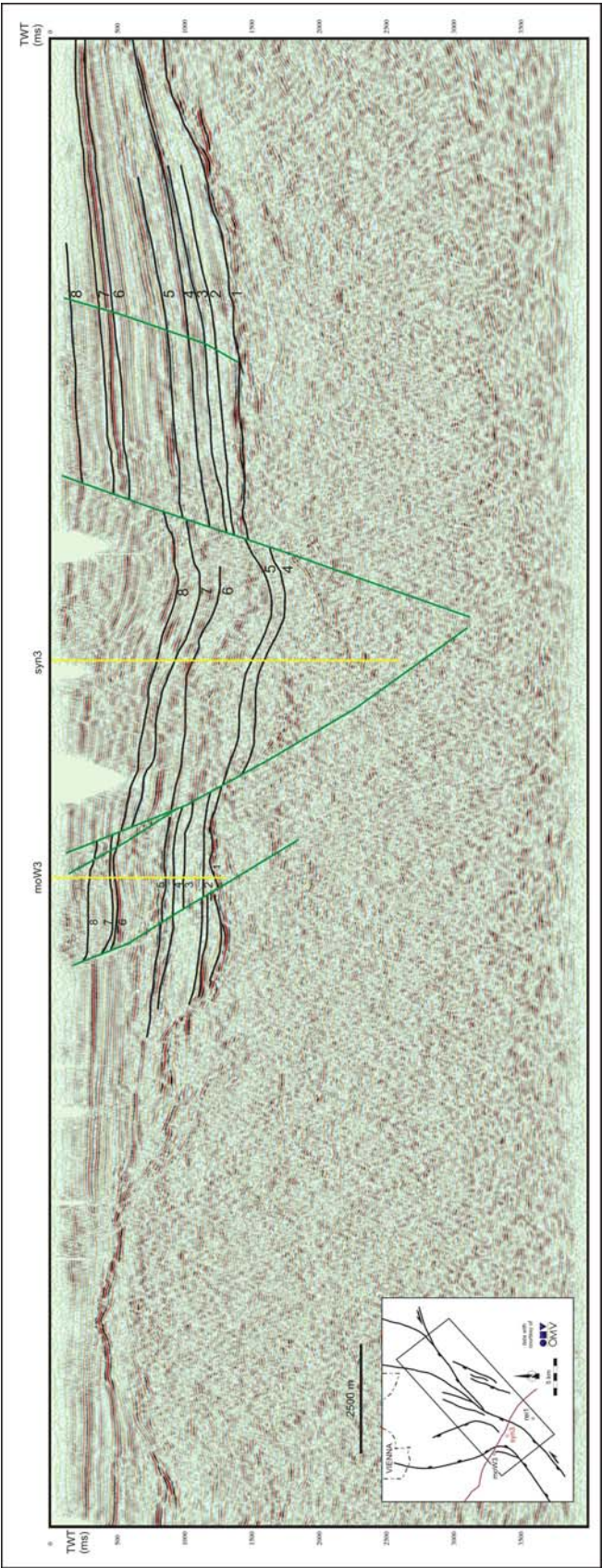
8.1 Seismic sections



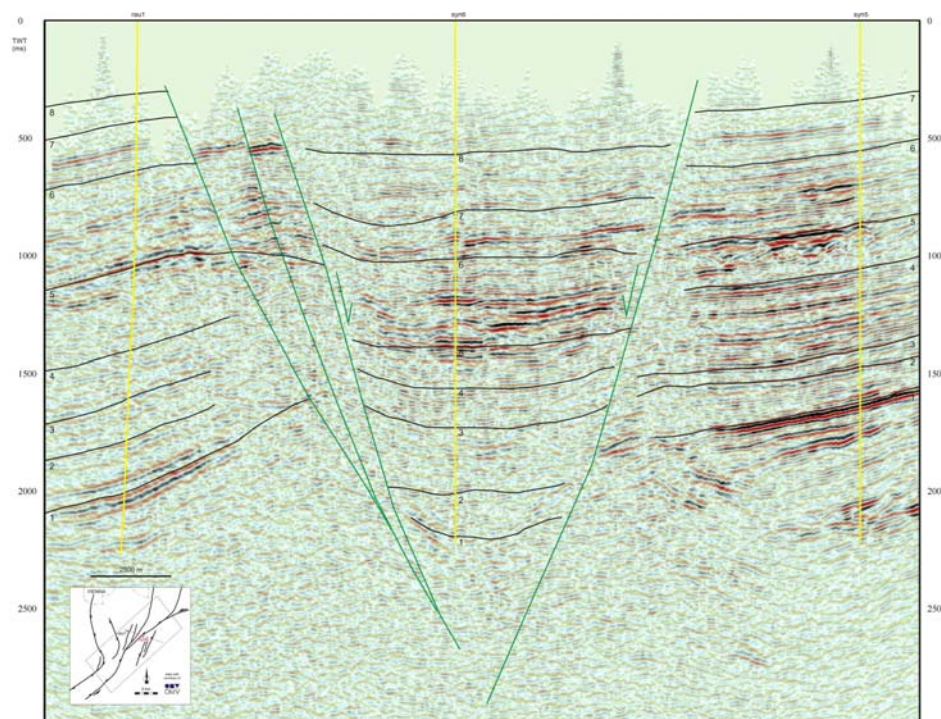
Appendix 1 - Fig. 1: Seismic section from the 3D cube Moosbrunn, showing well pair moW3 and rau1. These wells are situated on the footwall and hanging wall block of the Leopoldsdorf Fault (black lines: horizons tops - 9: Upper Pannonian, 8: Middle Pannonian, 7: Lower Pannonian, 6: Sarmatian, 5: Bulimina Rotalia Zone, 4: Spiroplectamina Zone, 3: Upper Lagenidae Zone, 2: Lower Lagenidae Zone, 1: Aderklaa Conglomerate, 0: Basement; yellow lines: well path; green lines: faults).



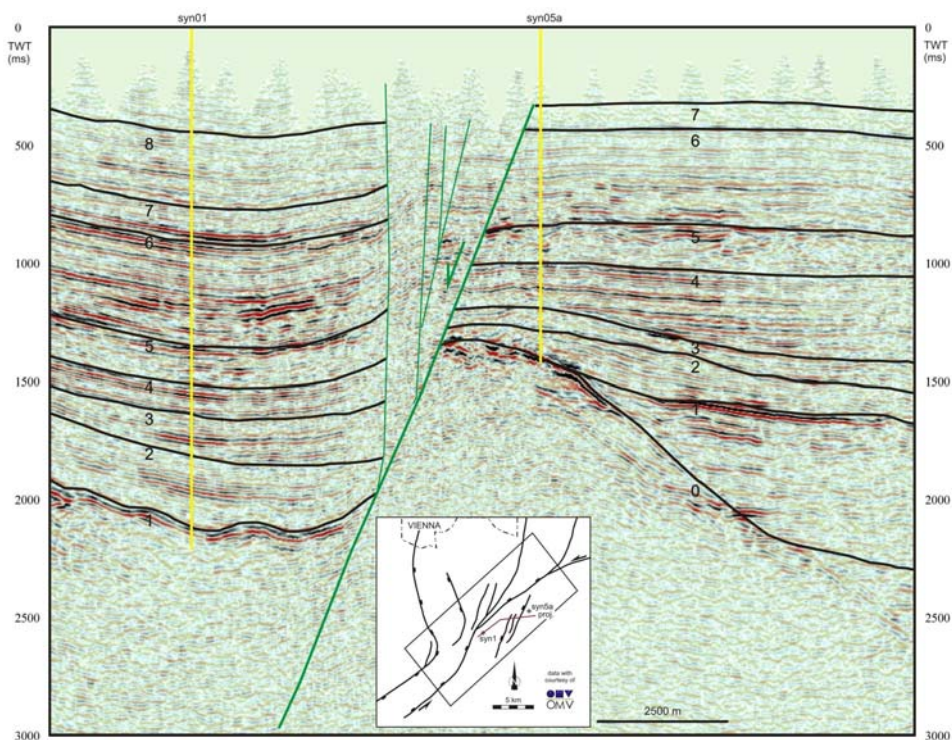
Appendix 1 - Fig. 2: Seismic section (2D) showing the Leopoldsdorf Fault and branches of the negative flower structure. Note that the surface leo is shown 2 times (black lines: horizons tops - 9: Upper Pannonian, 8: Middle Pannonian, 7: Lower Pannonian, 6: Bulimina Rotalia Zone, 4: Spiroplectamina Zone, 3: Upper Lagenidae Zone, 2: Lower Lagenidae Zone, 1: Aderklau Conglomerate, 0: Basement; yellow lines: well path; green lines: faults).



Appendix 1 - Fig. 3: Seismic line with the 2 branches of the southern part of the negative flower structure with faults leo and reis (black lines: horizons tops - 9: Upper Pannonian, 8: Middle Pannonian, 7: Lower Pannonian, 6: Sarmatian, 5: Bulimina Rotalia Zone, 4: Spiroplectamina Zone, 3: Upper Lagenidae Zone, 2: Lower Lagenidae Zone, 1: Aderklaa Conglomerate, 0: Basement; yellow lines: well path; green lines: faults).

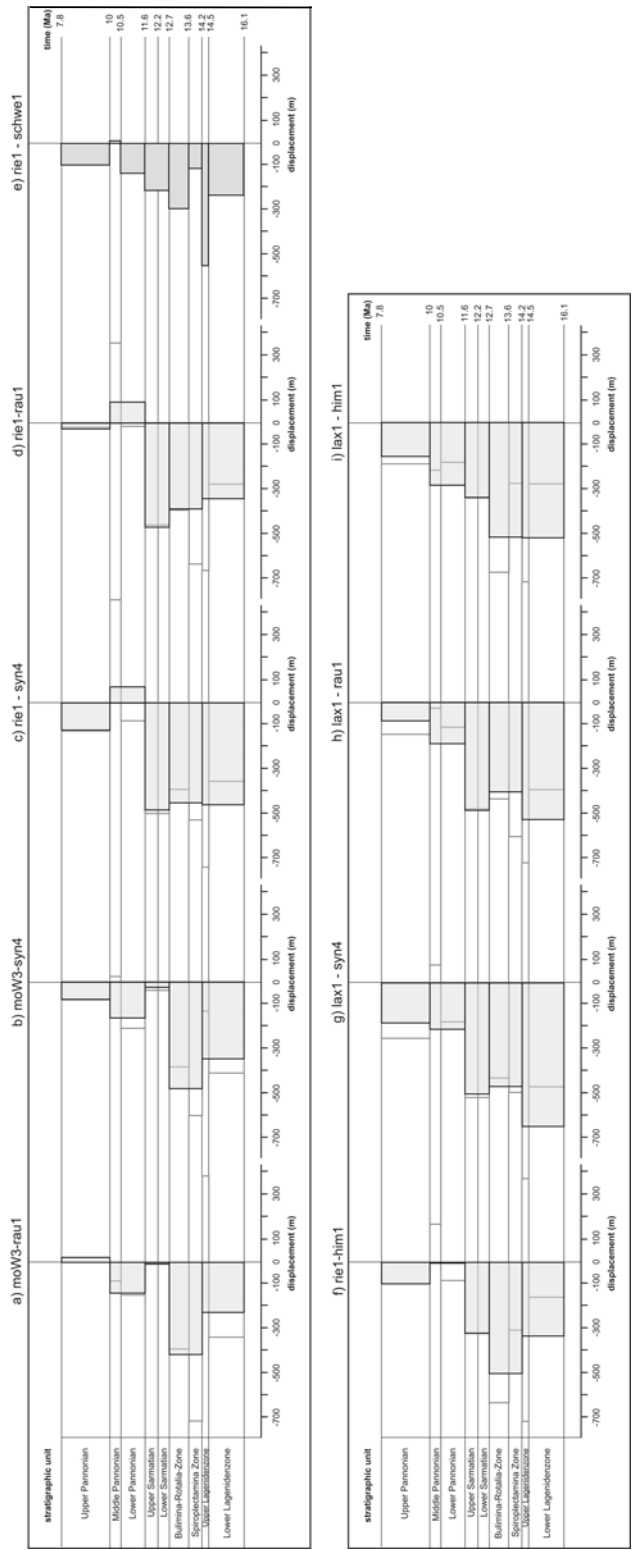


**Appendix 1 - Fig. 4: Arbitrary line through the 3D block Moosbrunn covering the northern branches of the negative flower structure.**



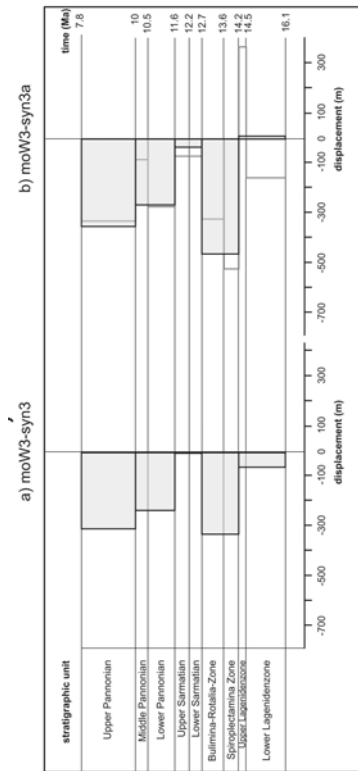
**Appendix 1 - Fig. 5: Arbitrary line (block Moosbrunn) showing fault kopf in detail (black lines: horizons tops - 9: Upper Pannonian, 8: Middle Pannonian, 7: Lower Pannonian, 6: Sarmatian, 5: Bulimina Rotalia Zone, 4: Spiroplectamina Zone, 3: Upper Lagenidae Zone, 2: Lower Lagenidae Zone, 1: Aderklaa Conglomerate, 0: Basement; yellow lines: well path; green lines: faults).**

8.2 Displacement Plots

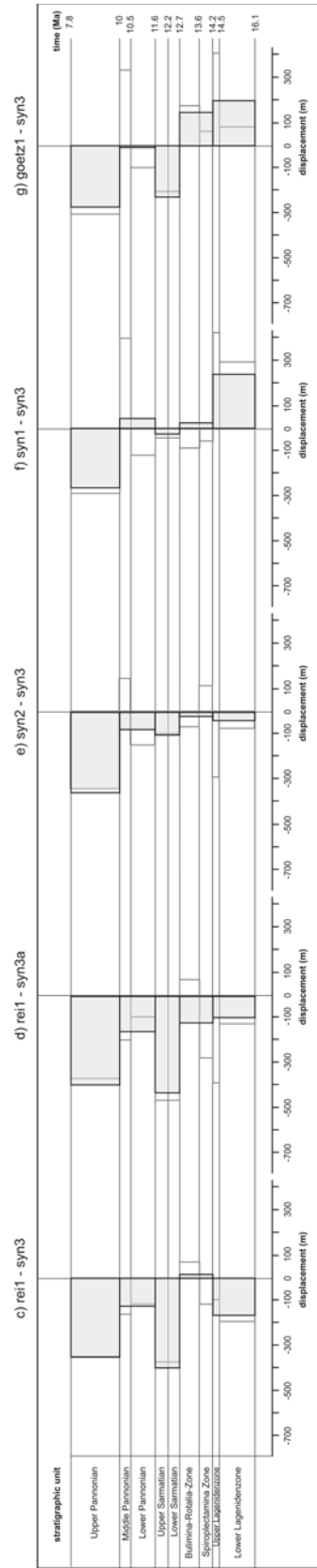


Appendix 1 – Fig. 1: Displacement rates along the Leopoldsdorf Fault (leo), including fault blocks A and D.

A)



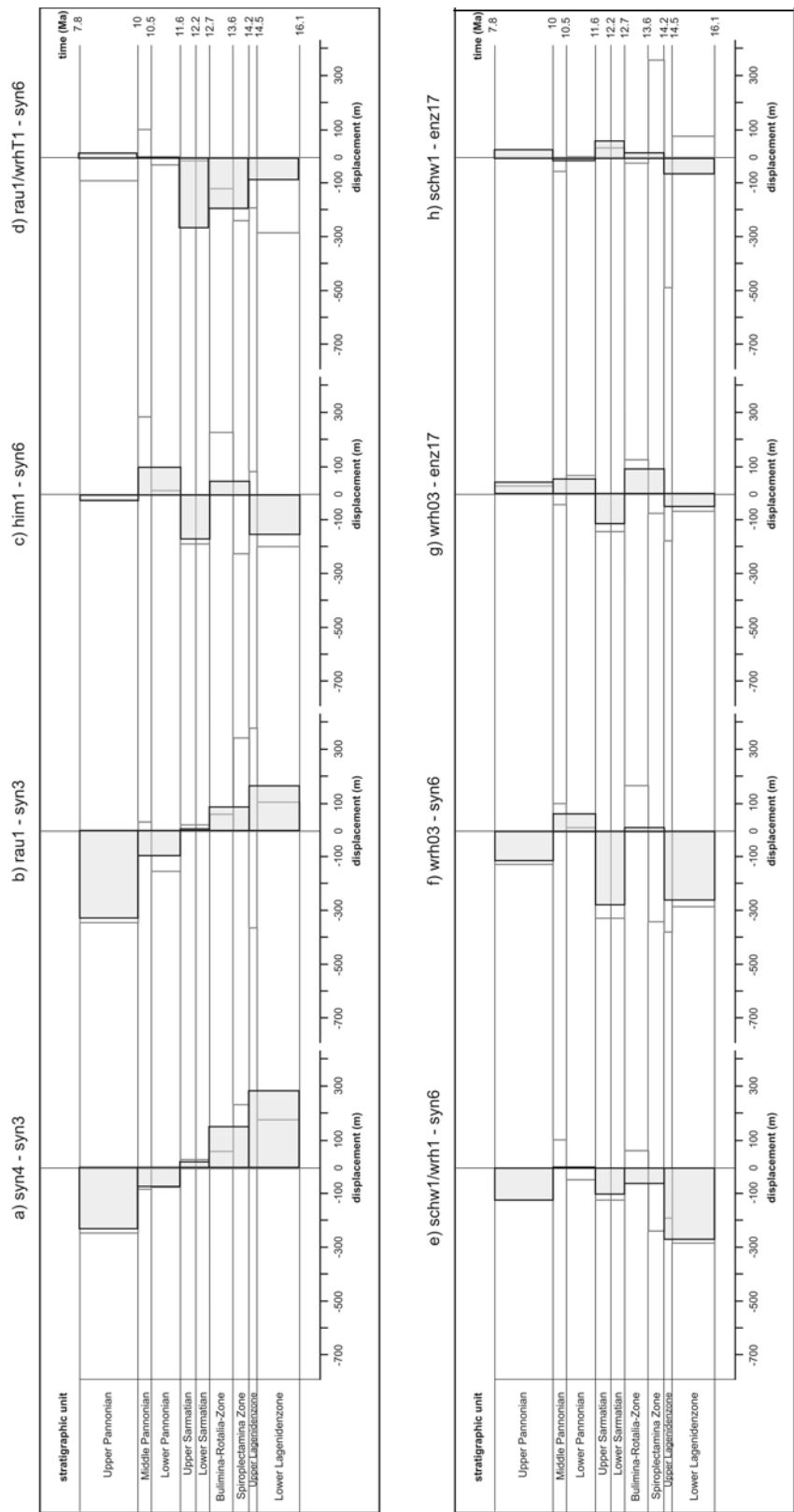
B)



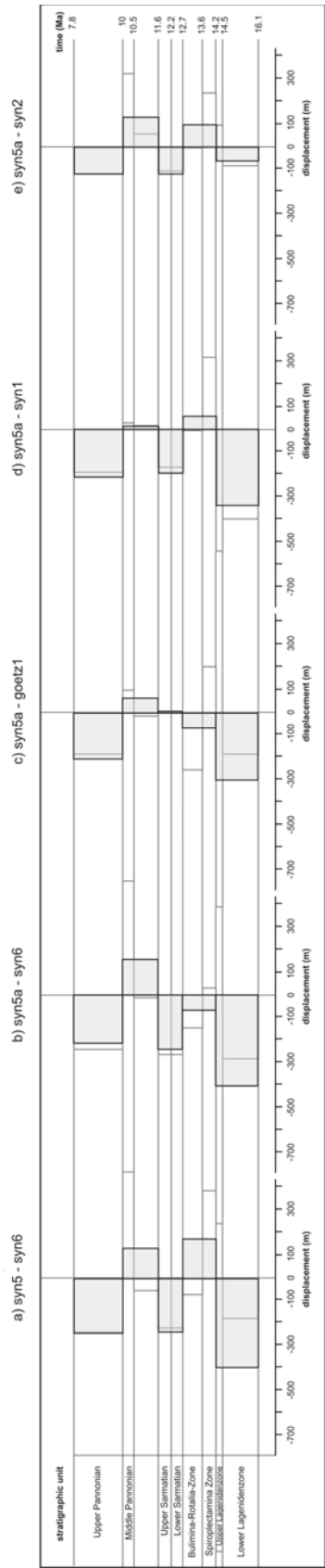
Appendix 1 - Fig. 2: Displacement rates of branches of the southern part of the negative flower structure.

A) Plots of well pairs of the Leopoldsdorf Fault (leo; Blocks A and B).

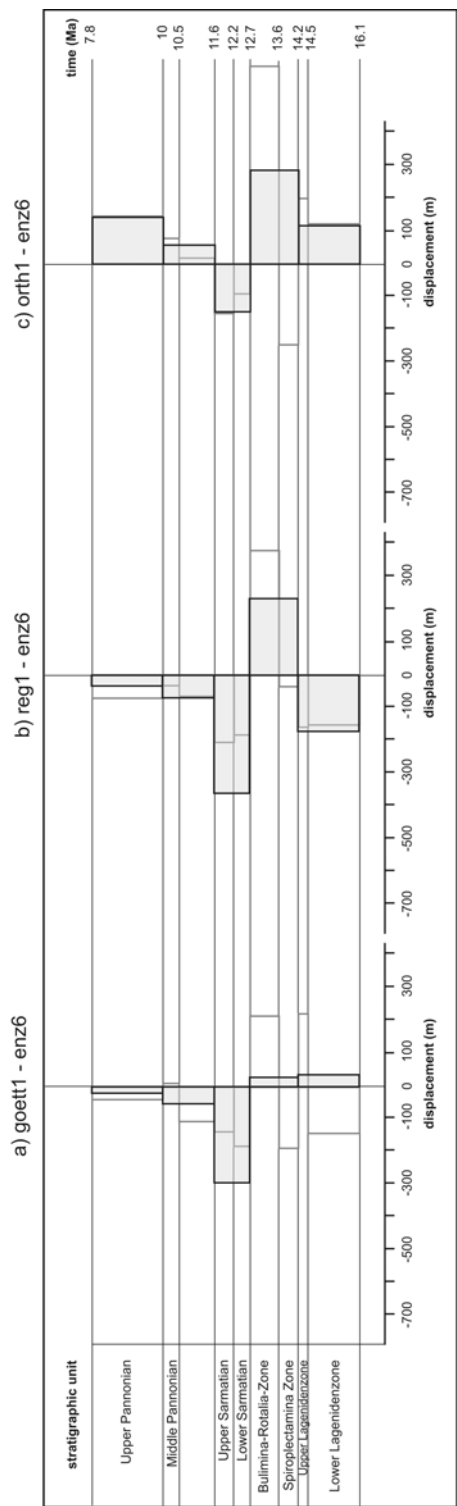
B) Plots of well pairs of the fault reits with blocks C and B.



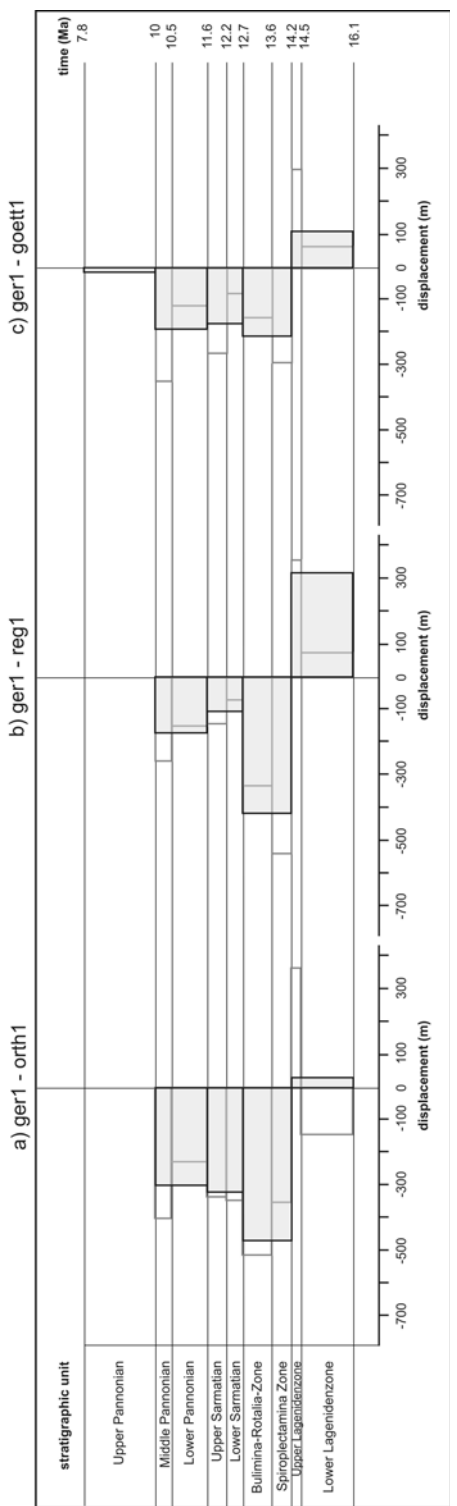
Appendix 1 - Fig. 3: Displacement rates of fault wrh with fault blocks D - B and D - E.



Appendix 1 - Fig. 4: Displacement rates of fault wrh with fault blocks F – E and F-C.



Appendix 1 - Fig. 5: Displacement rates along the fault engel, including fault blocks H and F.



Appendix 1 - Fig. 6: Displacement rates along the fault kopf, including fault blocks F and G.



### 8.3 Input Data for Subsidence Analysis

Units used in Tables

ID	StrataName	Thickness metres	Thickness_Min metres	Thickness_Max metres	Lithol_ID 0 = sand (stone)	Lithol %	Lithol_Min %	Lithol_Max %	Litho2_ID 3 = shale	Litho2 %	Litho2_Min %	Litho2_Max %
6	Lower Lagenid Z.											

#### Sollenau 1

ID	StrataName	Thickness	Thickness_Min	Thickness_Max	Lithol_ID	Lithol	Lithol_Min	Lithol_Max	Litho2_ID	Litho2	Litho2_Min	Litho2_Max
6	Lower Lagenid Z.	347	327	367	0	0.01	0.01	0.01	3	0.99	0.99	0.99
7	Upper Lagenid Z.	417	397	437	0	0.01	0.01	0.01	3	0.99	0.99	0.99
8	Spiroplectamina Z.	154	134	174	0	0.03	0.03	0.03	3	0.97	0.97	0.97
9	Bulimina Rotalia Z.	194	174	214	0	0.12	0.12	0.12	3	0.88	0.88	0.88
10	Lower Sarmatian	362	342	382	0	0.29	0.29	0.29	3	0.71	0.71	0.71
11	Upper Sarmatian	264	244	284	0	0.18	0.18	0.18	3	0.82	0.82	0.82
12	Lower Pannonian	32	12	52	0	0.06	0.06	0.06	3	0.94	0.94	0.94
13	Middle Pannonian	240	220	260	0	0.03	0.03	0.03	3	0.97	0.97	0.97
14	Upper Pannonian	299	279	319	0	0.11	0.11	0.11	3	0.89	0.89	0.89

#### Moosbrunn W3

ID	StrataName	Thickness	Thickness_Min	Thickness_Max	Lithol_ID	Lithol	Lithol_Min	Lithol_Max	Litho2_ID	Litho2	Litho2_Min	Litho2_Max
6	Lower Lagenid Z.	40	20	60	0	0.00	0.00	0.00	3	1.00	1.00	1.00
7	Upper Lagenid Z.	249	229	269	0	0.00	0.00	0.00	3	1.00	1.00	1.00
8	Spiroplectamina Z.	32	12	52	0	0.00	0.00	0.00	3	1.00	1.00	1.00
9	Bulimina Rotalia Z.	39	19	59	0	0.00	0.00	0.00	3	1.00	1.00	1.00
11	Sarmatian	470	450	490	0	0.14	0.14	0.14	3	0.86	0.86	0.86
12	Lower Pannonian	45	25	65	0	0.00	0.00	0.00	3	1.00	1.00	1.00
13	Middle Pannonian	113	93	133	0	0.64	0.64	0.64	3	0.36	0.36	0.36
14	Upper Pannonian	312	292	332	0	0.41	0.41	0.41	3	0.59	0.59	0.59

Riedenhof 1

ID	StrataName	Thickness	Thickness_Min	Thickness_Max	Litho1_ID	Litho1	Litho1_Min	Litho1_Max	Litho2_ID	Litho2	Litho2_Min	Litho2_Max
6	Lower Lagenid Z.	94	74	114	0	0.32	0.32	0.32	3	0.68	0.68	0.68
7	Upper Lagenid Z.	87	67	107	0	0.23	0.23	0.23	3	0.77	0.77	0.77
8	Spiropectamina Z.	52	32	72	0	0.00	0.00	0.00	3	1.00	1.00	1.00
9	Bulimina Rotalia Z.	34	14	54	0	0.00	0.00	0.00	3	1.00	1.00	1.00
11	Sarmatian	93	73	113	0	0.00	0.00	0.00	3	1.00	1.00	1.00
12	Lower Pannonian	131	111	151	0	0.00	0.00	0.00	3	1.00	1.00	1.00
13	Middle Pannonian	236	216	256	0	0.03	0.03	0.03	3	0.97	0.97	0.97
14	Upper Pannonian	207	187	227	0	0.04	0.04	0.04	3	0.96	0.96	0.96

Laxenburg 2

ID	StrataName	Thickness	Thickness_Min	Thickness_Max	Litho1_ID	Litho1	Litho1_Min	Litho1_Max	Litho2_ID	Litho2	Litho2_Min	Litho2_Max
8	Spiropectamina Z.	52	32	72	0	0.00	0.00	0.00	3	1.00	1.00	1.00
9	Bulimina Rotalia Z.	8	1	28	0	0.00	0.00	0.00	3	1.00	1.00	1.00
11	Sarmatian	71	51	91	0	0.14	0.14	0.14	3	0.86	0.86	0.86
12	Lower Pannonian	53	33	73	0	0.00	0.00	0.00	3	1.00	1.00	1.00
13	Middle Pannonian	102	82	122	0	0.64	0.64	0.64	3	0.36	0.36	0.36

Schwechat 1

ID	StrataName	Thickness	Thickness_Min	Thickness_Max	Litho1_ID	Litho1	Litho1_Min	Litho1_Max	Litho2_ID	Litho2	Litho2_Min	Litho2_Max
7	Upper Lagenid Z.	286	266	306	0	0.05	0.05	0.05	3	0.95	0.95	0.95
8	Spiropectamina Z.	206	186	226	0	0.05	0.05	0.05	3	0.95	0.95	0.95
9	Bulimina Rotalia Z.	113	93	133	0	0.03	0.03	0.03	3	0.97	0.97	0.97
10	Lower Sarmatian	239	219	259	0	0.08	0.08	0.08	3	0.92	0.92	0.92
11	Upper Sarmatian	322	302	342	0	0.21	0.21	0.21	3	0.79	0.79	0.79
12	Lower Pannonian	298	278	318	0	0.14	0.14	0.14	3	0.86	0.86	0.86
13	Middle Pannonian	299	279	319	0	0.16	0.16	0.16	3	0.84	0.84	0.84
14	Upper Pannonian	479	459	499	0	0.43	0.43	0.43	3	0.57	0.57	0.57

### Synthetic 1

ID	StrataName	Thickness	Thickness_Min	Thickness_Max	Litho1_ID	Litho1	Litho1_Min	Litho1_Max	Litho2_ID	Litho2	Litho2_Min	Litho2_Max
6	Lower Lagenid Z.	377	377	470	0	0.01	0.01	0.01	3	0.99	0.99	0.99
7	Upper Lagenid Z.	345	345	392	0	0.00	0.00	0.00	3	1.00	1.00	1.00
8	Spiropectamina Z.	331	284	331	0	0.01	0.01	0.01	3	0.99	0.99	0.99
9	Bulimina Rotalia Z.	351	351	351	0	0.12	0.12	0.12	3	0.88	0.88	0.88
11	Sarmatian	635	616	759	0	0.26	0.26	0.26	3	0.74	0.74	0.74
12	Lower Pannonian	281	157	292	0	0.01	0.01	0.01	3	0.99	0.99	0.99
13	Middle Pannonian	114	98	114	0	0.09	0.09	0.09	3	0.91	0.91	0.91
14	Upper Pannonian	541	541	565	0	0.15	0.15	0.15	3	0.85	0.85	0.85

### Himberg O1

ID	StrataName	Thickness	Thickness_Min	Thickness_Max	Litho1_ID	Litho1	Litho1_Min	Litho1_Max	Litho2_ID	Litho2	Litho2_Min	Litho2_Max
6	Lower Lagenid Z.	213	193	233	0	0.00	0.00	0.00	3	1.00	1.00	1.00
7	Upper Lagenid Z.	337	317	357	0	0.01	0.01	0.01	3	0.99	0.99	0.99
8	Spiropectamina Z.	200	180	220	0	0.00	0.00	0.00	3	1.00	1.00	1.00
9	Bulimina Rotalia Z.	500	480	520	0	0.05	0.05	0.05	3	0.95	0.95	0.95
11	Sarmatian	482	462	502	0	0.43	0.43	0.43	3	0.57	0.57	0.57
12	Lower Pannonian	238	218	258	0	0.01	0.01	0.01	3	0.99	0.99	0.99
13	Middle Pannonian	245	225	265	0	0.11	0.11	0.11	3	0.89	0.89	0.89
14	Upper Pannonian	485	465	505	0	0.26	0.26	0.26	3	0.74	0.74	0.74

### Rauchenwarth 1

ID	StrataName	Thickness	Thickness_Min	Thickness_Max	Litho1_ID	Litho1	Litho1_Min	Litho1_Max	Litho2_ID	Litho2	Litho2_Min	Litho2_Max
6	Lower Lagenid Z.	315	295	335	0	0.01	0.01	0.01	3	0.99	0.99	0.99
7	Upper Lagenid Z.	246	226	266	0	0.00	0.00	0.00	3	1.00	1.00	1.00
8	Spiropectamina Z.	324	304	344	0	0.01	0.01	0.01	3	0.99	0.99	0.99
9	Bulimina Rotalia Z.	374	354	394	0	0.12	0.12	0.12	3	0.88	0.88	0.88
11	Sarmatian	595	575	615	0	0.26	0.26	0.26	3	0.74	0.74	0.74
12	Lower Pannonian	199	179	219	0	0.01	0.01	0.01	3	0.99	0.99	0.99
13	Middle Pannonian	150	130	170	0	0.09	0.09	0.09	3	0.91	0.91	0.91

14	Upper Pannonian	316	296	336	0	0.15	0.15	0.15	3	0.85	0.85	0.85
----	-----------------	-----	-----	-----	---	------	------	------	---	------	------	------

Synthetic 3

ID	StrataName	Thickness	Thickness_Min	Thickness_Max	Litho1_ID	Litho1	Litho1_Min	Litho1_Max	Litho2_ID	Litho2	Litho2_Min	Litho2_Max
6	Lower Lagenid Z.	210	201	282	0	0.00	0.00	0.00	3	1.00	1.00	1.00
7	Upper Lagenid Z.	145	126	165	0	0.00	0.00	0.00	3	1.00	1.00	1.00
8	Spiroplectamina Z.	177	158	197	0	0.00	0.00	0.00	3	1.00	1.00	1.00
9	Bulimina Rotalia Z.	238	222	383	0	0.01	0.01	0.01	3	0.99	0.99	0.99
11	Sarmatian	543	345	705	0	0.12	0.12	0.12	3	0.88	0.88	0.88
12	Lower Pannonian	345	168	407	0	0.00	0.00	0.00	3	1.00	1.00	1.00
13	Middle Pannonian	133	123	163	0	0.07	0.07	0.07	3	0.93	0.93	0.93
14	Upper Pannonian	1025	1015	1035	0	0.26	0.26	0.26	3	0.74	0.74	0.74

Synthetic 3a

ID	StrataName	Thickness	Thickness_Min	Thickness_Max	Litho1_ID	Litho1	Litho1_Min	Litho1_Max	Litho2_ID	Litho2	Litho2_Min	Litho2_Max
6	Lower Lagenid Z.	165	151	165	0	0.00	0.00	0.00	3	1.00	1.00	1.00
7	Upper Lagenid Z.	190	190	190	0	0.00	0.00	0.00	3	1.00	1.00	1.00
8	Spiroplectamina Z.	240	240	240	0	0.00	0.00	0.00	3	1.00	1.00	1.00
9	Bulimina Rotalia Z.	258	258	258	0	0.01	0.01	0.01	3	0.99	0.99	0.99
11	Sarmatian	593	565	739	0	0.12	0.12	0.12	3	0.88	0.88	0.88
12	Lower Pannonian	340	195	368	0	0.00	0.00	0.00	3	1.00	1.00	1.00
13	Middle Pannonian	153	134	171	0	0.07	0.07	0.07	3	0.93	0.93	0.93
14	Upper Pannonian	1088	1070	1107	0	0.26	0.26	0.26	3	0.74	0.74	0.74

Schwadorf 1 + wrh

ID	StrataName	Thickness	Thickness_Min	Thickness_Max	Litho1_ID	Litho1	Litho1_Min	Litho1_Max	Litho2_ID	Litho2	Litho2_Min	Litho2_Max
6	Lower Lagenid Z.	139	119	159	0	0.00	0.00	0.00	3	1.00	1.00	1.00
7	Upper Lagenid Z.	265	245	285	0	0.00	0.00	0.00	3	1.00	1.00	1.00
8	Spiroplectamina Z.	181	161	201	0	0.00	0.00	0.00	3	1.00	1.00	1.00
9	Bulimina Rotalia Z.	363	343	383	0	0.12	0.12	0.12	3	0.88	0.88	0.88
11	Sarmatian	496	476	516	0	0.26	0.26	0.26	3	0.74	0.74	0.74
12	Lower Pannonian	189	169	209	0	0.04	0.04	0.04	3	0.96	0.96	0.96

13	Middle Pannonian	151	131	171	0	0.14	0.14	0.14	3	0.86	0.86	0.86
14	Upper Pannonian	238	218	258	0	0.00	0.00	0.00	3	1.00	1.00	1.00

#### Wienerherberg 1

ID	StrataName	Thickness	Thickness_Min	Thickness_Max	Litho1_ID	Litho1	Litho1_Min	Litho1_Max	Litho2_ID	Litho2	Litho2_Min	Litho2_Max
6	Lower Lagenid Z.	139	119	159	0	0.00	0.00	0.00	3	1.00	1.00	1.00
7	Upper Lagenid Z.	265	245	285	0	0.00	0.00	0.00	3	1.00	1.00	1.00
8	Spiroplectamina Z.	181	161	201	0	0.00	0.00	0.00	3	1.00	1.00	1.00
9	Bulimina Rotalia Z.	228	208	248	0	0.00	0.00	0.00	3	1.00	1.00	1.00
11	Sarmatian	193	173	213	0	0.14	0.14	0.14	3	0.86	0.86	0.86
12	Lower Pannonian	288	268	308	0	0.01	0.01	0.01	3	0.99	0.99	0.99
13	Middle Pannonian	248	228	268	0	0.02	0.02	0.02	3	0.98	0.98	0.98
14	Upper Pannonian	525	505	545	0	0.50	0.50	0.50	3	0.50	0.50	0.50

#### Wienerherberg T1

ID	StrataName	Thickness	Thickness_Min	Thickness_Max	Litho1_ID	Litho1	Litho1_Min	Litho1_Max	Litho2_ID	Litho2	Litho2_Min	Litho2_Max
6	Lower Lagenid Z.	198	178	218	0	0.00	0.00	0.00	3	1.00	1.00	1.00
7	Upper Lagenid Z.	268	248	288	0	0.00	0.00	0.00	3	1.00	1.00	1.00
8	Spiroplectamina Z.	204	184	224	0	0.00	0.00	0.00	3	1.00	1.00	1.00
9	Bulimina Rotalia Z.	234	214	254	0	0.19	0.19	0.19	3	0.81	0.81	0.81
11	Sarmatian	347	327	367	0	0.28	0.28	0.28	3	0.72	0.72	0.72
12	Lower Pannonian	237	217	257	0	0.00	0.00	0.00	3	1.00	1.00	1.00
13	Middle Pannonian	99	79	119	0	0.10	0.10	0.10	3	0.90	0.90	0.90
14	Upper Pannonian	527	507	547	0	0.05	0.05	0.05	3	0.95	0.95	0.95

#### Wienerherberg T3

ID	StrataName	Thickness	Thickness_Min	Thickness_Max	Litho1_ID	Litho1	Litho1_Min	Litho1_Max	Litho2_ID	Litho2	Litho2_Min	Litho2_Max
6	Lower Lagenid Z.	141	121	161	0	0.00	0.00	0.00	3	1.00	1.00	1.00
7	Upper Lagenid Z.	231	211	251	0	0.00	0.00	0.00	3	1.00	1.00	1.00
8	Spiroplectamina Z.	138	118	158	0	0.00	0.00	0.00	3	1.00	1.00	1.00
9	Bulimina Rotalia Z.	417	397	437	0	0.00	0.00	0.00	3	1.00	1.00	1.00
11	Sarmatian	303	283	323	0	0.19	0.19	0.19	3	0.81	0.81	0.81

12	Lower Pannonian	243	223	263	0	0.00	0.00	0.00	3	1.00	1.00	1.00
13	Middle Pannonian	153	133	173	0	0.18	0.18	0.18	3	0.82	0.82	0.82
14	Upper Pannonian	228	208	248	0	0.00	0.00	0.00	3	1.00	1.00	1.00

Reisenberg 1

ID	StrataName	Thickness	Thickness_Min	Thickness_Max	Litho1_ID	Litho1	Litho1_Min	Litho1_Max	Litho2_ID	Litho2	Litho2_Min	Litho2_Max
6	Lower Lagenid Z.	92	72	112	0	1.00	1.00	1.00	3	0.00	0.00	0.00
7	Upper Lagenid Z.	141	121	161	0	1.00	1.00	1.00	3	0.00	0.00	0.00
8	Spiroplectamina Z.	103	83	123	0	0.04	0.04	0.04	3	0.96	0.96	0.96
9	Bulimina Rotalia Z.	258	238	278	0	0.05	0.05	0.05	3	0.95	0.95	0.95
11	Sarmatian	184	164	204	0	0.37	0.37	0.37	3	0.63	0.63	0.63
12	Lower Pannonian	189	169	209	0	0.12	0.12	0.12	3	0.88	0.88	0.88
13	Middle Pannonian	54	34	74	0	0.00	0.00	0.00	3	1.00	1.00	1.00
14	Upper Pannonian	224	204	244	0	0.00	0.00	0.00	3	1.00	1.00	1.00

Synthetic 2

ID	StrataName	Thickness	Thickness_Min	Thickness_Max	Litho1_ID	Litho1	Litho1_Min	Litho1_Max	Litho2_ID	Litho2	Litho2_Min	Litho2_Max
6	Lower Lagenid Z.	207	203	224	0	1.00	1.00	1.00	3	0.00	0.00	0.00
7	Upper Lagenid Z.	107	97	114	0	1.00	1.00	1.00	3	0.00	0.00	0.00
8	Spiroplectamina Z.	182	182	188	0	0.04	0.04	0.04	3	0.96	0.96	0.96
9	Bulimina Rotalia Z.	204	196	211	0	0.05	0.05	0.05	3	0.95	0.95	0.95
11	Sarmatian	440	356	474	0	0.37	0.37	0.37	3	0.63	0.63	0.63
12	Lower Pannonian	153	119	237	0	0.12	0.12	0.12	3	0.88	0.88	0.88
13	Middle Pannonian	205	79	205	0	0.00	0.00	0.00	3	1.00	1.00	1.00
14	Upper Pannonian	245	245	245	0	0.00	0.00	0.00	3	1.00	1.00	1.00

Synthetic 1

ID	StrataName	Thickness	Thickness_Min	Thickness_Max	Litho1_ID	Litho1	Litho1_Min	Litho1_Max	Litho2_ID	Litho2	Litho2_Min	Litho2_Max
6	Lower Lagenid Z.	516	516	516	0	0.00	0.00	0.00	3	1.00	1.00	1.00
7	Upper Lagenid Z.	266	266	266	0	0.00	0.00	0.00	3	1.00	1.00	1.00
8	Spiroplectamina Z.	184	184	184	0	0.00	0.00	0.00	3	1.00	1.00	1.00
9	Bulimina Rotalia Z.	236	236	236	0	0.00	0.00	0.00	3	1.00	1.00	1.00

11	Sarmatian	565	418	612	0	0.14	0.14	0.14	3	0.86	0.86	0.86
12	Lower Pannonian	195	147	342	0	0.01	0.01	0.01	3	0.99	0.99	0.99
13	Middle Pannonian	328	328	328	0	0.02	0.02	0.02	3	0.98	0.98	0.98
14	Upper Pannonian	449	449	449	0	0.50	0.50	0.50	3	0.50	0.50	0.50

#### Götzendorf 1

ID	StrataName	Thickness	Thickness_Min	Thickness_Max	Litho1_ID	Litho1	Litho1_Min	Litho1_Max	Litho2_ID	Litho2	Litho2_Min	Litho2_Max
6	Lower Lagenid Z.	69	49	89	0	0.00	0.00	0.00	3	1.00	1.00	1.00
7	Upper Lagenid Z.	304	284	324	0	0.00	0.00	0.00	3	1.00	1.00	1.00
8	Spiroplectamina Z.	226	206	246	0	0.00	0.00	0.00	3	1.00	1.00	1.00
9	Bulimina Rotalia Z.	412	392	432	0	0.01	0.01	0.01	3	0.99	0.99	0.99
11	Sarmatian	370	350	390	0	0.12	0.12	0.12	3	0.88	0.88	0.88
12	Lower Pannonian	249	229	269	0	0.00	0.00	0.00	3	1.00	1.00	1.00
13	Middle Pannonian	297	277	317	0	0.07	0.07	0.07	3	0.93	0.93	0.93
14	Upper Pannonian	407	387	427	0	0.26	0.26	0.26	3	0.74	0.74	0.74

#### Synthetic 6

ID	StrataName	Thickness	Thickness_Min	Thickness_Max	Litho1_ID	Litho1	Litho1_Min	Litho1_Max	Litho2_ID	Litho2	Litho2_Min	Litho2_Max	Litho3_ID
6	Lower Lagenid Z.	377	377	470	0	0.00	0.00	0.00	3	1.00	1.00	1.00	0
7	Upper Lagenid Z.	345	345	392	0	0.00	0.00	0.00	3	1.00	1.00	1.00	0
8	Spiroplectamina Z.	331	284	331	0	0.00	0.00	0.00	3	1.00	1.00	1.00	0
9	Bulimina Rotalia Z.	351	351	351	0	0.00	0.00	0.00	3	1.00	1.00	1.00	0
11	Sarmatian	635	616	759	0	0.14	0.14	0.14	3	0.86	0.86	0.86	0
12	Lower Pannonian	281	157	292	0	0.01	0.01	0.01	3	0.99	0.99	0.99	0
13	Middle Pannonian	114	98	114	0	0.02	0.02	0.02	3	0.98	0.98	0.98	0
14	Upper Pannonian	541	541	565	0	0.50	0.50	0.50	3	0.50	0.50	0.50	0

#### Synthetic 5

ID	StrataName	Thickness	Thickness_Min	Thickness_Max	Litho1_ID	Litho1	Litho1_Min	Litho1_Max	Litho2_ID	Litho2	Litho2_Min	Litho2_Max	Litho3_ID
6	Lower Lagenid Z.	231	231	231	0	0.08	0.08	0.08	3	0.92	0.92	0.92	0
7	Upper Lagenid Z.	99	99	99	0	0.36	0.36	0.36	3	0.64	0.64	0.64	0
8	Spiroplectamina Z.	471	261	471	0	0.00	0.00	0.00	3	1.00	1.00	1.00	0

9	Bulimina Rotalia Z.	236	236		446	0	0.11	0.11	0.11	0.11	3	0.89	0.89	0.89
11	Sarmatian	374	353		458	0	0.10	0.10	0.10	0.10	3	0.90	0.90	0.90
12	Lower Pannonian	201	117		223	0	0.00	0.00	0.00	0.00	3	1.00	1.00	1.00
13	Middle Pannonian	310	310		310	0	0.00	0.00	0.00	0.00	3	1.00	1.00	1.00

Synthetic 5a

ID	StrataName	Thickness	Thickness_Min	Thickness_Max	Litho1_ID	Litho1	Litho1_Min	Litho1_Max	Litho2_ID	Litho2	Litho2_Min	Litho2_Max
6	Lower Lagenid Z.	142	142	142	0	0.08	0.08	0.08	3	0.92	0.92	0.92
7	Upper Lagenid Z.	129	129	129	0	0.36	0.36	0.36	3	0.64	0.64	0.64
8	Spiroplectamina Z.	261	261	261	0	0.00	0.00	0.00	3	1.00	1.00	1.00
9	Bulimina Rotalia Z.	209	209	209	0	0.11	0.11	0.11	3	0.89	0.89	0.89
11	Sarmatian	326	326	326	0	0.10	0.10	0.10	3	0.90	0.90	0.90
12	Lower Pannonian	216	216	216	0	0.00	0.00	0.00	3	1.00	1.00	1.00
13	Middle Pannonian	311	311	311	0	0.00	0.00	0.00	3	1.00	1.00	1.00

Göttlesbrunn 1

ID	StrataName	Thickness	Thickness_Min	Thickness_Max	Litho1_ID	Litho1	Litho1_Min	Litho1_Max	Litho2_ID	Litho2	Litho2_Min	Litho2_Max
6	Lower Lagenid Z.	91	71	111	0	0.08	0.08	0.08	3	0.92	0.92	0.92
7	Upper Lagenid Z.	363	343	383	0	0.36	0.36	0.36	3	0.64	0.64	0.64
8	Spiroplectamina Z.	169	149	189	0	0.00	0.00	0.00	3	1.00	1.00	1.00
9	Bulimina Rotalia Z.	410	390	430	0	0.11	0.11	0.11	3	0.89	0.89	0.89
10	Lower Sarmatian	94	74	114	0	0.12	0.12	0.12	3	0.88	0.88	0.88
11	Upper Sarmatian	161	141	181	0	0.09	0.09	0.09	3	0.91	0.91	0.91
12	Lower Pannonian	103	83	123	0	0.00	0.00	0.00	3	1.00	1.00	1.00
13	Middle Pannonian	147	127	167	0	0.00	0.00	0.00	3	1.00	1.00	1.00
14	Upper Pannonian	33	13	53	0	0.00	0.00	0.00	3	1.00	1.00	1.00

Gerhaus 1

ID	StrataName	Thickness	Thickness_Min	Thickness_Max	Litho1_ID	Litho1	Litho1_Min	Litho1_Max	Litho2_ID	Litho2	Litho2_Min	Litho2_Max
6	Lower Lagenid Z.	156	136	176	0	0.30	0.30	0.30	3	0.70	0.70	0.70
7	Upper Lagenid Z.	404	384	424	0	0.03	0.03	0.03	3	0.97	0.97	0.97
8	Spiroplectamina Z.	71	51	91	0	0.00	0.00	0.00	3	1.00	1.00	1.00

9	Bulmina Rotalia Z.	300	280	320	0	0.00	0.00	0.00	3	1.00	1.00	1.00
10	Lower Sarmatian	67	47	87	0	0.29	0.29	0.29	3	0.71	0.71	0.71
11	Upper Sarmatian	29	9	49	0	0.00	0.00	0.00	3	1.00	1.00	1.00

#### Regelsbrunn 1

ID	StrataName	Thickness	Thickness_Min	Thickness_Max	Lithol_ID	Lithol	Lithol_Min	Lithol_Max	Litho2_ID	Litho2	Litho2_Min	Litho2_Max
6	Lower Lagenid Z.	88	68	108	0	0.16	0.16	0.16	3	0.84	0.84	0.84
7	Upper Lagenid Z.	117	97	137	0	0.32	0.32	0.32	3	0.68	0.68	0.68
8	Spiroplectamina Z.	247	227	267	0	0.05	0.05	0.05	3	0.95	0.95	0.95
9	Bulmina Rotalia Z.	541	521	561	0	0.36	0.36	0.36	3	0.64	0.64	0.64
10	Lower Sarmatian	79	59	99	0	0.23	0.23	0.23	3	0.77	0.77	0.77
11	Upper Sarmatian	101	81	121	0	0.16	0.16	0.16	3	0.84	0.84	0.84
12	Lower Pannonian	163	143	183	0	0.80	0.80	0.80	3	0.20	0.20	0.20
13	Middle Pannonian	117	97	137	0	1.00	1.00	1.00	3	0.00	0.00	0.00

#### Engelhardtstetten 1

ID	StrataName	Thickness	Thickness_Min	Thickness_Max	Lithol_ID	Lithol	Lithol_Min	Lithol_Max	Litho2_ID	Litho2	Litho2_Min	Litho2_Max
6	Lower Lagenid Z.	303	293	313	0	0.44	0.35	0.44	3	0.56	0.56	0.65
7	Upper Lagenid Z.	173	163	183	0	0.53	0.53	0.60	3	0.47	0.40	0.47
8	Spiroplectamina Z.	299	289	309	0	0.03	0.03	0.05	3	0.97	0.95	0.97
9	Bulmina Rotalia Z.	257	247	267	0	0.43	0.43	0.50	3	0.57	0.50	0.57
10	Lower Sarmatian	263	253	273	0	0.45	0.45	0.45	3	1.00	0.55	0.55
11	Upper Sarmatian	128	118	138	0	0.54	0.54	0.54	3	1.00	0.46	0.46
12	Lower Pannonian	177	167	187	0	0.63	0.63	0.63	3	1.00	0.37	0.37
13	Middle Pannonian	205	195	215	0	0.77	0.77	0.77	3	1.00	0.23	0.23

#### Enzersdorf 17

ID	StrataName	Thickness	Thickness_Min	Thickness_Max	Lithol_ID	Lithol	Lithol_Min	Lithol_Max	Litho2_ID	Litho2	Litho2_Min	Litho2_Max
6	Lower Lagenid Z.	200	180	220	0	0.07	0.07	0.07	3	0.93	0.93	0.93
7	Upper Lagenid Z.	273	253	293	0	0.00	0.00	0.00	3	1.00	1.00	1.00
8	Spiroplectamina Z.	176	156	196	0	0.00	0.00	0.00	3	1.00	1.00	1.00
9	Bulmina Rotalia Z.	345	325	365	0	0.00	0.00	0.00	3	1.00	1.00	1.00

11	Sarmatian	453	433	473	0	0.29	0.29	0.29	0.29	0.71	0.71	0.71
12	Lower Pannonian	181	161	201	0	0.08	0.08	0.08	0.08	0.92	0.92	0.92
13	Middle Pannonian	166	146	186	0	0.11	0.11	0.11	0.11	0.89	0.89	0.89
14	Upper Pannonian	180	160	200	0	0.08	0.08	0.08	0.08	0.92	0.92	0.92

Enzersdorf 4

ID	StrataName	Thickness	Thickness_Min	Thickness_Max	Lithol_ID	Lithol	Lithol_Min	Lithol_Max	Litho2_ID	Litho2	Litho2_Min	Litho2_Max
6	Lower Lagenid Z.	18	0	38	0	0.00	0.00	0.00	3	1.00	0.80	1.00
7	Upper Lagenid Z.	207	187	227	0	0.00	0.00	0.00	3	1.00	0.90	1.00
8	Spiroplectamina Z.	387	367	407	0	0.00	0.00	0.00	3	1.00	0.80	1.00
9	Bulimina Rotalia Z.	263	243	283	0	0.02	0.02	0.02	3	0.98	0.80	1.00
10	Lower Sarmatian	269	249	289	0	0.31	0.30	0.31	3	0.69	0.50	0.90
11	Upper Sarmatian	265	245	285	0	0.42	0.30	0.42	3	0.58	0.40	0.80
12	Lower Pannonian	167	147	187	0	0.07	0.00	0.07	3	0.93	0.80	1.00
13	Middle Pannonian	115	95	135	0	0.24	0.10	0.24	3	0.76	0.60	1.00
14	Upper Pannonian	151	131	171	0	0.44	0.30	0.44	3	0.56	0.40	0.80

Enzersdorf 5

ID	StrataName	Thickness	Thickness_Min	Thickness_Max	Lithol_ID	Lithol	Lithol_Min	Lithol_Max	Litho2_ID	Litho2	Litho2_Min	Litho2_Max
6	Lower Lagenid Z.	29	9	49	0	0.00	0.00	0.00	3	1.00	1.00	1.00
7	Upper Lagenid Z.	212	192	232	0	0.02	0.02	0.02	3	0.98	0.98	0.98
8	Spiroplectamina Z.	264	244	284	0	0.04	0.04	0.04	3	0.96	0.96	0.96
9	Bulimina Rotalia Z.	310	290	330	0	0.06	0.06	0.06	3	0.94	0.94	0.94
10	Lower Sarmatian	216	196	236	0	0.24	0.24	0.24	3	0.76	0.76	0.76
11	Upper Sarmatian	282	262	302	0	0.19	0.19	0.19	3	0.81	0.81	0.81
12	Lower Pannonian	198	178	218	0	0.06	0.06	0.06	3	0.94	0.94	0.94
13	Middle Pannonian	159	139	179	0	0.18	0.18	0.18	3	0.82	0.82	0.82
14	Upper Pannonian	75	55	95	0	0.40	0.40	0.40	3	0.60	0.60	0.60

### Enzersdorf 6

ID	StrataName	Thickness	Thickness_Min	Thickness_Max	Lithol_ID	Lithol	Lithol_Min	Lithol_Max	Litho2_ID	Litho2	Litho2_Min	Litho2_Max
6	Lower Lagenid Z.	172	152	192	0	0.25	0.25	0.25	3	0.75	0.75	0.75
7	Upper Lagenid Z.	213	193	233	0	0.14	0.14	0.14	3	0.86	0.86	0.86
8	Spiroplectamina Z.	308	288	328	0	0.11	0.11	0.11	3	0.89	0.89	0.89
9	Bulimina Rotalia Z.	254	234	274	0	0.21	0.21	0.21	3	0.79	0.79	0.79
10	Lower Sarmatian	237	217	257	0	0.24	0.24	0.24	3	0.76	0.76	0.76
11	Upper Sarmatian	271	251	291	0	0.08	0.08	0.08	3	0.92	0.92	0.92
12	Lower Pannonian	199	179	219	0	0.03	0.03	0.03	3	0.97	0.97	0.97
13	Middle Pannonian	153	133	173	0	0.20	0.20	0.20	3	0.80	0.80	0.80
14	Upper Pannonian	82	62	102	0	1.00	1.00	1.00	3	0.00	0.00	0.00

### Fischamend T1

ID	StrataName	Thickness	Thickness_Min	Thickness_Max	Lithol_ID	Lithol	Lithol_Min	Lithol_Max	Litho2_ID	Litho2	Litho2_Min	Litho2_Max
6	Lower Lagenid Z.	229	209	249	0	0.00	0.00	0.00	3	1.00	1.00	1.00
7	Upper Lagenid Z.	351	331	371	0	0.22	0.22	0.22	3	0.78	0.78	0.78
8	Spiroplectamina Z.	182	162	202	0	0.02	0.02	0.02	3	0.98	0.98	0.98
9	Bulimina Rotalia Z.	574	554	594	0	0.17	0.17	0.17	3	0.83	0.83	0.83
11	Sarmatian	271	251	291	0	0.28	0.28	0.28	3	0.72	0.72	0.72
12	Lower Pannonian	552	532	572	0	0.31	0.31	0.31	3	0.69	0.69	0.69

### Orth O1

ID	StrataName	Thickness	Thickness_Min	Thickness_Max	Lithol_ID	Lithol	Lithol_Min	Lithol_Max	Litho2_ID	Litho2	Litho2_Min	Litho2_Max
6	Lower Lagenid Z.	269	249	289	0	0.02	0.02	0.02	3	0.98	0.98	0.98
7	Upper Lagenid Z.	310	290	330	0	0.55	0.55	0.55	3	0.45	0.45	0.45
8	Spiroplectamina Z.	206	186	226	0	0.12	0.12	0.12	3	0.88	0.88	0.88
9	Bulimina Rotalia Z.	698	678	718	0	0.12	0.12	0.12	3	0.88	0.88	0.88
10	Lower Sarmatian	262	242	282	0	0.01	0.01	0.01	3	0.00	0.00	0.00
11	Upper Sarmatian	222	202	242	0	0.01	0.01	0.01	3	0.00	0.00	0.00
12	Lower Pannonian	196	176	216	0	0.02	0.02	0.02	3	0.98	0.98	0.98
13	Middle Pannonian	188	168	208	0	0.02	0.02	0.02	3	0.98	0.98	0.98

14	Upper Pannonian	369	349	389	0	0.00	0.00	0.00	0.00	3	1.00	1.00	1.00
----	-----------------	-----	-----	-----	---	------	------	------	------	---	------	------	------

Wittau UT1

ID	StrataName	Thickness	Thickness_Min	Thickness_Max	Lithol_ID	Lithol	Lithol_Min	Lithol_Max	Litho2_ID	Litho2	Litho2_Min	Litho2_Max
6	Lower Lagenid Z.	159	149	169	0	0.00	0.00	0.00	3	1.00	1.00	1.00
7	Upper Lagenid Z.	513	503	523	0	0.18	0.18	0.25	3	0.82	0.75	0.82
8	Spiroplectamina Z.	263	253	273	0	0.00	0.00	0.00	3	1.00	1.00	1.00
9	Bulimina Rotalia Z.	314	304	324	0	0.67	0.67	0.67	3	0.33	0.33	0.33
10	Lower Sarmatian	543	533	553	0	0.44	0.44	0.44	3	0.56	0.56	0.56
11	Upper Sarmatian	367	357	377	0	0.35	0.35	0.35	3	0.65	0.65	0.65
12	Lower Pannonian	212	202	222	0	0.14	0.14	0.14	3	0.86	0.86	0.86
13	Middle Pannonian	257	247	267	0	0.29	0.29	0.29	3	0.71	0.71	0.71
14	Upper Pannonian	501	491	511	0	0.62	0.62	0.62	3	0.38	0.38	0.38

Essling 1

ID	StrataName	Thickness	Thickness_Min	Thickness_Max	Lithol_ID	Lithol	Lithol_Min	Lithol_Max	Litho2_ID	Litho2	Litho2_Min	Litho2_Max
6	Lower Lagenid Z.	258	248	268	0	0.00	0.00	0.00	3	1.00	1.00	1.00
7	Upper Lagenid Z.	298	288	308	0	0.00	0.00	0.25	3	1.00	0.75	1.00
8	Spiroplectamina Z.	239	229	249	0	0.00	0.00	0.55	3	1.00	0.45	1.00
9	Bulimina Rotalia Z.	167	157	177	0	0.00	0.00	0.00	3	1.00	1.00	1.00
10	Lower Sarmatian	496	486	506	0	0.41	0.41	0.41	3	0.59	0.59	0.59
11	Upper Sarmatian	202	192	212	0	0.23	0.23	0.23	3	0.77	0.77	0.77
12	Lower Pannonian	169	159	179	0	0.11	0.11	0.11	3	0.89	0.89	0.89
13	Middle Pannonian	222	212	232	0	0.23	0.23	0.23	3	0.77	0.77	0.77
14	Upper Pannonian	460	450	470	0	0.24	0.24	0.24	3	0.76	0.76	0.76

Raasdorf T2

ID	StrataName	Thickness	Thickness_Min	Thickness_Max	Lithol_ID	Lithol	Lithol_Min	Lithol_Max	Litho2_ID	Litho2	Litho2_Min	Litho2_Max
6	Lower Lagenid Z.	75	65	85	0	0.08	0.00	0.08	3	0.92	0.92	1.00
7	Upper Lagenid Z.	215	205	225	0	0.30	0.30	0.30	3	0.70	0.70	0.70
8	Spiroplectamina Z.	236	226	246	0	0.00	0.00	0.00	3	1.00	1.00	1.00
9	Bulimina Rotalia Z.	84	74	94	0	0.07	0.07	0.07	3	0.93	0.93	0.93

10	Lower Sarmatian	465	455	475	0	0.30	0.30	0.30	3	0.70	0.70	0.70
11	Upper Sarmatian	200	190	210	0	0.49	0.49	0.49	3	0.51	0.51	0.51
12	Lower Pannonian	204	194	214	0	0.25	0.25	0.25	3	0.75	0.75	0.75
13	Middle Pannonian	219	209	229	0	0.40	0.40	0.40	3	0.60	0.60	0.60
14	Upper Pannonian	364	354	374	0	0.68	0.68	0.68	3	0.32	0.32	0.32

#### Aderklaa 78

ID	StrataName	Thickness	Thickness_Min	Thickness_Max	Lithol_ID	Lithol	Lithol_Min	Lithol_Max	Litho2_ID	Litho2	Litho2_Min	Litho2_Max
6	Lower Lagenid Z.	95	85	105	0	0.85	0.61	0.90	3	0.15	0.15	0.15
7	Upper Lagenid Z.	186	176	196	0	0.50	0.50	0.52	3	0.50	0.50	0.50
8	Spiroplectamina Z.	226	216	236	0	0.00	0.00	0.09	3	1.00	1.00	1.00
9	Bulimina Rotalia Z.	72	62	82	0	0.05	0.00	0.08	3	0.95	0.95	0.95
10	Lower Sarmatian	296	286	306	0	0.22	0.22	0.22	3	0.78	0.78	0.78
11	Upper Sarmatian	182	172	192	0	0.33	0.33	0.33	3	0.67	0.67	0.67
12	Lower Pannonian	160	150	170	0	0.34	0.34	0.34	3	0.66	0.66	0.66
13	Middle Pannonian	219	209	229	0	0.41	0.41	0.41	3	0.59	0.59	0.59
14	Upper Pannonian	439	429	449	0	0.49	0.49	0.49	3	0.51	0.51	0.51

#### Aderklaa UT1

ID	StrataName	Thickness	Thickness_Min	Thickness_Max	Lithol_ID	Lithol	Lithol_Min	Lithol_Max	Litho2_ID	Litho2	Litho2_Min	Litho2_Max
6	Lower Lagenid Z.	195	185	205	0	0.86	0.86	0.90	3	0.14	0.10	0.14
7	Upper Lagenid Z.	190	180	200	0	0.53	0.53	0.65	3	0.47	0.35	0.47
8	Spiroplectamina Z.	375	365	385	0	0.17	0.15	0.17	3	0.83	0.83	0.85
9	Bulimina Rotalia Z.	250	240	260	0	0.44	0.44	0.55	3	0.56	0.45	0.56
10	Lower Sarmatian	435	425	445	0	0.24	0.24	0.24	3	0.76	0.76	0.76
11	Upper Sarmatian	278	268	288	0	0.26	0.26	0.26	3	0.74	0.74	0.74
12	Lower Pannonian	372	362	382	0	0.33	0.33	0.33	3	0.67	0.67	0.67
13	Middle Pannonian	605	595	615	0	0.42	0.42	0.42	3	0.58	0.58	0.58

Markgrafneusiedl 1

ID	StrataName	Thickness	Thickness_Min	Thickness_Max	Lithol_ID	Lithol	Lithol_Min	Lithol_Max	Litho2_ID	Litho2	Litho2_Min	Litho2_Max
6	Lower Lagenid Z.	116	116	116	0	0.45	0.45	0.45	3	0.55	0.55	0.55
7	Upper Lagenid Z.	176	176	176	0	0.31	0.31	0.31	3	0.69	0.69	0.69
8	Spiroplectamina Z.	304	304	304	0	0.03	0.03	0.03	3	0.97	0.97	0.97
9	Bulimina Rotalia Z.	174	174	174	0	0.31	0.31	0.31	3	0.69	0.69	0.69
10	Lower Sarmatian	434	434	434	0	0.14	0.14	0.14	3	0.86	0.86	0.86
11	Upper Sarmatian	212	212	212	0	0.32	0.32	0.32	3	0.68	0.68	0.68
12	Lower Pannonian	250	250	250	0	0.26	0.26	0.26	3	0.74	0.74	0.74
14	Upper Pannonian	530	530	530	0	0.50	0.50	0.50	3	0.50	0.50	0.50

Glinzendorf T1

ID	StrataName	Thickness	Thickness_Min	Thickness_Max	Lithol_ID	Lithol	Lithol_Min	Lithol_Max	Litho2_ID	Litho2	Litho2_Min	Litho2_Max
6	Lower Lagenid Z.	27	17	37	0	0.11	0.00	0.11	3	0.89	0.89	1.00
7	Upper Lagenid Z.	175	165	185	0	0.30	0.30	0.35	3	0.70	0.65	0.70
8	Spiroplectamina Z.	364	354	374	0	0.00	0.00	0.00	3	1.00	1.00	1.00
9	Bulimina Rotalia Z.	92	82	102	0	0.39	0.35	0.40	3	0.61	0.60	0.65
10	Lower Sarmatian	529	519	539	0	0.25	0.25	0.25	3	0.75	0.75	0.75
11	Upper Sarmatian	245	235	255	0	0.36	0.36	0.36	3	0.64	0.64	0.64
12	Lower Pannonian	208	198	218	0	0.18	0.18	0.18	3	0.82	0.82	0.82
13	Middle Pannonian	150	140	160	0	0.47	0.47	0.47	3	0.53	0.53	0.53
14	Upper Pannonian	290	280	300	0	0.61	0.61	0.61	3	0.39	0.39	0.39

Leopoldau 1

ID	StrataName	Thickness	Thickness_Min	Thickness_Max	Lithol_ID	Lithol	Lithol_Min	Lithol_Max	Litho2_ID	Litho2	Litho2_Min	Litho2_Max
7	Upper Lagenid Z.	75	65	85	0	0.85	0.85	0.85	3	0.15	0.15	0.15
8	Spiroplectamina Z.	271	261	281	0	0.48	0.48	0.48	3	0.52	0.52	0.52
9	Bulimina Rotalia Z.	380	370	390	0	0.61	0.61	0.61	3	0.39	0.39	0.39
10	Lower Sarmatian	158	148	168	0	0.84	0.84	0.84	3	0.16	0.16	0.16
11	Upper Sarmatian	180	170	190	0	0.76	0.76	0.76	3	0.24	0.24	0.24
12	Lower Pannonian	241	231	251	0	0.63	0.63	0.63	3	0.37	0.37	0.37

13	Middle Pannonian	141	131	151	0	0.61	0.61	0.61	0.39	0.39	0.39
14	Upper Pannonian	13	3	23	0	0.92	0.92	0.92	0.08	0.08	0.08

#### Untersiebenbrunn T1

ID	StrataName	Thickness	Thickness_Min	Thickness_Max	Lithol_ID	Lithol	Lithol_Min	Lithol_Max	Litho2_ID	Litho2	Litho2_Min	Litho2_Max
6	Lower Lagenid Z.	99	99	99	0	0.00	0.00	0.00	3	1.00	1.00	1.00
7	Upper Lagenid Z.	198	198	198	0	0.69	0.69	0.69	3	0.31	0.31	0.31
8	Spiroplectammina Z.	368	368	368	0	0.07	0.07	0.07	3	0.93	0.93	0.93
9	Bulimina Rotalia Z.	90	90	90	0	0.31	0.31	0.31	3	0.69	0.69	0.69
10	Lower Sarmatian	578	578	578	0	0.37	0.37	0.37	3	0.63	0.63	0.63
11	Upper Sarmatian	230	230	230	0	0.48	0.48	0.48	3	0.52	0.52	0.52
12	Lower Pannonian	298	298	298	0	0.34	0.34	0.34	3	0.66	0.66	0.66
13	Middle Pannonian	194	194	194	0	0.51	0.51	0.51	3	0.49	0.49	0.49
14	Upper Pannonian	460	460	460	0	0.76	0.76	0.76	3	0.24	0.24	0.24

#### Oberweiden T1

ID	StrataName	Thickness	Thickness_Min	Thickness_Max	Lithol_ID	Lithol	Lithol_Min	Lithol_Max	Litho2_ID	Litho2	Litho2_Min	Litho2_Max
6	Upper Lagenid Z.	156	156	156	0	0.77	0.77	0.77	3	0.23	0.23	0.23
8	Spiroplectammina Z.	443	443	443	0	0.32	0.32	0.32	3	0.68	0.68	0.68
9	Bulimina Rotalia Z.	327	327	327	0	0.13	0.13	0.13	3	0.87	0.87	0.87
10	Lower Sarmatian	172	172	172	0	0.31	0.31	0.31	3	0.69	0.69	0.69
11	Upper Sarmatian	206	206	206	0	0.20	0.20	0.20	3	0.80	0.80	0.80
12	Lower Pannonian	328	328	328	0	0.27	0.27	0.27	3	0.73	0.73	0.73
13	Middle Pannonian	444	444	444	0	0.26	0.26	0.26	3	0.74	0.74	0.74

#### Zwerndorf T1

ID	StrataName	Thickness	Thickness_Min	Thickness_Max	Lithol_ID	Lithol	Lithol_Min	Lithol_Max	Litho2_ID	Litho2	Litho2_Min	Litho2_Max
7	Upper Lagenid Z.	25	25	25	0	0.68	0.68	0.68	3	0.32	0.32	0.32
8	Spiroplectammina Z.	375	375	375	0	0.38	0.38	0.38	3	0.62	0.62	0.62
9	Bulimina Rotalia Z.	384	384	384	0	0.08	0.08	0.08	3	0.92	0.92	0.92
10	Lower Sarmatian	141	141	141	0	0.27	0.27	0.27	3	0.73	0.73	0.73
11	Upper Sarmatian	211	211	211	0	0.32	0.32	0.32	3	0.68	0.68	0.68

12	Lower Pannonian	307	307	307	0	0.32	0.32	0.32	0.32	0.68	0.68	0.68
13	Middle Pannonian	116	116	116	0	0.73	0.73	0.73	0.73	0.27	0.27	0.27
14	Upper Pannonian	316	316	316	0	0.52	0.52	0.52	0.52	0.48	0.48	0.48

Tallesbrunn S1

ID	StrataName	Thickness	Thickness_Min	Thickness_Max	Litho1_ID	Litho1	Litho1_Min	Litho1_Max	Litho2_ID	Litho2	Litho2_Min	Litho2_Max
7	Upper Lagenid Z.	49	49	49	0	0.35	0.35	0.35	3	0.65	0.65	0.65
8	Spiroplectanina Z.	370	370	370	0	0.12	0.12	0.12	3	0.88	0.88	0.88
9	Bulimina Rotalia Z.	419	419	419	0	0.05	0.05	0.05	3	0.95	0.95	0.95
10	Lower Sarmatian	137	137	137	0	0.42	0.42	0.42	3	0.58	0.58	0.58
11	Upper Sarmatian	229	229	229	0	0.21	0.21	0.21	3	0.79	0.79	0.79
12	Lower Pannonian	284	284	284	0	0.45	0.45	0.45	3	0.55	0.55	0.55
13	Middle Pannonian	157	157	157	0	0.75	0.75	0.75	3	0.25	0.25	0.25
14	Upper Pannonian	274	274	274	0	0.78	0.78	0.78	3	0.22	0.22	0.22

Tallesbrunn T1

ID	StrataName	Thickness	Thickness_Min	Thickness_Max	Litho1_ID	Litho1	Litho1_Min	Litho1_Max	Litho2_ID	Litho2	Litho2_Min	Litho2_Max
7	Upper Lagenid Z.	25	25	25	0	0.08	0.08	0.08	3	0.92	0.92	0.92
8	Spiroplectanina Z.	427	427	427	0	0.20	0.20	0.20	3	0.80	0.80	0.80
9	Bulimina Rotalia Z.	414	414	414	0	0.36	0.36	0.36	3	0.64	0.64	0.64
10	Lower Sarmatian	120	120	120	0	0.14	0.14	0.14	3	0.86	0.86	0.86
11	Upper Sarmatian	178	178	178	0	0.16	0.16	0.16	3	0.84	0.84	0.84
12	Lower Pannonian	290	290	290	0	0.24	0.24	0.24	3	0.76	0.76	0.76
14	Middle/Upper Pannonian	413	413	413	0	0.56	0.56	0.56	3	0.44	0.44	0.44

Tallesbrunn W2

ID	StrataName	Thickness	Thickness_Min	Thickness_Max	Litho1_ID	Litho1	Litho1_Min	Litho1_Max	Litho2_ID	Litho2	Litho2_Min	Litho2_Max
9	Badenian	807	807	807	0	0.19	0.19	0.19	3	0.81	0.81	0.81
11	Sarmatian	356	356	356	0	0.50	0.50	0.50	3	0.50	0.50	0.50
12	Lower Pannonian	293	293	293	0	0.05	0.05	0.05	3	1.29	1.29	1.29
14	Middle/Upper Pannonian	394	394	394	0	0.52	0.52	0.52	3	0.48	0.48	0.48

Prottes TS1

ID	StrataName	Thickness	Thickness_Min	Thickness_Max	Lithol_ID	Lithol	Lithol_Min	Lithol_Max	Litho1_Max	Litho2_ID	Litho2	Litho2_Min	Litho2_Max
9	Badenian	702	702	702	0	0.19	0.19	0.19	0.19	3	0.81	0.81	0.81
11	Sarmatian	295	295	295	0	0.29	0.29	0.29	0.29	3	0.71	0.71	0.71
12	Lower Pannonian	292	292	292	0	0.23	0.23	0.23	0.23	3	0.77	0.77	0.77
14	Middle/Upper Pannonian	383	383	383	0	0.58	0.58	0.58	0.58	3	0.42	0.42	0.42

Spannberg T3

ID	StrataName	Thickness	Thickness_Min	Thickness_Max	Lithol_ID	Lithol	Lithol_Min	Lithol_Max	Litho2_ID	Litho2	Litho2_Min	Litho2_Max	Litho3_ID
9	Badenian	731	731	731	0	0.18	0.18	0.18	3	0.82	0.82	0.82	0
10	Lower Sarmatian	40	40	40	0	0.02	0.02	0.02	3	0.98	0.98	0.98	0
11	Upper Sarmatian	271	271	271	0	0.21	0.21	0.21	3	0.79	0.79	0.79	0
12	Lower Pannonian	321	321	321	0	0.16	0.16	0.16	3	0.84	0.84	0.84	0
14	Middle Pannonian	510	510	510	0	0.35	0.35	0.35	3	0.65	0.65	0.65	0

Spannberg T1

ID	StrataName	Thickness	Thickness_Min	Thickness_Max	Lithol_ID	Lithol	Lithol_Min	Lithol_Max	Litho1_Max	Litho2_ID	Litho2	Litho2_Min	Litho2_Max
8	Spiroplectamina Z.	172	172	172	0	0.38	0.38	0.38	0.38	3	0.62	0.62	0.62
9	Bulimina Rotalia Z.	412	412	412	0	0.18	0.18	0.18	0.18	3	0.82	0.82	0.82
10	Lower Sarmatian	128	128	128	0	0.24	0.24	0.24	0.24	3	0.76	0.76	0.76
11	Upper Sarmatian	308	308	308	0	0.24	0.24	0.24	0.24	3	0.76	0.76	0.76
12	Lower Pannonian	330	330	330	0	0.38	0.38	0.38	0.38	3	0.62	0.62	0.62
13	Middle Pannonian	185	185	185	0	0.45	0.45	0.45	0.45	3	0.55	0.55	0.55
14	Upper Pannonian	277	277	277	0	0.65	0.65	0.65	0.65	3	0.35	0.35	0.35

Ebenthal T1

ID	StrataName	Thickness	Thickness_Min	Thickness_Max	Lithol_ID	Lithol	Lithol_Min	Lithol_Max	Litho1_Max	Litho2_ID	Litho2	Litho2_Min	Litho2_Max
7	Upper Lagenid Z.	122	122	122	0	0.73	0.73	0.73	0.73	3	0.27	0.27	0.27
8	Spiroplectamina Z.	377	377	377	0	0.41	0.41	0.41	0.41	3	0.59	0.59	0.59
9	Bulimina Rotalia Z.	507	507	507	0	0.68	0.68	0.68	0.68	3	0.32	0.32	0.32
10	Lower Sarmatian	204	204	204	0	0.74	0.74	0.74	0.74	3	0.26	0.26	0.26

11	Upper Sarmatian	255		255		255	0	0.57	0.57	0.57	3	0.43	0.43	0.43
12	Lower Pannonian	285		285		285	0	0.71	0.71	0.71	3	0.29	0.29	0.29
13	Middle Pannonian	65		65		65	0	0.66	0.66	0.66	3	0.34	0.34	0.34
14	Upper Pannonian	525		525		525	0	0.38	0.38	0.38	3	0.62	0.62	0.62

**Zistersdorf 4**

ID	StrataName	Thickness	Thickness_Min	Thickness_Max	Litho1_ID	Litho1	Litho1_Min	Litho1_Max	Litho2_ID	Litho2	Litho2_Min	Litho2_Max
8	Spiropectamina Z.	495	495	495	0	0.61	0.61	0.61	3	0.39	0.39	0.39
9	Bulimina Rotalia Z.	1262	1262	1262	0	0.44	0.44	0.44	3	0.56	0.56	0.56
10	Lower Sarmatian	258	258	258	0	0.00	0.00	0.00	3	1.00	1.00	1.00
11	Upper Sarmatian	860	860	860	0	0.35	0.35	0.35	3	0.65	0.65	0.65
12	Lower Pannonian	527	527	527	0	0.67	0.67	0.67	3	0.33	0.33	0.33
13	Middle Pannonian	103	103	103	0	0.35	0.35	0.35	3	0.65	0.65	0.65
14	Upper Pannonian	70	70	70	0	0.45	0.45	0.45	3	0.55	0.55	0.55

## **9     Appendix 2**

### ***Curriculum Vitae***



## ***Curriculum Vitae***

Mag. Monika Hölzel  
Geologist/Sedimentologist  
born on 11<sup>th</sup> October 1977 in Vienna

### Education

<i>1996</i>	School leaving exam, Neusprachliches Gymnasium, Wien 21
<i>1996 - 2003</i>	Study Earth Sciences, Geology (University Vienna)
<i>2001 – 2003</i>	Diploma Thesis (M. Wagneich, B. Grasemann): Sedimentologische Bearbeitung der Ingering Formation, Austria.
<i>06.2003</i>	Final Exam
<i>2004 - 2008</i>	PhD Thesis in Geology (University Vienna): Quantification of tectonic movement along Miocene faults in the Vienna Basin (M. Wagneich).

### Professional Life

<i>since 08. 2008</i>	Geoscientist at RAG (Rohoelaufsuchungsgesellschaft-AG)
<i>01.2007 – 07.2008</i>	Project at the University Vienna: Karpatian Tectonics financed by OMV together with K. Decker, A. Zamolyi.
<i>01.2006; 02.2008; 02 2009</i>	Lectures: 3D Seismic Interpretation together with R. Hinsch.
<i>12.2005 – 05.2006</i>	Project at RAG: Re-assignment of field outlines.
<i>11.2005 &amp; 11.2006</i>	Lectures: Software applications in Geology (University Vienna).
<i>08.2005</i>	Structural Mapping in order of the Geological Survey of Austria: Totes Gebirge.
<i>01. – 06.2004</i>	Geotechnical Data Management at the ARC Seibersdorf: Zustandserhebung Schutzdämme Lobau – March.
<i>01. – 08.2002</i>	Project at RAG: Digitalising of borehole data.
<i>2001 – 2002</i>	Internet research for thecrystalweb.org (virtual museum of crystals, financed by Swarovski).
<i>1999 – 2002</i>	Work at the laboratory of the Museum of Natural History Vienna (Department of Mineralogy and Petrology).
<i>1999 – 2003</i>	Diverse tutorials at the Institutes of Petrology and Geology (rock microscopy, general geology, excursions).

---

Short Courses

*Sedimentation and Tectonic in Compressive Settings*, P. van der Beek, R. Zoetemeijer, S. Gupta u.a. (Grenoble/F)

*Diagenesis of clastic sediments*, R. Hesse and R. Gaupp (Jena/D)

*Seismische Stratigraphie*, J. Schlaf

*Basin Formation and Basin Modelling*, S. Cloething

*Global Inventory of Fold-Thrust Belts: Petroleum Geology*, D. Roeder

*Pressures, sealing and hydrocarbon column heights*, R. Swarbrick

*Visual Basic-Programming*, ZID-BOKU

---

Scholarships

01.2006 – 06.2006	Forschungsstipendium of the University Vienna (Project)
02. 2005	Förderungsstipendium of the University Vienna (PhD)
06.2004 – 11.2005	DOC Scholarship of the Austrian Academy of Sciences (PhD)
06. 2002	OEAW-Scholarship Commission of Stratigraphy (Diploma Thesis)
02.2001	Förderungsstipendium of the University Vienna (Diploma Thesis)

### **List of Publications**

#### Scientific Articles

- Hölzel, M., Wagreich, M. (submitted 2009). Middle to Upper Miocene fault history analysis of the southern Vienna Basin (Austria). *Marine and Petroleum Geology*.
- Hölzel, M., Decker, K., Zamolyi, A., Strauss, P., Wagreich, M. (submitted 2008): Lower Miocene structural evolution of the central Vienna Basin (Austria). *Marine and Petroleum Geology*.
- Hölzel, M., Wagreich, M., Faber R., Strauss, P. (2008). Regional subsidence analysis in the Vienna Basin (Austria). *Austrian Journal of Earth Sciences*, 101, 88 –89.
- Hölzel, M., Faber, R., Wagreich, M. (2008). DeCompactionTool: Software for subsidence analysis including statistical error quantification. *Computers and Geosciences*, 34, 1454-1460.
- Hölzel, M. (2006): Bericht 2005 über geologische Aufnahmen im Toten Gebirge auf Blatt 97 Bad Mitterndorf. *Jahrbuch Geol. B.-A.*, 146 (1+2), 82-84.
- Hölzel, M., Wagreich M., Grasemann, B. (2006): Numerical modelling of clast rotation during soft-sediment deformation: A case study in Miocene delta deposits. *International Journal of Earth Sciences*, 95 (5), 921-928.
- Hölzel, M., Wagreich, M. (2004): Sedimentology of a Miocene Delta Complex: The Type Section of the Ingering Formation (Fohnsdorf Basin, Austria). *Austrian Journal of Earth Sciences* 95/96, 80-86.
- Hoelzel, M. (2004): StratDraw - Automatic generation of stratigraphic sections from tabulated field data. *Computers and Geosciences* 30 (7), 785-789.

#### Reports

- Hölzel, M., Zamolyi A., Decker, K. (2007): Tectonic evolution of the Vienna Basin and the Waschberg Zone during the Early Miocene. unpubl. OMV-Karpetec Mid Term Report, 98 pp.
- Hölzel, M. (2005): Geologische Kartierung des Gebietes Bösenbühel – Gr. Hochkasten – Hebenkas (Totes Gebirge). unpubl. Report Geol. B.-A., 14 pp.
- Hölzel, M. (2005): Quantification of tectonic movement along Miocene faults in the southern Vienna Basin. unpubl., DOC Scholarship Final Report, 16 pp.

#### Selected Conference Abstracts

- Hölzel, M., Zamolyi A., Decker, K. (2008): Tectonic evolution of the Vienna Basin and the Waschberg Zone during the Early Miocene. *Erdwissenschaftliches Kolloquium – OEGG*, University Vienna. (Talk)
- Decker, K., Hölzel, M., Strauss, P., Wagreich, M., Zamolyi, A. (2007): Tectonic evolution of the Alpine-Carpathian transition during the Early Miocene. EGU2007-A-02712, Vienna. (Poster)
- Hölzel, M., Wagreich, M. (2007): Fault backstripping: How to quantify normal faulting in the southern Vienna Basin. EGU2007-A-09476, Vienna. (Poster)

Hölzel, M., Faber, R., Wagreich, M. (2006): A software tool for error quantification of subsidence calculations based on Monte Carlo Simulation. Abstracts Pangeo Austria, Innsbruck, 114-115. (Poster)

Hölzel, M., Faber, R., Wagreich, M. (2006): A new software tool for statistical error quantification of subsidence calculations. Abstracts COG Salzburg, p.15. (Poster, Talk)

Hölzel, M., Wagreich, M. (2006): Miocene fault activity in the southern Vienna Basin based on fault backstripping. Geophysical Research Abstracts, Vol. 8, 06999 (Abstracts EGU06). (Talk)

Hölzel, M., Faber, R., Wagreich, M. (2006): A new software tool for statistical error quantification of subsidence calculations. Sediment 2006 – Schriftenreihe d. Deutschen Gesellschaft für Geowissenschaften, 45, p 95. (Poster)

Hölzel, M., Wagreich, M., 2005, Miocene faulting recorded in backstripped sediments of the southern Vienna Basin. Sediment05 – Abstracts, Schriftenreihe der Deutschen Gesellschaft für Geowissenschaften, 38, p. 75. (Talk)

Hölzel, M., Ebner, M., Grasemann, B., Wagreich, M. (2004): Soft sediment deformation with anisotropic volume loss. (Talk)

Hölzel, M., Wagreich, M., Grasemann, B. (2002): Quantifizierung von synsedimentärer Deformation in einem miozänen Delta (Ingering-Formation, Fohnsdorfer Tertiärbecken). Abstracts Pangeo Austria, Salzburg, p. 76. (Poster)

Hölzel, M., Wagreich, M., Grasemann, B. (2001): Sedimentologie und Quantifizierung von synsedimentärer Deformation in der Ingering-Formation (Fohnsdorfer Tertiärbecken). Mitteilungen Geoaustria, 45, 164-166. (Talk)